Addis Ababa University

Addis Ababa Institute of Technology

School of Mechanical and Industrial Engineering

MOUNTING PLATE, STRESS CONCENTRATION AND DAMAGE TOLERANCE ANALYSIS FOR ANTENNA INSTALLATIONS ON PRESSURIZED TRANSPORT AIRCRAFT USING THE FEM

By: - Woldeyesus Mideksa

A thesis is submitted to the school of Graduate Studies of Addis Ababa University in partial fulfilment of the requirement of the Degree of Master of Science in Mechanical Engineering (Mechanical Design Stream)

Advisor: - Behailu Mamo

July, 2021

Addis Ababa, Ethiopia

Addis Ababa University

Addis Ababa Institute of Technology

School of Mechanical and Industrial Engineering

MOUNTING PLATE, STRESS CONCENTRATION AND DAMAGE TOLERANCE ANALYSIS FOR ANTENNA INSTALLATIONS ON PRESSURIZED TRANSPORT AIRCRAFT USING THE FEM

By

Woldeyesus Mideksa

Approved by board of Examiners

_____	_____	_____
Chairman, SMIE	Signature	Date
Behailu Mamo	_____	_____
Thesis Advisor	Signature	Date
_____	_____	_____
Internal Examiner	Signature	Date
_____	_____	_____
External Examiner	Signature	Date

July, 2021

Addis Ababa

Ethiopia

Name of the advisor: Behailu Mamo

Candidate's Declaration

I hereby declare that the work which is being presented in this thesis entitled "**MOUNTING PLATE, STRESS CONCENTRATION AND DAMAGE TOLERANCE ANALYSIS FOR ANTENNA INSTALLATIONS ON PRESSURIZED TRANSPORT AIRCRAFT USING THE FEM** " is original work of my own, has not been presented for a degree in any other university and that all sources of material used for the thesis have been duly acknowledged.

_____ _____

Woldeyesus Mideksa **(**Candidate) Date

This is to certify that the above declaration made by the candidate is correct to the best of my knowledge.

_____ _____

Behailu Mamo **(Thesis Advisor**) Date

Acknowledgement

First and foremost, praise and thanks to God, the Almighty, and Yahweh for His showers of blessings throughout my research work to complete this thesis successfully. I would like to express my deep and sincere gratitude to my thesis advisor, Mr. Behailu Mamo, for having the patience to help me to work on this thesis and for providing invaluable guidance and encouragement throughout the course of this thesis project. His vision, sincerity, and motivation have deeply inspired me. He has taught me how to carry out and present the thesis as clearly as possible. It was a great privilege and honor to work and study under his guidance. I am extremely grateful for what he has offered me. I would also like to thank him for his friendship, empathy, and great sense of humor.

I would like to express my deep appreciation to Ethiopian Airlines, who employed me at the very beginning and has been giving to me different pragmatic courses related to different civil aircraft systems and acquired engineering and maintenance knowledge, skills, and competencies to understand state-of-the-art aircraft systems engineering, structures engineering, and aircraft and component reliability engineering, and aviation related regulations training.

I would also like to thank Boeing commercial aircraft manufacturing company for shaping me more in aircraft systems engineering and maintenance activities and introducing me to a lot of aviation and aircraft knowledge with unlimited manuals and documents.

I am grateful to my parents for their love, prayers, care, and sacrifices in educating and preparing me for my future endeavours. I am very much thankful to my wife, Yeshihareg Tilahun, and my sons, Macron & Roobson Woldeyesus, and my sister, Dr. Tigist Mideksa, for their love, understanding, prayers, and continuing support and encouragement during my thesis work.

In addition, I would like to express my heartfelt appreciation and gratitude to Dr. Mulugeta Hailemariam (Internal Examiner) for his intelligent remarks, insightful comments, and challenging questions.

Finally, my thanks go to all the people who have supported me in completing this thesis work, directly or indirectly.

Abstract

During the in-service life of a given aircraft, different antennas are installed on the fuselage of the aircraft for different operational and regulatory requirements. These antennas are part of the Communication, Navigation and surveillance (CNS) systems of aircraft. Antennas play the greatest role in enhancing the operational safety and functionality of a given civil or military aircraft by providing reliable communication and navigation systems. During antenna installation, the fuselage skin loses its structural integrity. Taking this into consideration and also fracture mechanics as a basic principle, damage tolerance analysis for antenna installations on pressurized transport airplanes has been studied. For skin modifications, first from a static strength point of view, the elliptical antenna mounting plate is compared with those of circular and rectangular mounting plates. Next, based on the first result, from the stress concentration factor point of view, the best antenna cut-out shape was studied by comparing antenna cut-out shapes such as elliptical, circular, and square cut-outs for mounting plates subjected to biaxial loads. Then, considering the best mounting plate shape and antenna cut-out, i.e., having the lowest stress concentration factor, damage tolerance analysis (DTA) is done using Linear Elastic Fracture Mechanics (LEFM) and the establishing inspection type and inspection threshold are studied. To perform the above activities, a special tool, Finite Element Analysis (FEA), i.e., ANSYS application software, was used to perform static and fatigue simulations along the potential crack growth path for a flaw initiating from the antenna cut-out normal to the stress application direction. The output from finite element modelling and analysis is compared with the analytical for the safe installation of the antenna. With respect to the above framework, the study was done, and the result shows that the circular mounting plate is relatively better than those of the rectangular mounting plate and the elliptical mounting plate. With regard to the cut-out shape, for the applied biaxial tension loads, a circular cut-out is relatively better than those of the square and elliptical cut-out shapes. A circular mounting plate with a circular antenna cut-out is better than an elliptical or rectangular mounting plate. Starting with the initial crack length of a_i and the progressive crack length of a_{i+1} to the critical crack length value ac, which is calculated using the fracture toughness of the skin materials, an estimated inspection type and inspection threshold (damage detection) were established.

Key words: Antenna Installation Plate, antenna cut-out & stress concentration for biaxial tension load, Damage Tolerance Design and Analysis, Stress Intensity Factor (SIF) and Inspection Interval,

Table of Contents

List of tables

List of figures

Abbreviation

- a: Crack Length
- A/C : Aircraft
- AASA: Aging Airplane Safety Act
- AASR: Aging Airplane Safety Rule
- AAWG: Airworthiness Assurance Working Group
- AC: Advisory Circular
- a_c : Critical Crack Length
- A_f: Cross-sectional area of each fastener
- a_f : Final Crack Length
- a_i : Initial Crack Length
- a_{min}: Minimum Detectable Crack Length
- AMM: Aircraft Maintenance Manual
- D: Antenna connector cut-out hole
- d: Diameter, hole or fastener diameter
- da : Change In Crack Length
- DADT: Durability And Damage Tolerance
- dN: Change In Number Of Cycles
- DT: Damage Tolerance
- DTA: Damage Tolerance Analysis
- e: Edge Margin
- E: Modulus of elasticity or Young's Modulus in tension
- e/D: Ratio of edge distance (centre of the hole to edge of the sheet) to hole diameter (bearing strength).
- EASA : European Aviation Safety Agency
- E_c: Modulus of elasticity in compression; average
- FAA: Federal Aviation Administration
- FAR: Federal Aviation Regulation
- F_{brg} : Design Yield Allowable
- F_{bru}: Design ultimate bearing stress(ksi)
- F_{bry}: Design bearing yield stress(ksi)
- F_{cy}: Design compressive yield stress
- F_{du}: Design Tension Allowable

— FEA:Finite Element Analysis

— FEM:Finite Element Method

— Fsu:Ultimate shear strength of the fastener material,

— $F_{tu:}$Ultimate tensile strength of the material (allowable)(ksi)

— $F_{ty:}$Yield tensile strength of the material (allowable)(ksi)

— G: Modulus of rigidity (shear modulus).

— GAG :Ground Air Ground

— GVI : general visual inspection

— HFEC :high frequency eddy current

— K :stress intensity factor

— Kc : Fracture toughness

— Kc :K value at critical crack length

— KIC : Fracture toughness for mode I failure

— Ksi :1000 pound per square inch

— K_{tg} :Gross Area Stress Concentration factor

— ΔK: Change of Stress Intensity Factor

— L: Longitudinal (grain direction)

— LEFM: Linear Elastic Fracture Mechanics

— LFEC: Low frequency eddy current

— LT:Long Transverse(grain direction)

— M or Ma: Mach number

— MED: Multiple element damage

— MFEC: medium frequency eddy current

— MMPDS: Metallic Materials Properties Development and Standardization

— MS: Margins of Safety

— MSD: multiple site damage

— NDI: Non-Destructive Inspection

— NDT: Non Destructive Testing

— N_i: Number of Cycles to Fatigue Failure

— $N_{\underline{O}}$: Damage Detection Period

— NPRMs: Notice of Proposed Rulemaking

— NTSB: National Transportation Safety Board

— OEM: Original Equipment Manufacturer

— P:Fastener pitch

— ΔP: Cabin Differential Pressure

— POD: probability of detection

— PSI :Pound Per Square Inch

— R:Stress ratio

— Re_x:Reynolds number (Re)

— Satcom: Satellite communication

— SCF1: Single shear correction factor

— SCF2: Double Shear Correction Factor

— σ_{gross} : Gross, or Far Field Stress

— Skin Bay :Area Between 2 Adjacent Frames and Stringers

— σ_{net} : Net Area Stress

— σ_{peak} : Peak Stress

— SRM: Structural Repair Manual

— ST:Short Transverse(grain direction)

— STA: station

— STC: Supplemental Type Certificates

— STG: Structure Task Group

— TC: Transport Canada

— t_p: Thickness of mounting plate

— t_s:skin thickness

— WFD: Widespread Fatigue Damage

— β :Geometric constant (unit-less)

— ν: Kinematic viscosity of the fluid (m^2/s).

— σ Remote:(Far-Field) Uniform Stress

— σ_{rs}: Residual Stress

— v:Poisson's ratio

Chapter One

1.1 Introduction

Today, with thousands of aircraft airborne at any time, communication and navigation systems are essential to safe, successful, and target-based flight. For all these communication, navigation, and surveillance systems, different antenna types, which are part of the communication and navigation systems, play a vital role. Aircraft structural modification, specifically to the fuselage, is performed on a wide range of platforms to install various types of antennas, ranging from pure civil aircraft (commercial and private) to pure military models, with intermediate scenarios (mission aircraft, military derivatives). [1][2][3].

Damage tolerance is an evaluation of the strength, detailed design, and fabrication that must show that catastrophic failure due to fatigue and corrosion, manufacturing defects, or accidental damage will be avoided throughout the operational life of the airplane [2][3].

The damage tolerance principle requires that any airplane damage be detected and repaired before the strength fails below the regulatory fail-safe capability. Achieving this goal requires a combination of efficient design, thorough analysis, adequate inspections, and appropriate repairs to insure the long-term safety of the aircraft structure [3].

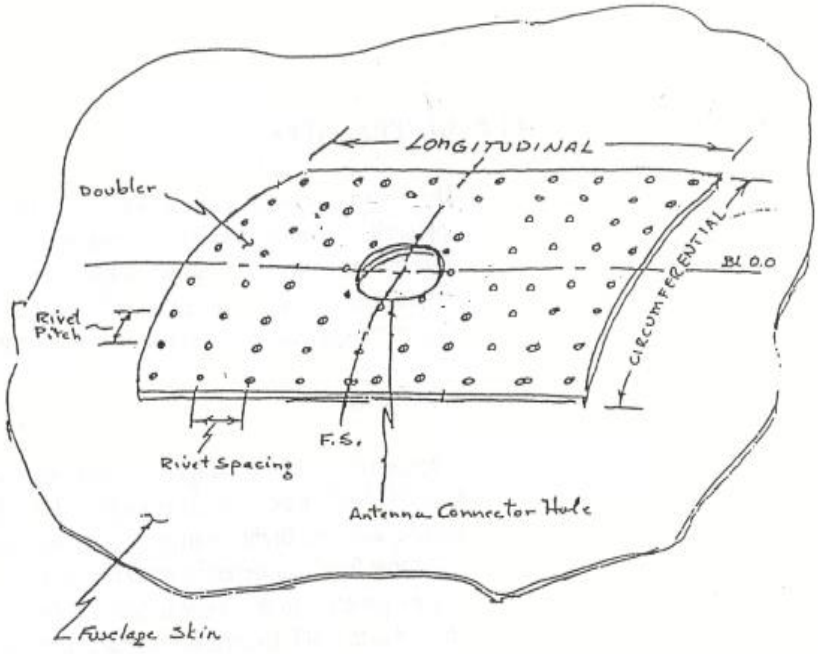

Figure 1.1: Typical Antenna Installation

After a certain service life of the aircraft, the antenna mounting plate and fuselage skin adjacent to the antenna are subject to crack initiation and propagation for a variety of reasons, the most significant of

which are fretting, corrosion, and fatigue. A certain crack in the fuselage skin can propagate to the critical length, which is the point where the fuselage skin structure cannot sustain the limit load. When the fuselage skin cannot sustain the limit load, this can result in possible rapid decompression and loss of aircraft structural integrity [4].

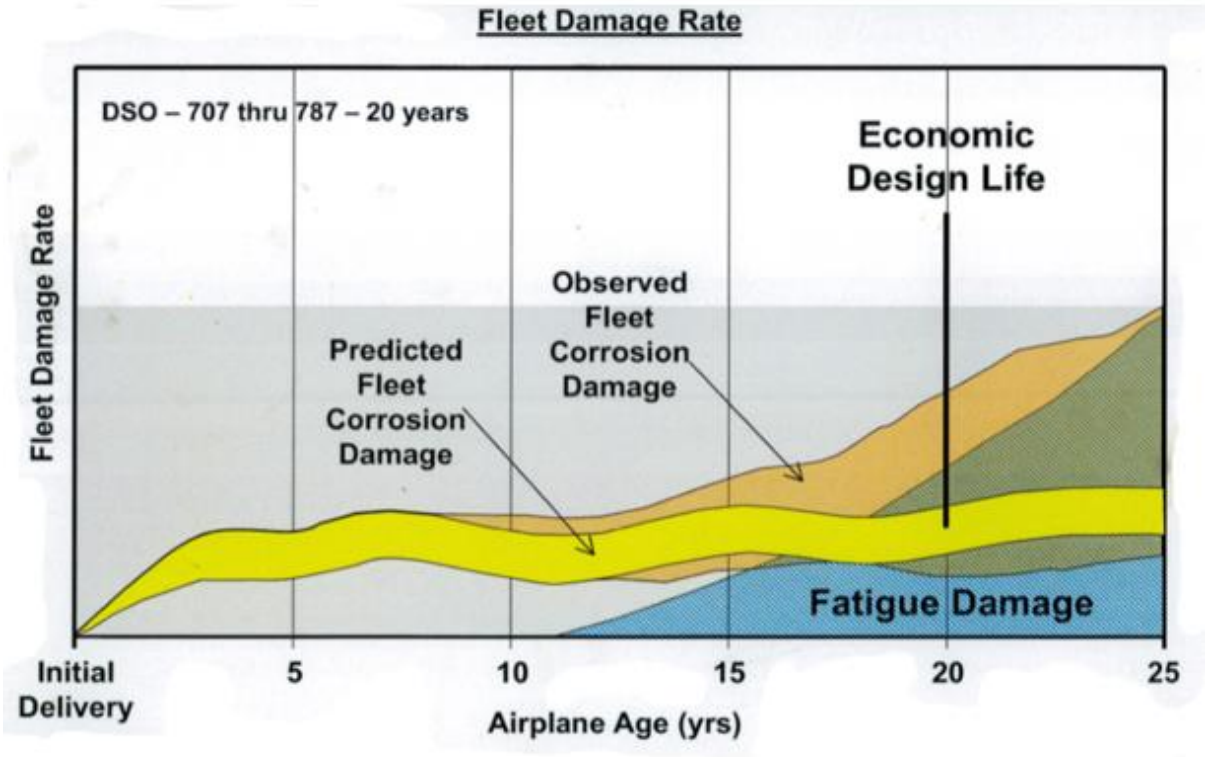

Figure 1.2: B7X7 Fleet Damage Rate related with fatigue and corrosion [4]

1.1.1 Damage Tolerance Design, Damage Tolerance Analysis and Residual Strength

Fracture analysis: The approaches provide a simplified methodology for predicting the fracture of flawed structural components in the elastic-plastic and fully plastic regimes of material deformation. Damage tolerance is the attribute of the structure that permits it to retain its required residual strength for a period of use after the structure has sustained a given level of fatigue, corrosion, accidental or discrete source damage. [1][2]. In other words, it is the ability of the structure to sustain damage in the form of cracks without catastrophic consequences until such time as the damaged component can be repaired or until the economic service life has expired and the airplane or component is retired. [3][5] [4].

Damage Tolerance Analysis for antenna plates is the application of Fracture Mechanics to assess how a fuselage skin, antenna plate, and antenna cut-out failed. Damage tolerance analysis begins with the same static strength calculations as a non-damage tolerant structure. This includes analyses of ultimate, limit, and fail-safe design conditions. [3[4][5].

Residual strength: The strength capability of a structure after the structure has been damaged due to fatigue, corrosion, or discrete source damage depends on The residual strength capability includes consideration of static strength, fracture, and stiffness. It can then be used to determine the critical crack length, which corresponds to the lowest residual strength capability that satisfies the regulatory fail-safe requirements [2-3].

1.1.2 Crack Growth (Damage)

Different locations of the antenna mounting plate and fuselage skin need to be evaluated to determine the damage tolerance characteristics. A longitudinal crack at the antenna cut-out hole is considered. Consistent with this, some candidate cracking scenarios are discussed in detail. Crack growth is used to determine the rate at which the cracks grow from a detectable length to the critical length. A crack growth curve is then generated and used to determine the inspection type and the number of inspection opportunities available to detect a given crack with a given inspection method [6].

1.1.3 Inspections Program (Damage Detection)

The result of damage tolerance evaluation can be used to establish inspection requirements that will mitigate a failure due to fatigue. Given the damage tolerance characteristics of the antenna plate and aircraft fuselage skin and the detectable crack size, one is ready to determine when the inspection should start (i.e., threshold) and how often it should be performed (i.e. interval). The inspection intervals are based on the crack growth curve. They are chosen to give a high probability of detecting the fatigue crack before it grows to the critical length. Typically, at least two opportunities to find a crack before it reaches critical length are desired [6].

1.2 Statement of the Problem

During production by original equipment the manufacturer or during in-service life of the aircraft by the operators antennas are installed on the fuselage of the aircraft for the purpose of enhancing communication, navigation, or surveillance systems of the aircraft. The installation has a direct effect on structural integrity of the aircraft fuselage. After installation, the antenna systems have been encountering different failures, which lead minimum of operational delays and flight cancellations, and maximum of a direct effect on manoeuvrability and aircraft safety. Flight delays and cancellations may have an impact on the revenue flight of the given aircraft, which may have a gradual impact on dispatch

reliability and fleet on-time performance, as well as the operators' business plan and strategy. From a safety point of view, potentially developed cracks in the fuselage crown skin and mounting plate could lead to loss of structural integrity of the airplane and decompression of the aircraft.

During flight, an undictated skin crack can propagate around the antenna and result in separation of the antenna from the airplane and an inability to maintain cabin pressure within the fuselage of an aircraft.

Cracks in the fuselage skin that are not found and repaired can propagate to the point where the fuselage skin structure cannot sustain the limit load. When the fuselage skin cannot sustain the limit load, this can result in possible rapid decompression and loss of structural integrity. Cracking in the skin or surrounding structure could remain undetected. Continued operation with undetected cracks could result in crack growth, possibly leading to separation of the antenna from the airplane and rapid depressurization.

The typical antenna faced corrosion, pitting, and delamination between skin, mounting plate, and seal following water and moisture intrusion into the interface. The water intrusion has resulted in antenna corrosion and pitting that renders the antenna inoperable. Consequently, a crack in the fuselage structure started to be initiated.

To address in-service issues related to various antenna installations, aircraft manufacturers issued a variety of modification bulletins or maintenance documents. Most of the time, the
documents address crack initiation, propagation, inspection, and corrective modification or repair of existing defects. In this thesis, the effect of mounting plate shape, antenna cut-out shape, and damage tolerance analysis was studied. Following that, optimizing maintenance inspection type and inspection intervals are addressed. By doing so, they address a possibility and have the potential to improve the aircraft's safety and reliability.

1.3 Objective

1.3.1 General objective

The general objective of this thesis is to study the impact of mounting plates and antenna cut-outs on the structural integrity of the fuselage of pressurized transport airplanes and, using different concepts of fracture mechanics, perform damage tolerance analysis on the installed antenna.

1.3.2 Specific objectives

In this research, there are three specific objectives studied and listed as follows in chronological order:

I. From the static strength point of view, the elliptical antenna mounting plate compared with those of circular and rectangular mounting plates.

II. From the stress concentration factor point of view, antenna cut-out shapes such as elliptical, circular, and square were compared with each other and the best cut-out was selected.

III. Based on the above two specific results, i.e., the best mounting plate and the best antenna cut out, Damage tolerance analysis at the antenna cut-out was performed, and then an estimated inspection type and inspection threshold (damage detection) were performed.

1.4 Scope and Limitation

1.4.1 Load Types

Antenna installations are typically located on the fuselage skin, bounded by frames and longerons, away from discontinuities like doors and windows. Load environments contributing to the crack growth of a modified skin include the following:
For most of the fuselage, the stress state is mainly biaxial loading (circumferential and longitudinal) due to pressure plus vertical inertia fuselage bending (longitudinal) only. Other types of loading could be reasonably ignored.

1.4.2 Other Possibilities of Crack Initiation

There are other possibilities of crack initiation at different locations in the antenna plate and associated fuselage skin due to discrete sources of damage. It may be due to a bird strike or hit. Damage caused by a foreign object, such as a lightning strike, is not considered in this thesis.

1.4.3 Thermal Stress and Strain Effect

Aircraft external temperatures fluctuate between -65 and +180 degrees Fahrenheit. Temperature-related stress and strain (thermal stress and strain) are ignored entirely in this thesis.

1.4.4 Crack initiation and propagation (DTA-interest area)

FEA is used to validate stress levels, locations of high stress concentrations and possible impact of stress-field of nearby antenna locations. Based on the observation DTA performed at the antenna cut-out at the critical location with the highest Von Mises stress and highest stress concentration.
Riveting effects joining the mounting plate and the skin are ignored since the stress applied to the mounting plate and rivets is relatively lower than at the critical location i.e. antenna cut out (Refer to figure 4.12 to 4.35 as depicted at page number 77 to 89).

DTA Perform on the skin and only Mode-I (stress orthogonal to the local plane of the crack surface) considered. Mode-II (stress parallel to the crack surface but orthogonal to the crack front) and Mode-III (stress parallel to the crack surface and to the crack front) are not considered.

1.5 Organization of the Thesis

This thesis is structured into five chapters. In the first chapter, the background information and the statements of the research problems are discussed and elaborated. The unresolved issue of aircraft antenna-related anomalies and failures and its main and specific objectives are elaborated on in this chapter. In chapter two, a review of literature related to this study with up-to-date relevant information is mentioned. In Chapter three, materials, methods for the thesis are related to each of the specific objectives, along with the theoretical concept illustrated and also the boundary condition is identified here according to cabin pressure applied to the aircraft fuselage. In Chapter four, results and discussion for each of the specific objectives developed. In chapter Five, the conclusion of the thesis work, Validity and Applicability and future work are proposed

Chapter Two

2.1 Literature Review

This section is focused implicitly on overview materials, manufacturing processes, methods, loading and boundary conditions, and failure modes, explicitly on failures associated with aircraft and the aerospace industry, stress concentration and fatigue.

At present, commercial aircraft are composed of many antennas located on the fuselage structure and used for communication, navigation, and radar activity [7].

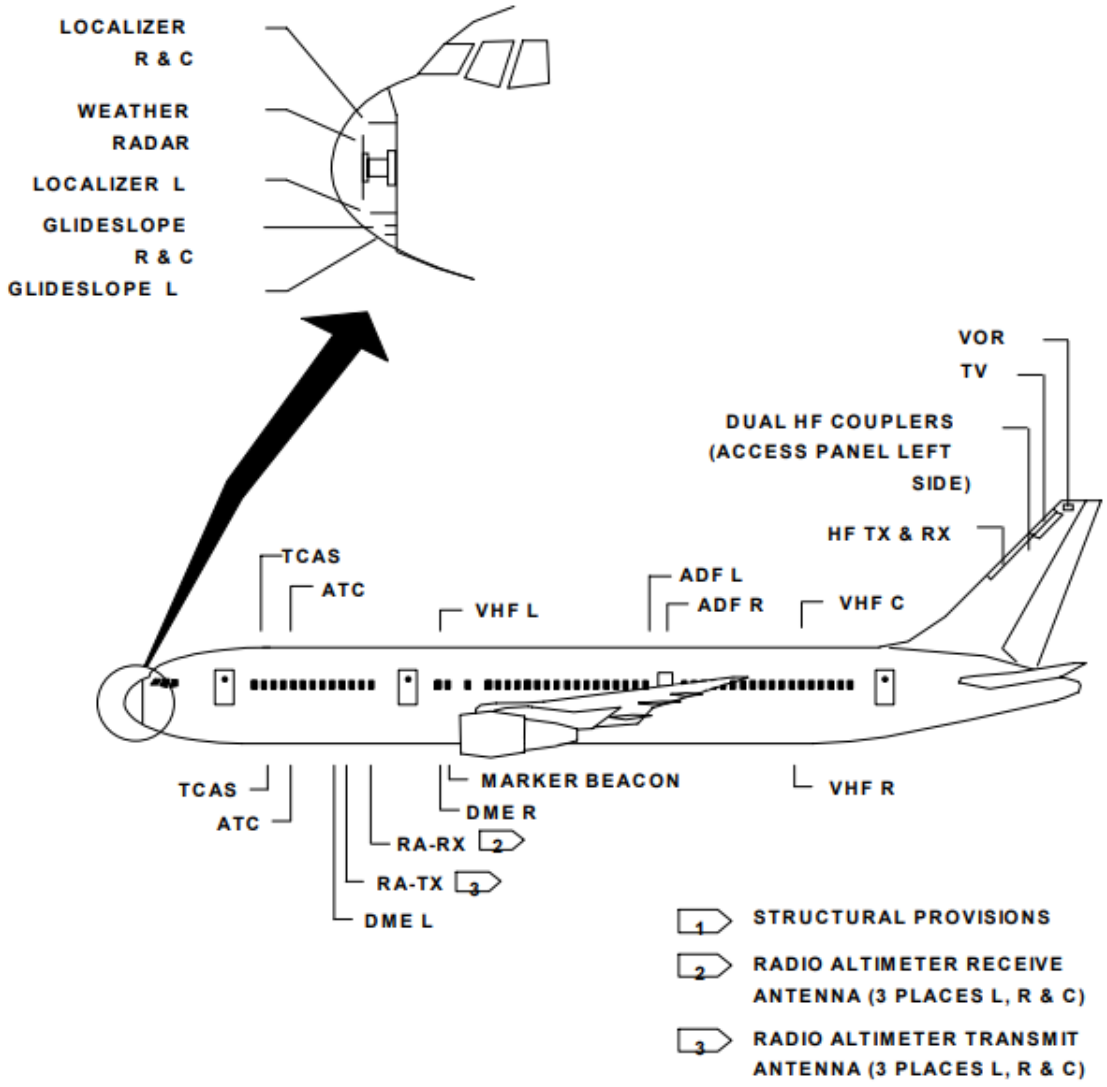

Figure 2.1: Different Antenna Locations on commercial aircraft [7]

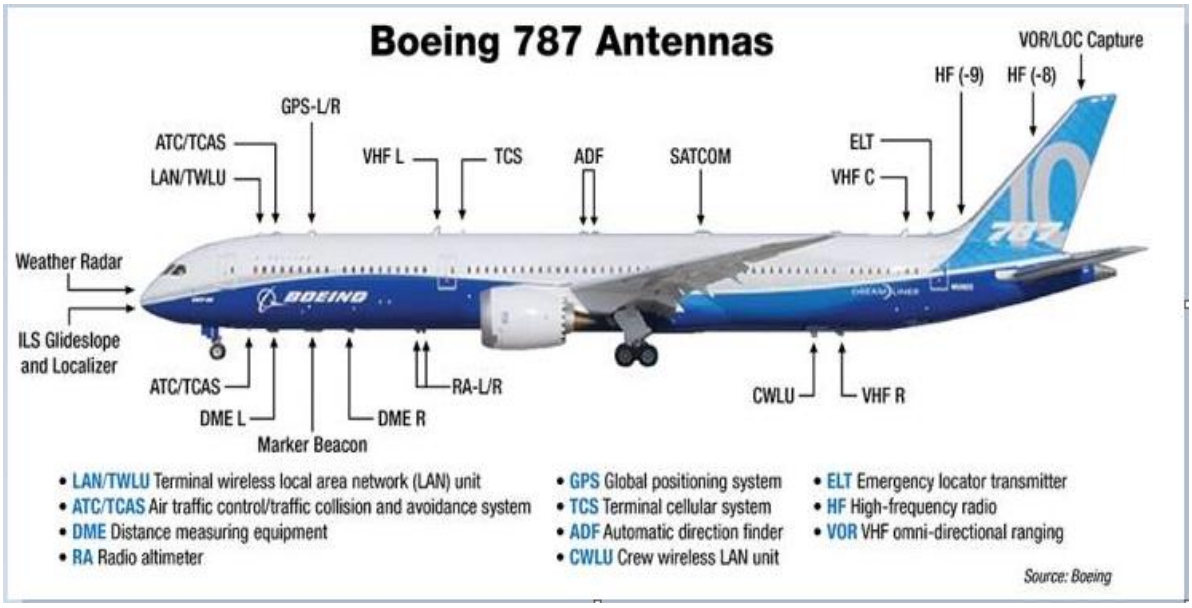

Figure 2.2: Different Antenna Locations on modern commercial aircraft [8]

Different design and manufacturing organizations, research centres, and regulatory bodies perform antenna installation and have damage tolerance evaluations studied on antenna modifications (e.g., alterations, repairs, and STC's). [8][9].

The above figures depict the significance of antennas, antenna type, and location on civil aircraft.

2.2 Modification

It means a design change that generally results in a change to the configuration of a product, component, or appliance.

2.3 Repair

Means a design change that is intended to return the product, component, or appliance to its original or properly modified configuration. FAA AC 43.13-1B and 43.13-2B

2.4 Alterations

It means an alteration not listed in the aircraft, aircraft engine, or propeller specifications FAR Part 43.5. That might appreciably affect weight, balance, structural strength, performance, power plant operation, flight characteristics, or other qualities affecting airworthiness; or That is not done according to accepted practices or cannot be done by elementary operations.

2.5 Supplemental Type Certificates (STC)

A Supplemental Type Certificate (STC) is an FAA or EASA approved major modification or repair to an existing type certified aircraft, engine or propeller. As it adds to the existing type certificate, it is deemed 'supplemental'. As its name suggests, an STC is a certificate. It defines the product design change, states how the modification affects the existing type design, and lists serial number effectively.

FAR Part 21 sections 21.111 through 21.119. Section 21.113, Requirement of supplemental type certificate, AC 21-40A, Application Guide for Obtaining a Supplemental Type Certificate

Before antenna modification, the complete analysis, such as static strength analysis and damage tolerance analysis, must be validated. The modification must be able to meet both the limit load and ultimate load criteria. Often, loads are not available, and the modification must be designed to the structure's original capability. If a formal damage tolerance or fatigue assessment needs to be conducted, the operating load environment is required. [8-10].

2.6 Static Strength Analysis

Typical antenna installations on the fuselage of civil airplanes generally involve cutting a hole in the fuselage skin for the antenna connector. A mounting plate (doublers) is then mechanically fastened to the skin around the skin cut-out. To assess the static strength of the modified skin, three independent criteria are used to evaluate the margins of safety of the mounting plate and fasteners:

- The mounting plate allowable.
- The joint allowable. and
- The shear allowable.

2.7 Damage tolerance analysis

To perform the damage tolerance analysis of a modified skin for antenna installations, critical locations in the skin must first be determined. Assumptions of initial flaws at fracture critical locations and the continuing damage need to be made. The stress spectrum must also be prescribed. In addition, the following data are needed [2] [9] [10]:

- Crack growth rate data of the skin material
- Fracture toughness of the skin material
- Stress intensity factors of relevant crack configurations

B777 has faced corrosion at Satcom Antenna due to a braided wire bonding jumper having insufficient clearance from the skin. The jumper wore into the skin; the fretting and the presence of corrosion are factors that can lead to the fuselage skin cracking. [11]

Modifying an aircraft must be done in a safe way so that the safe operation of the aircraft is not compromised. Compliance must be shown towards endorsement and airworthiness regulations so as to install a modification and allow for revenue flight. Certification from a regulatory body is an overwhelming process where damage tolerance analysis (DTA) is a mandatory part. Most analysis-based methodologies, such as stress analysis, finite element methods, and crack growth analysis, were developed by utilizing proven methods and recommended theories with adequate conventionality. The resulting methodology provides the tools to estimate crack growth and the corresponding critical crack

length that would cause a structural failure. This also enables the establishment of inspection intervals, which are required for continued airworthiness. [12]

A simplified approach to damage tolerance analysis (DTA) of riveted fuselage skin repairs has been incorporated. Static strength and damage tolerance analysis methods for skin modifications to antenna installations on the fuselage of commuter airplanes were performed. First, three types of antenna installations are presented, defined in terms of the mounting plate geometry. For rectangular and circular mounting plates, the static strength and damage tolerance analysis has been addressed, but for elliptical mounting plates, the analysis has not been performed, but rather the elliptical mounting plate installations to be considered in the future work. [12] [13]

2.8 Major fatigue related events in aviation industry

DE Havilland comet, 1954. The first pressurized jet passenger aircraft started service in 1951. In 1954, four days after one of the aircraft was inspected, it crashed into the Mediterranean Sea, and an identical airframe was subjected to repeated re-pressurization and over-pressurization. After 3,057 flight cycles, the pressure hull failed due to metal fatigue. Stress around the window corners were found to be higher than expected or previously tested. This situation was made worse by the use of punch rivets in those areas, which produced residual stress and possible micro-cracks. All comets of the initial design were removed from service, and a redesigned configuration was developed. [13-15]

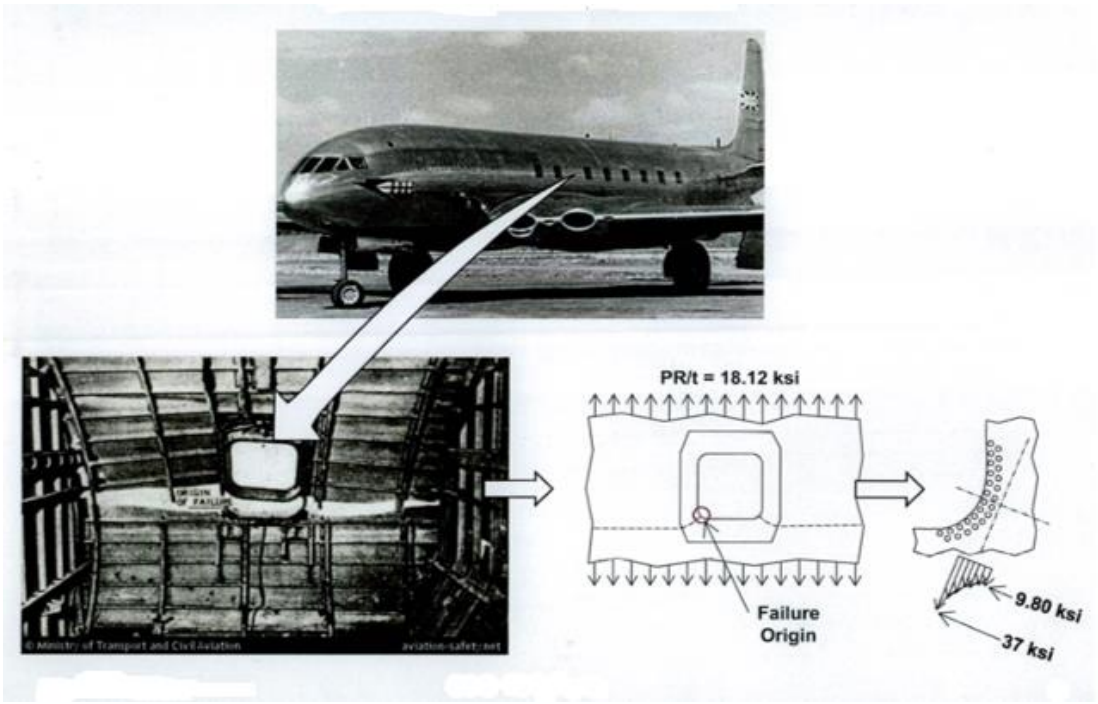

Figure 2.3: The pressurized fuselage failed due to metal fatigue and stress around the window corners, which produced residual stress and possible micro-cracks. [16]

General Dynamics F-111, 1960's: This was the first aircraft designed for "safe life", basically designed for a finite life after which parts must be replaced. The major structural components of the F-111 were made from relatively new high-strength steel, D6AC.ground test articles and flight aircraft experienced premature failures. Failures occurred at stress levels below the rated strength of the material. Testing of D6AC material found the strength of the material to be consistent but the toughness (ability to absorb energy without failure) to be highly variable. The steel used was not initially tested for toughness. After further testing, the fatigue life of the F-111 was found to be on the order of a few hundred hours. Surface protection was also found to be a factor in premature failures as the loss of corrosion protection led to surface defects that provided a site of opportunity for crack initiation. Critical crack lengths were very small. [15-18]

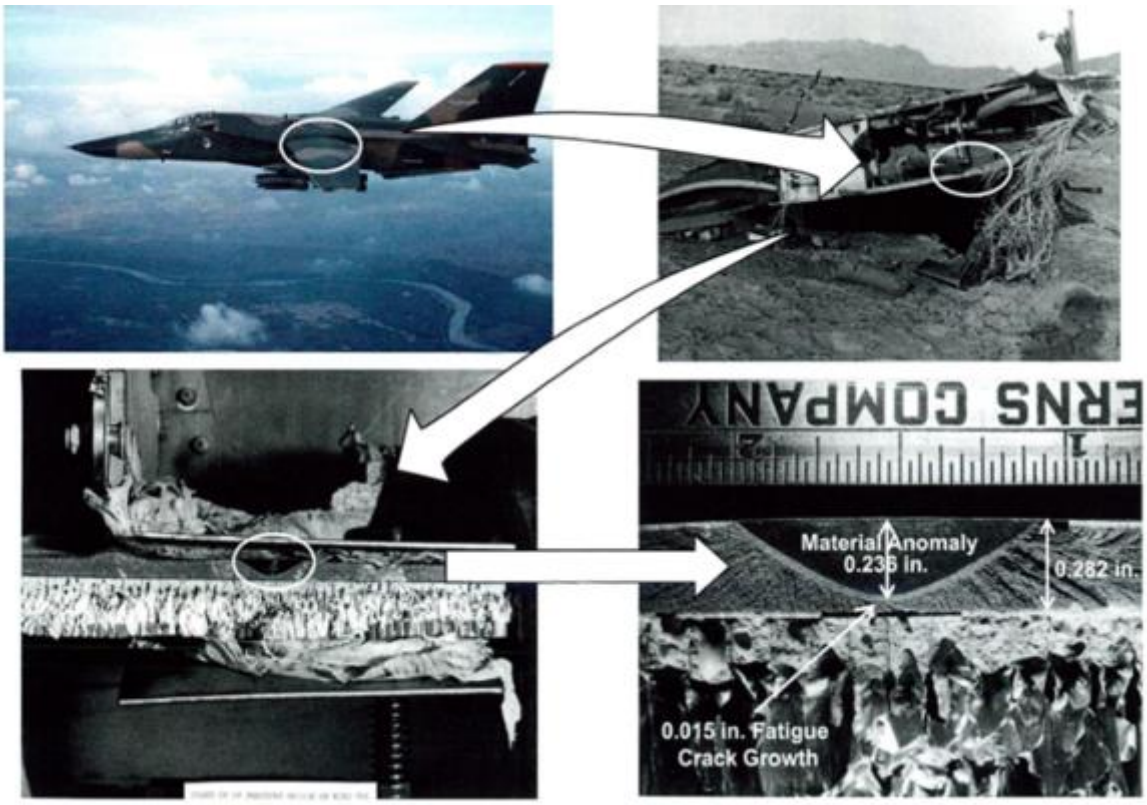

Figure 2.4: Failure occurs at a stress level below the rated strength of the material and material toughness is different from expected. [16]

In 1974, The USAF issued MIL A-8344, which defined damage tolerance (DT) as the basis for new design aircraft.

Dan-Air Service, Boeing 707, and 1977.The aircraft lost pitch control following the loss of the right horizontal stabilizer and elevator as a result of fatigue failure in the upper rear spar chord. The crack originated at a fastener hole in the upper chord. Of the rear spar. The aircraft had been designed based on fail-safe loading of multiple load paths. The fail-safe design had not prevented the structural

failure due to an inadequate inspection program. As a result of this accident, the FAA amended FAR 25.571 requiring damage tolerance designed and associated inspections [15, 18-22].

Figure 2.5: structural failure of the horizontal stabilizer rear spar, fatigue cracking began at a fastener hole in the upper chord [16]

In 1978, the FAA issued a ruling requiring all aircraft certified after that date to be designed for durability and damage tolerance (FAR part 25, Amendment 45, DADT).

Aloha Flight 243, Boeing 737-200, 1988.The aircraft was 19 years old with an incredible 89090 cycles (the 737 was initially designed for 75,000 cycles). The national transportation safety board

(NTSB) concluded the accident was caused by metal fatigue associated with corrosion. Areas where fatigue cracking was found were associated with two-layer bounded skin. The bound lines were found to have failed, permitting moisture to enter the gap between the two layers. Corrosion developed,

spreading the two layers apart, producing residual stress in the skin. The age of the aircraft and the high number of cycles had produced cracks at the sites created by the spread of corrosion. The salt air environment was also a factor [16] [23] [24]

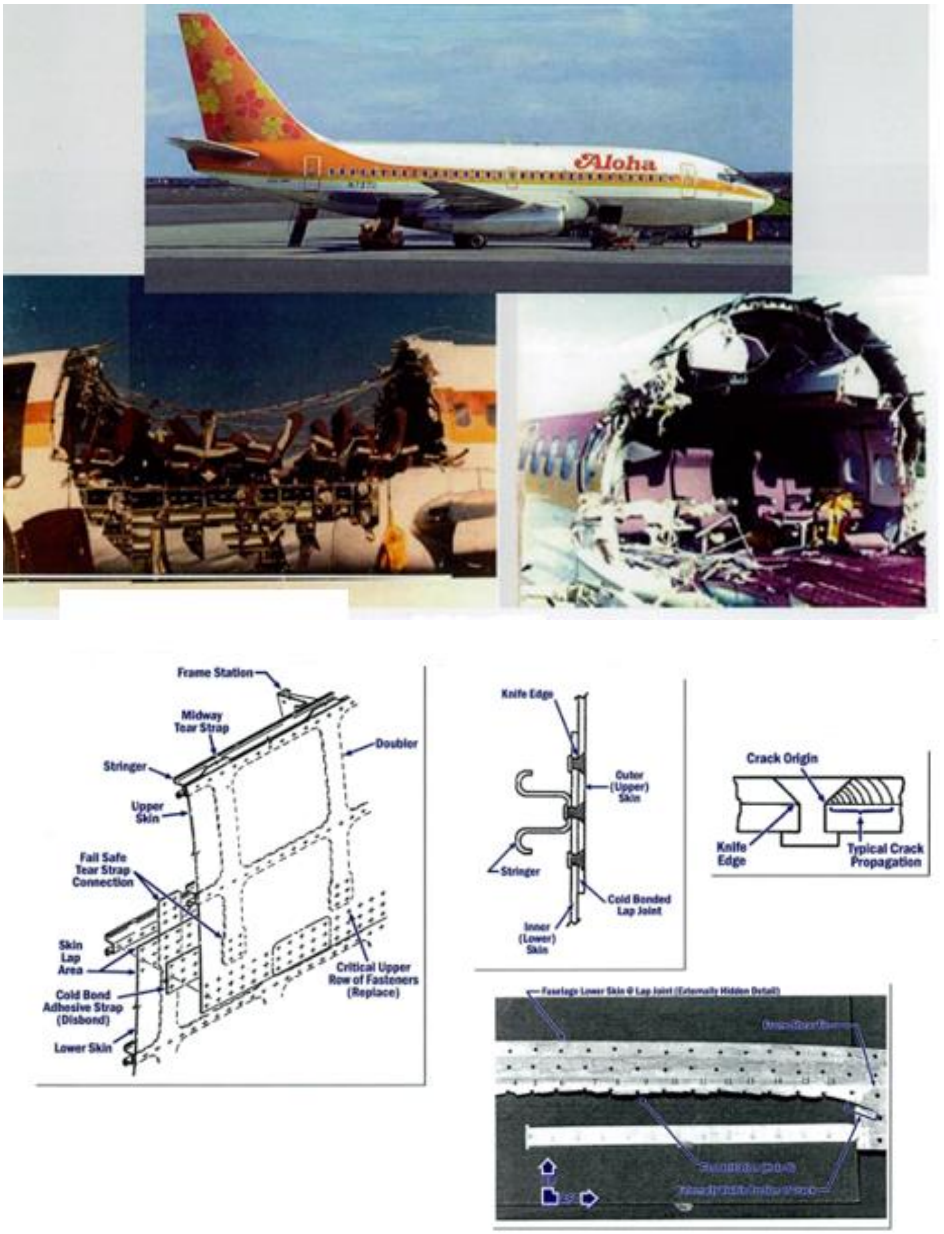

Figure 2.6: Fuselage remains after the emergency landing and area where the fatigue cracking initiated from the knife edge associated with the countersunk lap joint rivet holes [16]

The Airworthiness Assurance Working Group (AAWG), the Hawaii accident drew attention to fatigue problems with the airframe structure, as well as maintenance, inspection and repair issues. The AAWG designated 11 airplane models as “aging airplanes” and chartered model-specific Structure Task Group (STG) to address five (5) issues that contributed to the 1988 accident and Widespread Fatigue Damage (WFD).

The aging airplane safety act of 1991(AASA). The U, S. Congress required the FAA to declare a rule to assure the continued airworthiness of aging aircraft. In response to the AASA, over the next fourteen

years, the FAA issued two Notices of Proposed Rulemaking (NPRMs) and an interim final rule, which was finalized in 2005. The final aging airplane safety rule (AASR) affects airplane certified after January 1, 1958 with:

- Seating capacity of 30 or greater or
- Maximum payload of 7500lbs or more.

The AASR required a damage tolerance (DT) based maintenance program whether the airplane was certified as damage tolerant or not. The operators must revise their maintenance program and show their implementation plans to comply with the AASR requirements. They should not pass December 20, 2010 without an FAA –approved program.

"Mechanical failure" is defined as a material's lack of load carrying capability. Mechanical failure mechanisms include fracture, thermal stress, wear, yielding, and corrosion. Fracture failure of the material is due to defects in the form of porosities, cracks, or voids in the material. Cracks are observed in many structures for several reasons. Cracks might appear during the production process or subsequently as a result of environmental or loading conditions. When a component or a structural part has fractures, its structural integrity is greatly compromised. The relation between stresses, cracks, and fracture strength is studied using fracture mechanics.

To summarize, In the in-service life of any aircraft, different antennas may be installed or relocated from their existing locations for different operational or regulatory requirements. Structural modification for antenna installation is a mandatory activity for installing antennas on the fuselage of aircraft. Existing aircraft skin, mounting plate, and fasteners, i.e., rivets, are parts involved in the modification task. The modification involves a mounting plate that is mechanically fastened to the skin around the cut-out by rivets. Antenna cut-outs on the skin and mounting plate induce stress concentration. At the same time, mounting plate shape and joint mechanism affect structural integrity in the vicinity of installation;
Consequently, it affects load sharing and distribution capability of the structural members in the vicinity of the antenna. In service life of the aircraft Static strength and fatigue load caring capacity affected.
Static strength and fatigue load affect the durability of the installed antenna systems. Using damage tolerance basic principles and analysis, to alleviate failure related to these affected loads and stress concentrations, an inspection threshold (damage detection) should be established. By doing so, it is possible to reduce the catastrophic decompression failure of the aircraft. Finally, at the end, the safe and successful operation of the aircraft could be achieved.

Chapter Three

3.1 Material and Methods

3.1.1 Material

Aerospace material applications are heavy on process specifications approved by the FAA and strength values developed based on extensive FAA-approved testing as well as actual fleet flight experience. One of the most commonly used documents in this regard is MMPDS (Metallic Materials Properties Development and Standardization) [27] [28]

Humans without wings flying at 30,000 to 40,000 feet above sea level while sitting in a seat inside a pressurized barrel is unnatural and also not a joke. At the same time, it is a serious business and extremely risky. And without quality materials to help us do that, it is simply impossible. Part 25-603 of the 14 CFR—Materials

The Boeing Structural Repair Manual (SRM) Chapter 51-30-01-0G-0 specifies that the material used on the aircraft's fuselage is 2024-T3. Mechanical properties for 2024-T3 were obtained from the Handbook of Metallic Materials Properties Development and Standardization (MMPDS). MMPDS at Table 3.2.4.0(e1). Provide design Mechanical and Physical Properties of Clad 2024 Aluminium Alloy Sheet and Plate. In this thesis, the properties for 2024-T3 alloys are shown in table 3.1 for easy reference since these data are used later in many of the calculations found in the next chapters.

Table 3.1: Mechanical and Physical Properties of 2024-T3 Clad Sheet and Plate [27] [28]

Temper		-T3		
Cross Section (in^2)		ALL		1. A 10% Reduction in bearing strength has been applied to represent wet pin values 2. The addition of e/D ratio:1.7 by linear interpolation
Thickness(in) **Thickness(mm)**		.063-.128 1.60 -3.2512		
BASIS		A	B	
Mechanical Properties				
F_{tu}, [ksi/MPa]	L	62/427.475	63/434.37	
	LT	61/420.58	62/427.475	
F_{ty}, [ksi/MPa]	L	45/310.264	47/324.054	
	LT	40/275.79	42/289.58	
F_{cy}, [ksi/MPa]	L	37/255.106	39/268.896	
	LT	43/296.475	45/310.264	
F_{su}[ksi/MPa]		38/262.001	39/268.896	
F_{bru}[ksi/MPa]				
	e/D=1.5	91/627.423	92/634.318	
	e/D = 1.7	99/682.581	101/696.37	
	e/D = 2.0	112/772.213	114/786.002	
F_{bry} [ksi/MPa]				
	e/D = 1.5	63/434.37	65/448.159	
	e/D = 1.7	68/468.843	71/489.528	
	e/D = 2.0	75/517.107	79/544.686	
G [Psi/ MPa]		**3,800,000/26200.07771**		
E [Psi/ MPa]		10,500,000/72394.951576		
E_c10^6 [Psi/ MPa]		10,700,000/73773.903035		
μ(elastic region)		0.33		

Table 3.2: Material properties used for the analysis [27] [28]

Material		Young's modulus	Poisson's ratio
Rivets	2024-T3	72.4 GPa	0.33
Plates	2024-T-3	72.4GPa	0.33

Table 3.3: Table 2.1 Fracture Toughness of 2024-t3 plates in different direction [29] [30]

Mechanical Properties	Metric	English	Comments
Fracture Toughness	26 MPa-$m^{½}$	23.7 ksi-$in^{½}$	$K_{(IC)}$ in S-L Direction
Fracture Toughness	32 MPa-$m^{½}$	29.1 ksi-$in^{½}$	$K_{(IC)}$ in T-L Direction
Fracture Toughness	37 MPa-$m^{½}$	33.7 ksi-$in^{½}$	$K_{(IC)}$ in L-T Direction

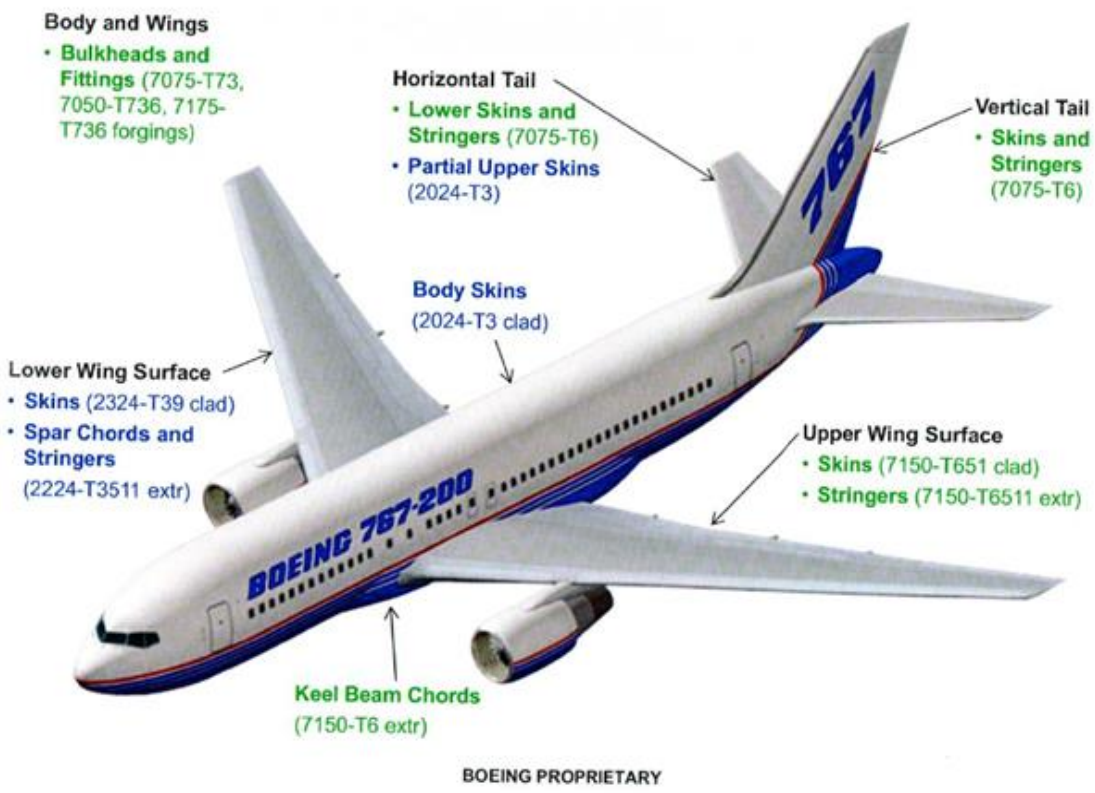

Figure 3.1: Aluminium alloy applications B737-500, B747-300/400, B757, B767 models aircraft [31]

3.1.2 Methods

In this thesis, the static strength analysis method for skin modifications to antenna installation is first described using analytical and FEA/FEM. Next, the elliptical antenna mounting plate is compared with the circular and rectangular mounting plates. Then, next, for the given cut-out (i.e., circular cut-out, square cut-out, and elliptical cut-out with orientation lateral and horizontal axis) for each of the mounting plates, which means elliptical, circular, and rectangular antenna mounting plate stress concentration factors compared with each other, the best antenna mounting plate and less stress-concentration cut-out shape are selected. Finally, this document studies damage tolerance analysis for the best selected antenna installation plate and establishes the methods to develop an inspection type and inspection interval.

3.1.3 Flow chart for each of the specific objectives

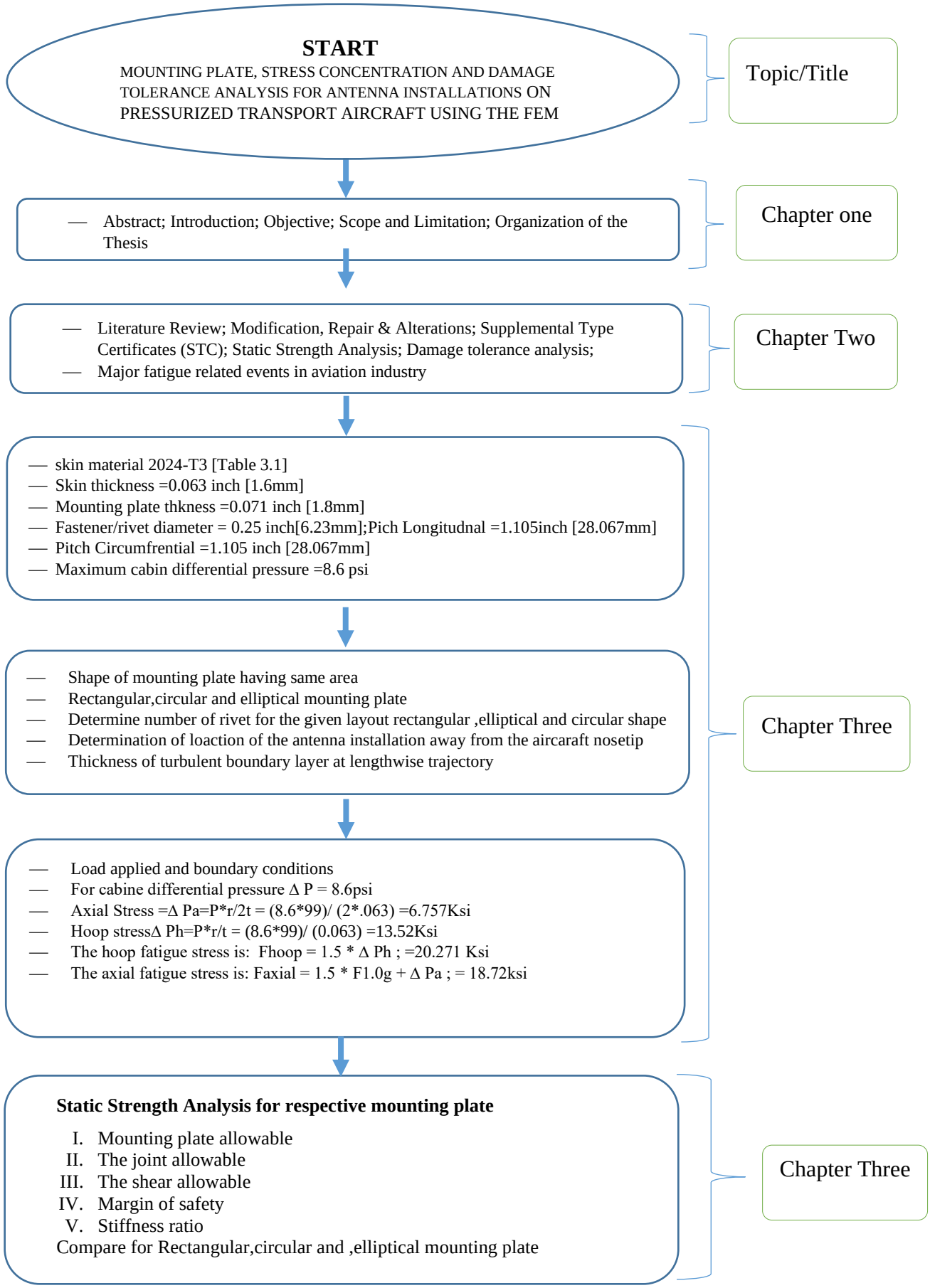

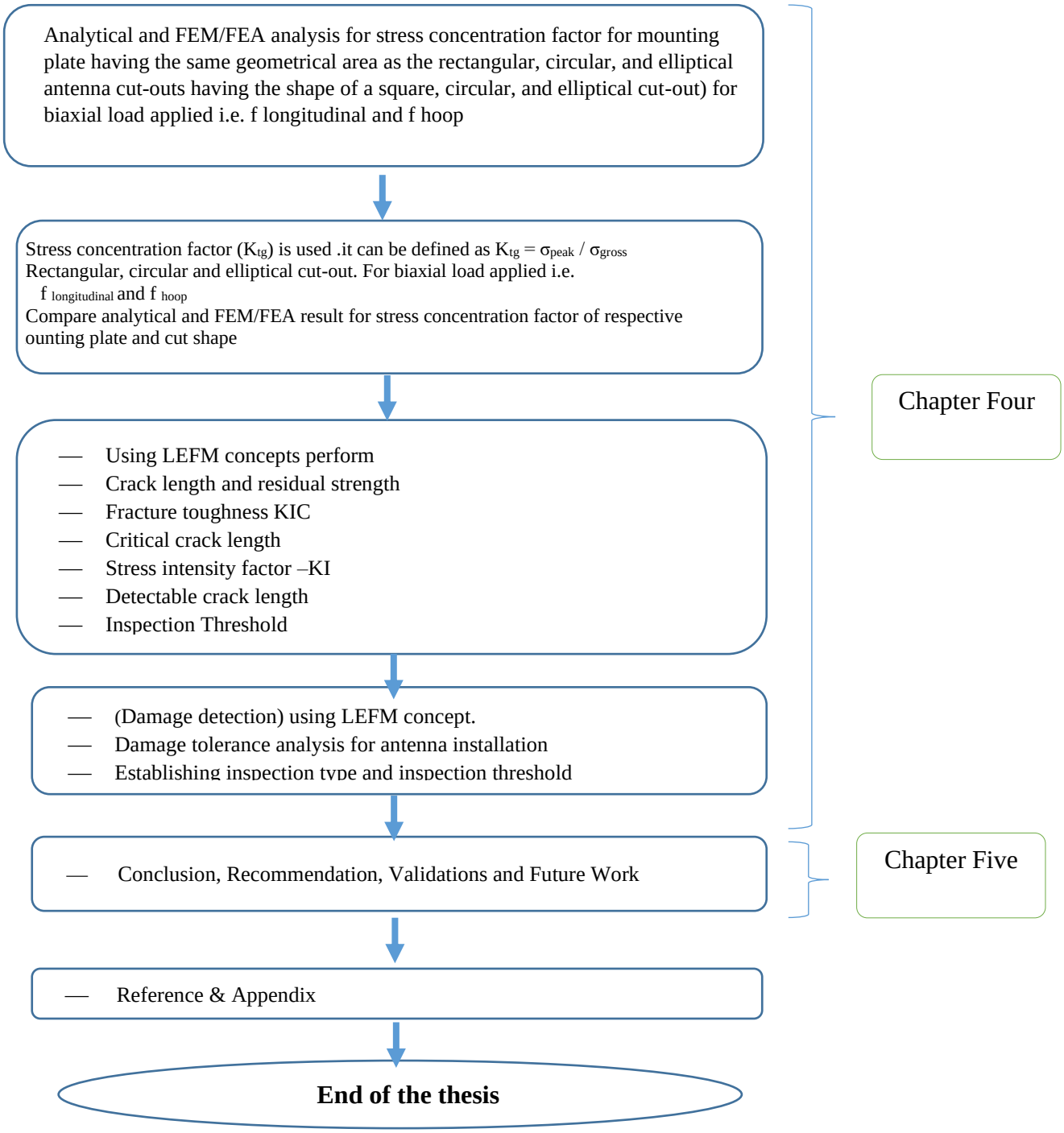

Figure 3.2 Flow chart of the thesis structure.

3.2 Mechanics and Basics Principles

3.2.1 Gross area stress

Using the methods described below, external load (i.e., cabin pressurization load) is converted to internal load (i.e., axial skin tension stress).

Commercial airplanes are pressurized to maintain the comfort level of passengers during flight. The fuselage skin behaves like a thin-walled pressure vessel, such as a balloon. The difference in pressure inside and outside the passenger cabin (Δ P) produces axial and radial tension loads.

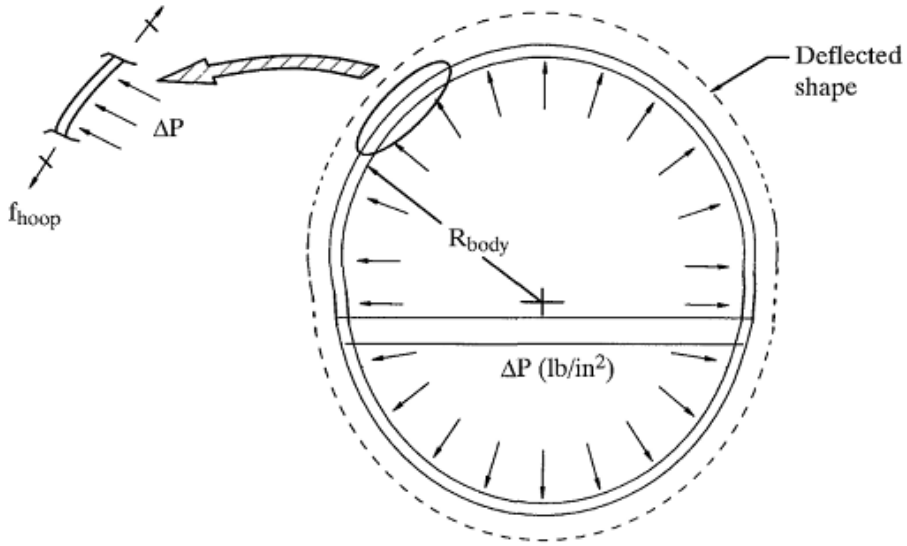

Figure 3.3: Effect of △P on fuselage skin

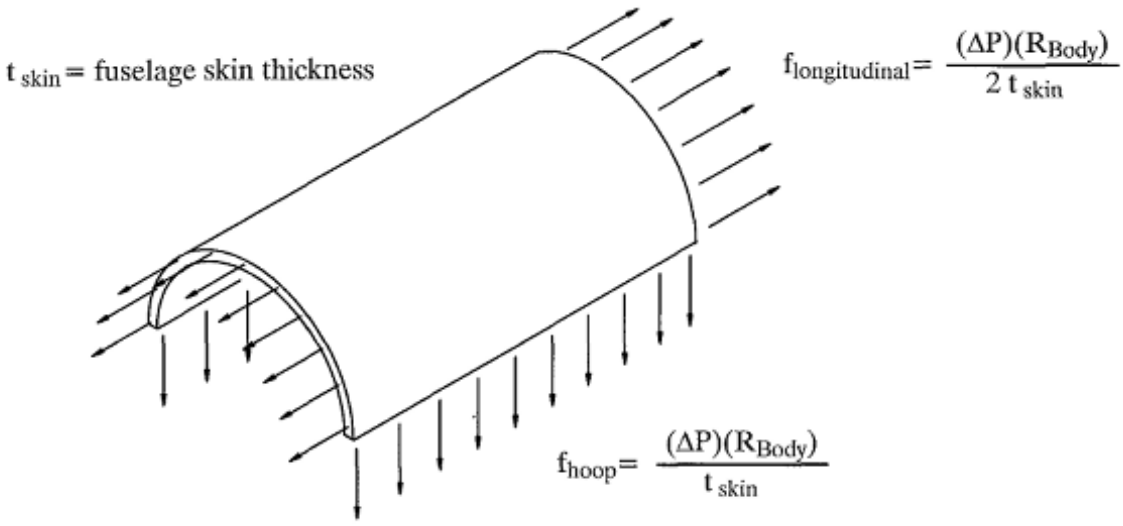

Figure 3.4: Stress resulting from applied cabin pressure

3.2.2 Hoop stress

The stress in the hoop direction is assumed to be due to pressure only and is given by ,

$$f_{Hoop} = \frac{\Delta P * R}{t} \quad (3.1)$$

Where,

ΔP = cabin differential pressure, psi

t=Fuselage skin thickness, in

R= Fuselage cabin radius, in

3.2.3 Longitudinal stress

The stress in the longitudinal direction is assumed to be due to pressure and vertical fuselage bending due to inertia (i.e. vertical acceleration) and is given by

$$f_{longitudinal} = \frac{\Delta PR}{2t} + n_z \sigma_{1G} \quad (3.2)$$

Where,

ΔP = cabin differential pressure, psi

t=Fuselage skin thickness, in

R= Fuselage cabin radius, in

n_z = Vertical load factor

σ_{1G} = 1G stress at antenna location

FAA/SWIFT Method to determine fuselage skin stress

- conservative method to obtain fuselage skin stresses
- fuselage skin stress is a function of inertia loads and cabin pressure loads
- FAA has recommended the following values be used for a typical fatigue stress
- Longitudinal: $F_{axial} = 1.5 * F_{1.0g} + \Delta P_a$
- circumferential (hoop): $F_{hoop} = 1.5 * \Delta Ph$

$F_{1.0g}$=1.0 g inertia stress at 70% payload

ΔP_a = axial stress due to pressure (cabin differential pressure)

ΔP_h = hoop stress due to pressure (cabin differential pressure)

P= Maximum cabin differential pressure = 8.6 psi

r=Skin radius = 99.0”

t=Skin thickness (gauge) = 0.063”

The hoop maximum stress is simply

$F_{hoop} = 1.5 * \Delta P_h$

$= 1.5 * 13.52$

=20.271 Ksi

F_{axial} = 18.72ksi

3.3 Boundary layer criteria (cruise flight small α and β):

For smooth upstream boundaries, the boundary layer starts out as a laminar boundary layer in which the fluid particles move in smooth layers. As the laminar boundary layer increases in thickness, it becomes unstable and finally transforms into a turbulent boundary layer in which fluid particles move in haphazard paths. When the boundary layer has become turbulent, there is still a very thin layer next to the boundary layer that has laminar motion. It is called the laminar sublayer.[32][33]

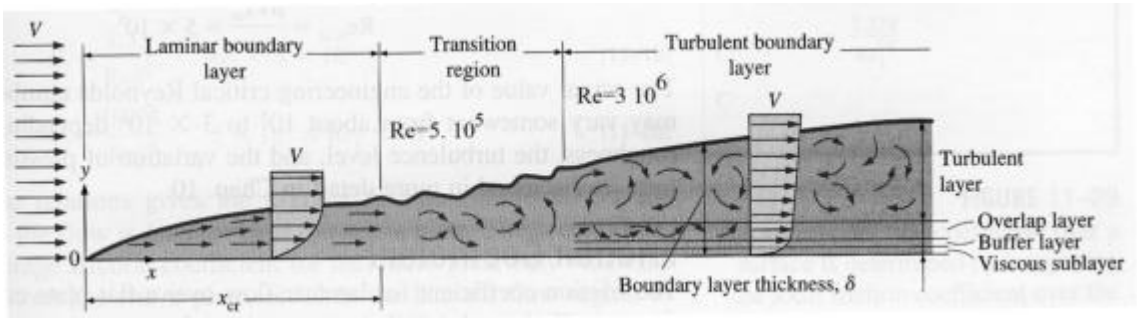

Figure 3.5: The development of the boundary layer for flow over a flat plate, and the different flow regimes.

3.4 Fuselage Station Diagrams

The fuselage station diagram gives a reference system to find components, features, and major fuselage structural openings in relation to a datum plane. The datum plane model (i.e., B767-300) is perpendicular to the fuselage centreline and is located 92.50 inches forward of the airplane's nose.

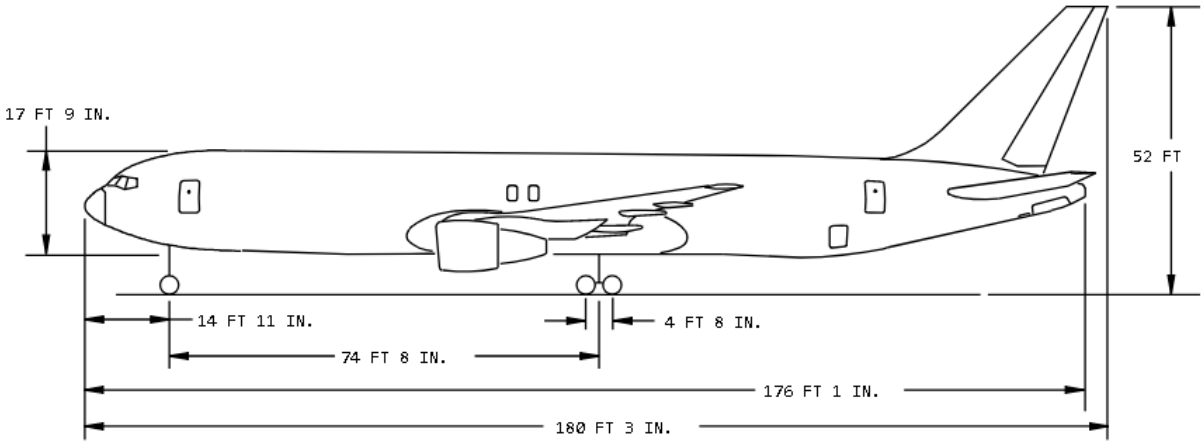

Figure 3.6: General - Principal Dimensions [34]

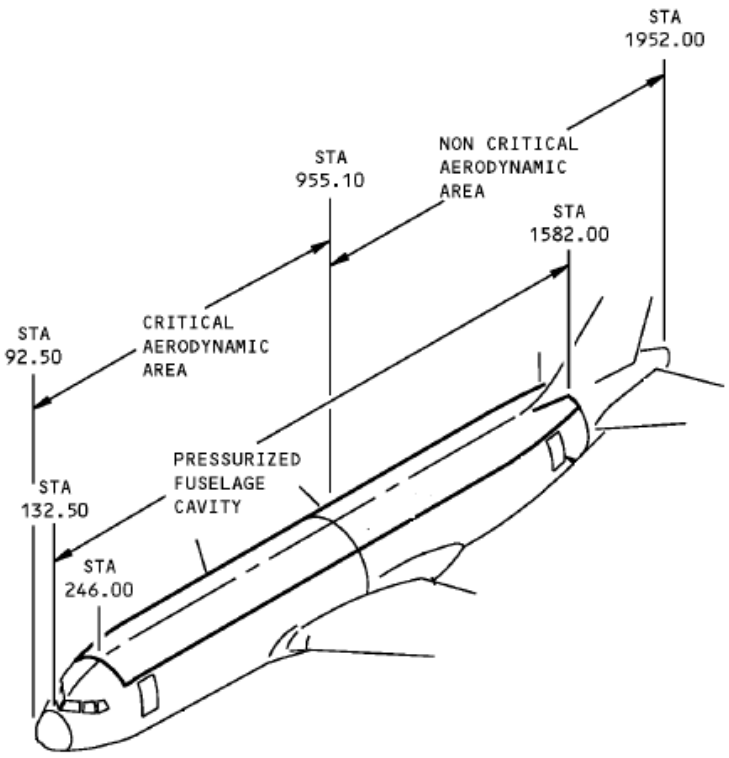

Figure 3.7: Fuselage Skin critical aerodynamic area, non-critical aerodynamic area and pressurized fuselage cavity as a function of fuselage station (STA) number [35].

From the above figure ,Critical aerodynamic length becomes the difference of = 955.10 inch -92.50 inch =862.6 inch (22meater) And non critical aerodynamic length becomes length greater than 22 meter from the nose tip of the aircraft .

identification	section
41	SECTION 41
43	SECTION 43
45	SECTION 45
46	SECTION 46
48	SECTION 48

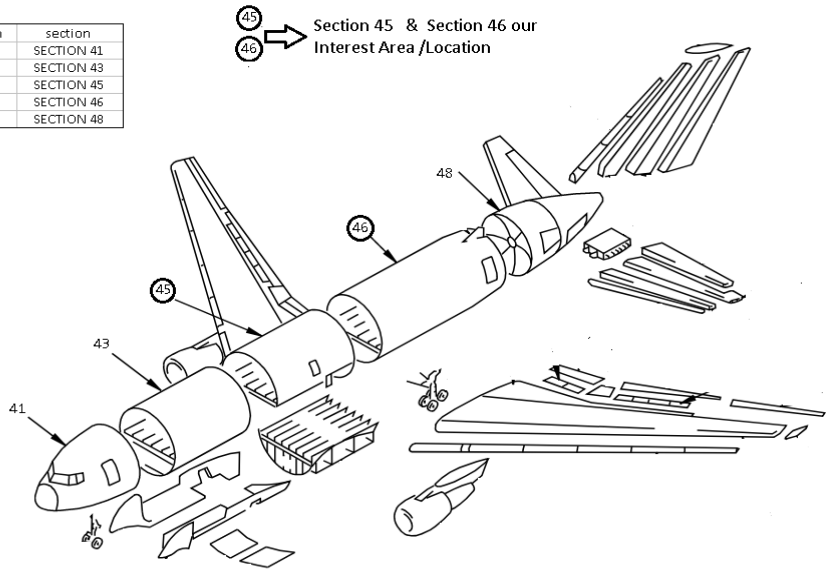

Figure 3.8 Major Assembly and Installation Breakdown: section 45 and section 46 location [36]

The development of the boundary layer, Fuselage Station Diagrams, aircraft General-Principal Dimensions, and major assembly and installation breakdown will be used in fixing the optimal location of the antenna to be installed.

3.5 Determination of the location of antenna installation away from the aircraft nose tip

The following Assumptions have been made in order to determine the location of the antenna installation away from the aircraft nose tip.

1) From the aircraft's detailed specification document, the A/C is flying at an altitude of 10 to 13 km with a speed of Mach 0.86 M.
2) At an altitude of 10 kilometers above sea level and a temperature of T = -50 °C, the speed of sound in meters per second is a=299.8m/s.
3) U_∞ is true airspeed
4) Kinematic viscosity: $V=1.49*10^{-5}$
5) The critical aerodynamic length becomes 22 meters from the nose tip of the aircraft.
6) Lengthwise trajectory (antenna location on fuselage): x greater or equal to 22 [m] from the aircraft's nose tip.
7) Air flows over the upper surface of the fuselage of the aircraft can be considered as flow over a flat plate.

3.5.1 By definition Mach Number (M): Mach number is the ratio between the true airspeed of the aircraft and the local speed of sound. Since it is a ratio, it is a dimensionless quantity. The word "local" has significant importance in the definition. Due to the airflow around the contours of the plane, there is most often an increase in its temperature, and this increases the speed of sound in that locality.

$$M=\frac{U_\infty}{a} \qquad (3.3)$$

$$U_\infty = M*a \qquad (3.4)$$

$U_\infty = 0.860*299.8$ m/s

U_∞= true airspeed in m/s=257.82 m/s

3.5.2 Reynolds number: Reynolds number is the ratio of inertial forces to viscous forces within a fluid that is subjected to relative internal movement due to different fluid velocities, which is known as

a boundary layer in the case of a bounding surface such as the interior of a pipe. A similar effect is created by the introduction of a stream of higher velocity fluid, such as the hot gases from a flame in the air. This relative movement generates fluid friction, which is a factor in developing turbulent flow. Counteracting this effect is the viscosity of the fluid, which as it increases, progressively inhibits turbulence as more kinetic energy is absorbed by a more viscous fluid. The Reynolds number quantifies the relative importance of these two types of forces for given flow conditions and is a guide to when turbulent flow will occur in a particular situation. [37]

With respect to laminar and turbulent flow regimes:

- Laminar flow occurs at low Reynolds numbers, where viscous forces are dominant, and is characterized by smooth, constant fluid motion.
- Turbulent flow occurs at high Reynolds numbers and is dominated by inertial forces, which tend to produce chaotic eddies, vortices, and other flow instabilities.
- The form of the Reynolds number can be derived as follows [38]

$$\mathrm{Re} = \frac{\mathrm{InertiaForce}}{\mathrm{Viscousforce}} = \frac{\mathrm{ma}}{\tau \mathrm{A}} = \frac{\rho \mathrm{V}\frac{\mathrm{du}}{\mathrm{dt}}}{\mu \frac{\mathrm{du}}{\mathrm{dy}}.\mathrm{A}} \propto \frac{\rho \mathrm{L}^3 \frac{\mathrm{du}}{\mathrm{dt}}}{\mu \frac{\mathrm{du}}{\mathrm{dy}}.\mathrm{L}^2} = \frac{\rho \mathrm{L}\frac{\mathrm{dy}}{\mathrm{dt}}}{\mu} \propto \frac{\rho \mathrm{u_o L}\frac{\mathrm{dy}}{\mathrm{dt}}}{\mu} = \frac{\mathrm{u_o L}}{\nu} \qquad (3.5)$$

The Reynolds number is defined as [37]

$$\mathrm{Rex} = \frac{\mathrm{u_o L}}{\nu} \qquad (3.6)$$

Where:

- ρ is the density of the fluid (SI units: kg/m^3)
- $u_o = \mathrm{U}_\infty$ is the velocity of the fluid with respect to the object (m/s)
- $x=L$ is a characteristic linear dimension (m)
- μ is the dynamic viscosity of the fluid (Pa·s or N·s/m^2 or kg/m·s)
- ν is the kinematic viscosity of the fluid (m^2/s).

By using equation (3.6) $\mathrm{Rex} = \frac{U_\infty * x}{V} = \frac{257.82\ \mathrm{m/s} * \cdot\ 22\mathrm{m}}{1.49 * 10-5\ \mathrm{m2/s}} = 380{,}673{,}826.00$

The turbulent boundary layer started with a Reynolds number greater than or equal to 3 x 10^6. Therefore, we can deduce that the location of the antenna mounting plate is within the turbulent boundary layer.

The boundary layer thickness should give us a hint if the antenna is fully exposed to the free flow and more likely affected by flow excitation and/or buffering.

Thickness of the turbulent boundary layer at the end of the lengthwise trajectory (antenna location on fuselage): x greater than or equal to 22 [m] from the aircraft's nose tip.

$$\delta(x)=\frac{0.37*x}{\sqrt[5]{Rex}} \tag{3.7}$$

$$\delta(x) = 0.156[m]$$

In this case our antenna installation $\delta(x)$ less than 0.156[m] at the location x greater than or equal to 22 [m] from the nose tip of the aircraft.

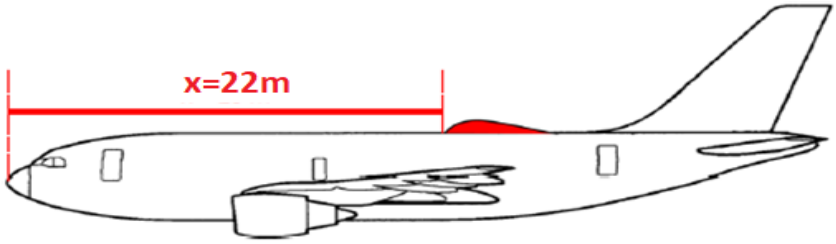

Figure 3.9: Lengthwise trajectory (antenna location on fuselage) [41]

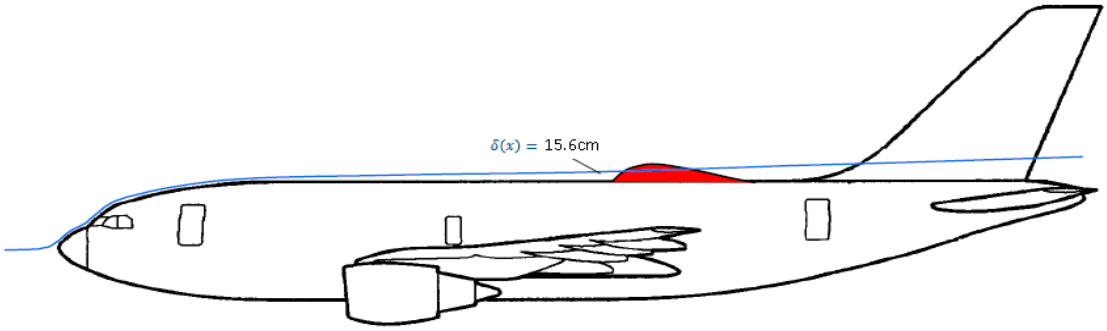

Figure 3.10: Thickness of turbulent boundary layer at Lengthwise trajectory (antenna location on fuselage): x greater than or equal to 22 [m] from the nose tip of the aircraft [41]

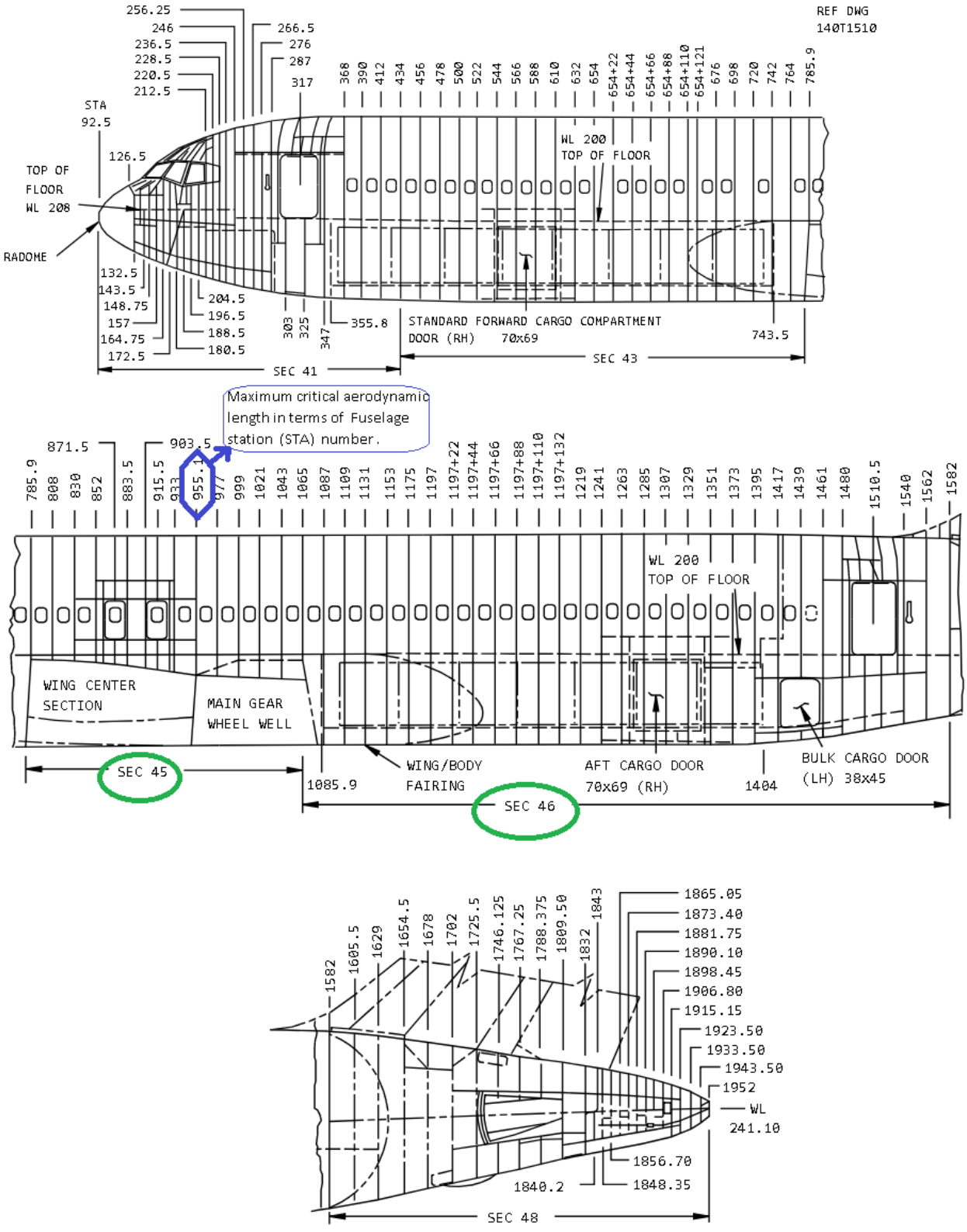

Figure 3.11: Fuselage Station Diagram [42]

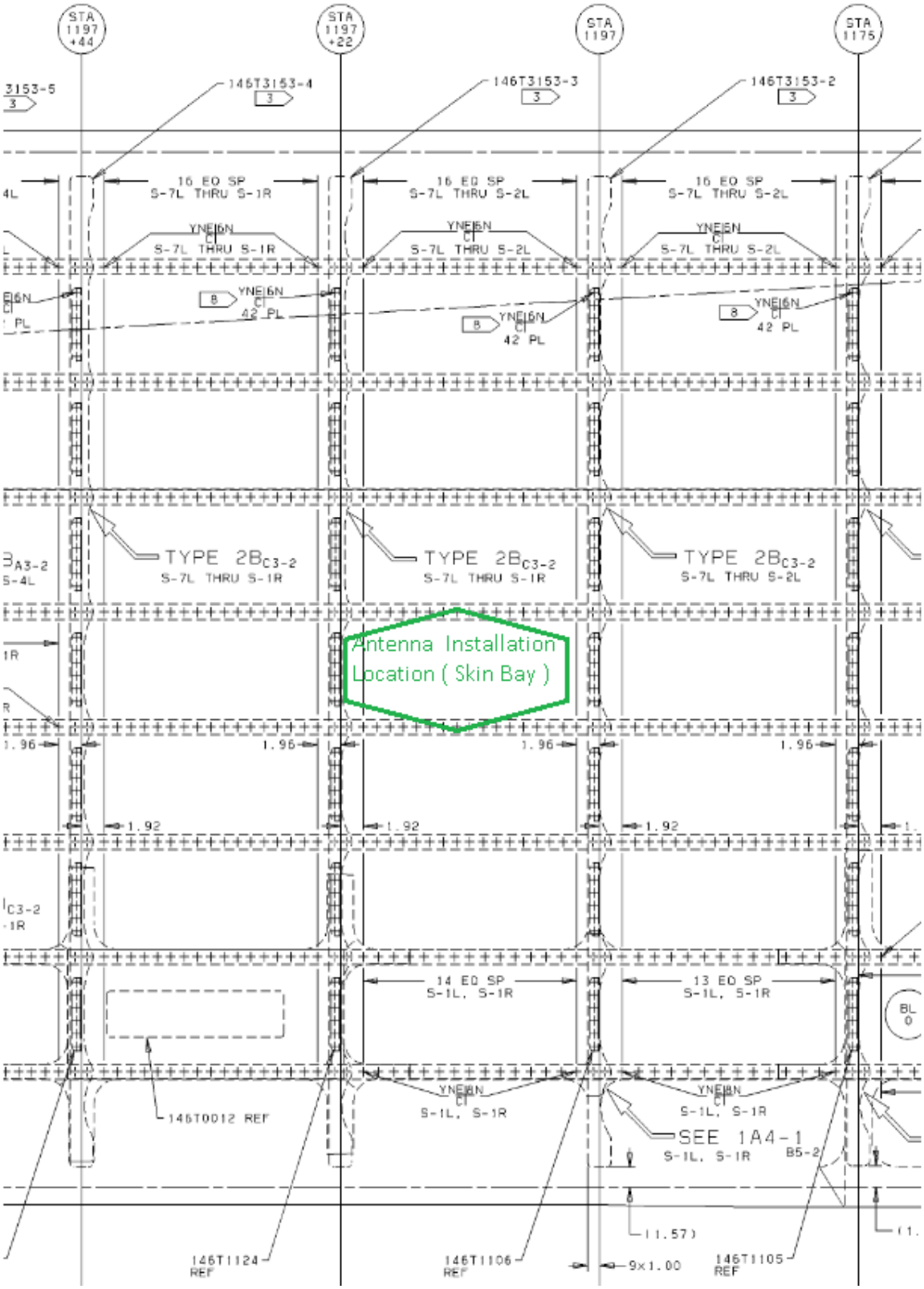

Figure 3.12: Skin Bay- Area between 2 Adjacent Frames and Stringers at which is antenna installation location. [43]

Modern civil aircraft utilize different antenna types by mounting them at different locations on the aircraft fuselage. The overall dimensions of different antenna types are depicted in the above table.

Table 3.4: Antenna type and their overall dimension used on civil aircraft [44]

	Antenna description	Long [Inch]	Width [inch]	Tall[inch]
1	Communication Antennas	5	3	10
2	ADF	12”	6	1
3	GPS **	4	4	0.5
4	Transponder and DME	5	2	1
5	TCAS	15.26	7.77	7.64
6	ADF LOOP	30	10.62	1.77
7	GLIDESLOPE	2	4.6	6.9
8	COM WHIP BENT			
9	COM WHIP			
10	ELT			
11	ADF COMBINED SENSE LOOP			
12	MARKER			
13	COMBINED COM/VOR			
14	DME/TRANSPONDER BLADE			
15	VOR BLADES	66.25	6.5	7.947
16	VOR RABBIT EAR			
17	SAT-COM			

****GPS Antennas**: They require a direct line of sight with the satellites they receive signals from, so they are typically mounted on the top of the fuselage. Communication antennas can cause interference with GPS antennas, so they should be mounted as far from each other as practicable.

3.6 Skin Bay (Area between 2 Adjacent Frames and Stringers) physical dimension

As indicated in the above-mentioned figures 3.8 and 3.9, the fuselage skin's critical aerodynamic length is 22.00 meters away from the nose tip of the aircraft. We can fix the open area and exact location of the antenna installation location (Skin Bay) based on physical existing dimensions and Boeing drawing numbers 146T3151_dwg_0003 and 146T3151_DWG_0004 at Section 46 and Stations Numbers 1197 to 1219.

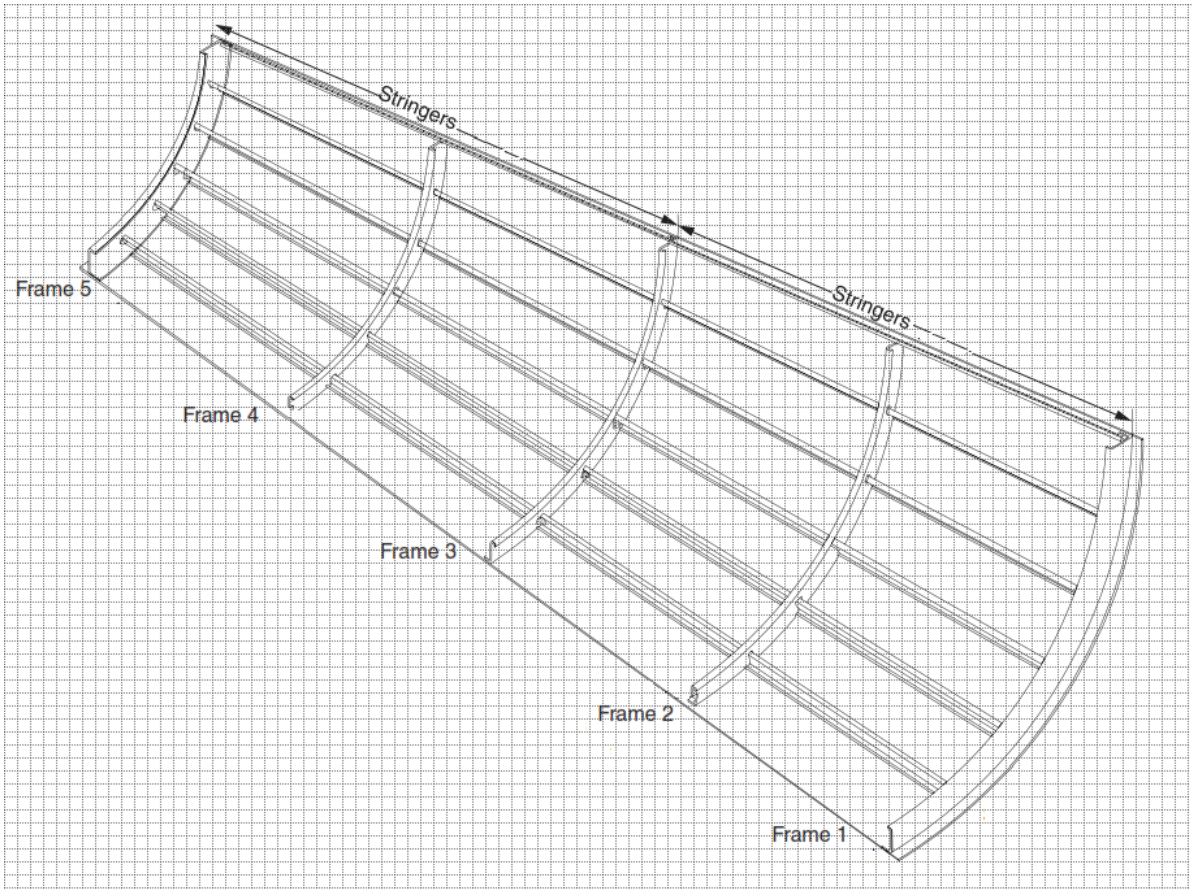

Figure 3.13: Layout of quarter fuselage, Frame, stringer and Skin Bay physical location [45]

Frame: Maintains fuselage shape, transfer shear loads, resists frame bending, provide support for stringer column buckling

Stringer: Reacts Axial Bending Loads, Resists Skin Buckling, Resists Frame Rotation

Skin: Reacts to pressure and bending loads; reacts to in-plane tension and compression stress; reacts to in-plane shear stresses

From Frame to frame = 18 inch [457.2mm]

Stringer to stringer = 8 inch [203.2mm]

Pitch $_{long}$ = 1.105 inch[28.067mm]

Pitch $_{circum}$ = 1.105 inch[28.067mm]

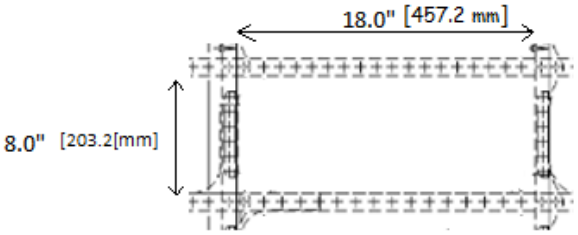

Figure 3.14: Geometry of mounting plate having same area [43]

In this paper for equal area of rectangular, circular and elliptical mounting plate static strength of the mounting plate will be analysed.

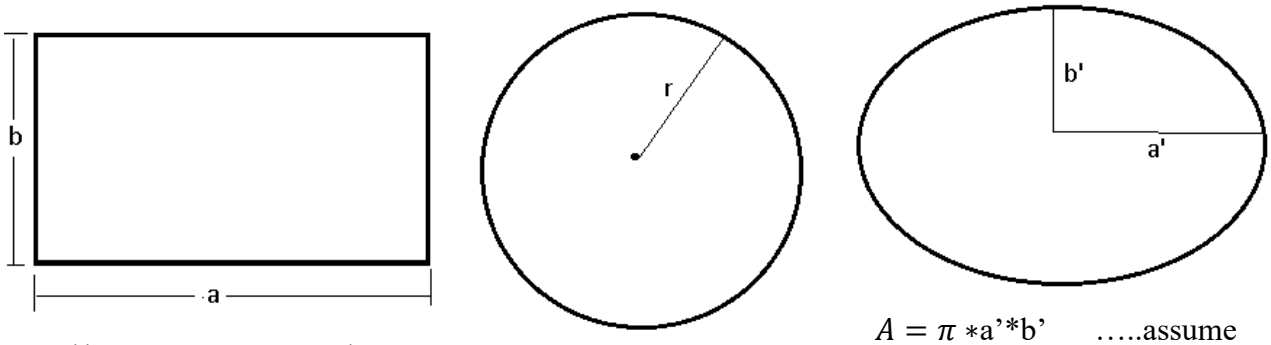

A= a*b …..assume a=2b

$A = \pi r^2$

$A = \pi * a' * b'$ …..assume a'=2b'

Figure 3.15: Geometry of mounting plate having same area.

Considering the indicated assumptions for the sides of the rectangular mounting plate and the major and minor diameters of the elliptical mounting plate, the physical dimension of the respective mounting plate is indicated in the table below.

Table 3.5: Mounting Plate Geometrical Shape final over all dimension

Item number	Mounting Plate Shape	Length [inch]	Length [inch]
I.	Rectangular	With length a =10”	With width b= 5”
II.	Elliptical	Major diameter 5.656”	Minor diameter =2.828”
III.	Circular	Diameter =7.98”	Diameter =7.98”

3.7 Mechanical fastening methods and Rivets

Large and complicated structures are typically only possible to manufacture when they are made up of smaller sections that are put together using a variety of joining techniques. Manufacturing components separately and then assembling them into a single product is easier and less expensive than producing the entire product at once. To ensure manufacturability and lower overall production costs, certain fastening and joining methods should be used.

Rivets are permanent, non-threaded, one-piece fasteners that join parts together by fitting through a pre-drilled hole and deforming the head by mechanically upsetting it from one end. Rivets are the most widely used mechanical fasteners, especially in aircraft fuselage structures. Hundreds of thousands of rivets

are utilized in the construction and assembly of a large aircraft. The solid rivet with a universal head is one of the most widely used rivet types in aircraft fuselage manufacturing and repair processes [46].

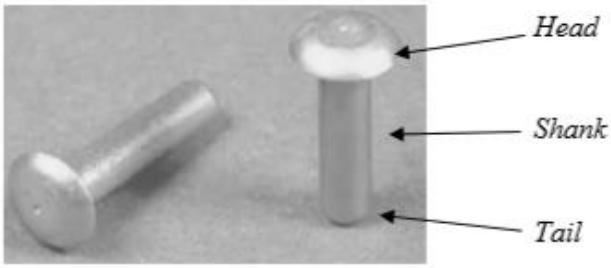

Figure 3.16 Solid rivet having universal head [46]

3.8 Determination of Number of Rivets

Rivets are used to join mechanically the antenna mounting plate with the fuselage skin and transfer loads to the structure. Optimize rivets must be used to ensure that each individual rivet load is less than the maximum allowable load.

3.8.1 For Rectangular Mounting Plate Determination of Number of Rivets

Rectangular Geometry/Shape Having Dimension Longitudinal Length = 10.00" &Circumferential width = 5.00"

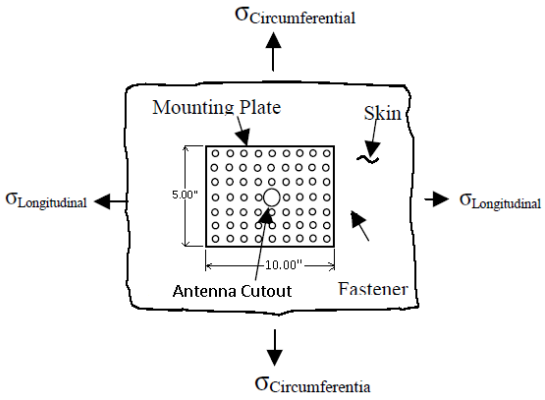

- skin material 2024-T3 [Table 3.1]
- Skin thickness =0.063 inch [1.6mm]
- Mounting plate thkness =0.071 inch [1.8mm]
- Fastener/rivet diameter = 0.25 inch[6.23mm]
- Pich $_{\text{Longitudnal}}$ =1.105 inch [28.067mm]
- Pitch $_{\text{Circumfrential}}$ =1.105 inch [28.067mm]

Figure 3.17: Rivets Layout and Determination of number of rivets for rectangular mounting plate-typical.

The mounting plate installed in the longitudinal direction as indicate in figure below.

$$L = 2\left(e - \frac{d}{2}\right) + nd + (n-1)(p-d) \qquad (3.8)$$

$$L = 2e + np - p$$

Where:

L= Length of rectangular mounting plate; n= number of rivet in a single row

e= edge margin; e/d=2 ;d=rivet diameter =0.25"

p= pitch for both longitudinal and circumferential direction = 1.105"

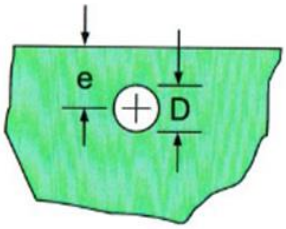

e = distance to edge, or "edge margin"
D = diameter of hole

- e/D is tested at 1.5 and 2.0
- EM is also used for "edge margin"
- For countersink fasteners, D equals the average diameter (D_{avg})

Figure 3.18: Edge margin rivet hole diameter "D" how to consider in fixing the rivets layout and rivet quantity. [47]

Consider length of a mounting plate L= 2e + np-p, the number of required fastener /rivet can be calculated as follow

n = (L-2e +p)/p

Along the longitudinal direction L=10.00" & P = 1.105 the number of rivet calculated with

n= 9.145

Let n= 9

The new p becomes 1.125"

Along the circumferential direction L=5.00" & P = 1.105 the number of rivet calculated with

n=4.62

Let n= 5

The new p becomes 1.105"

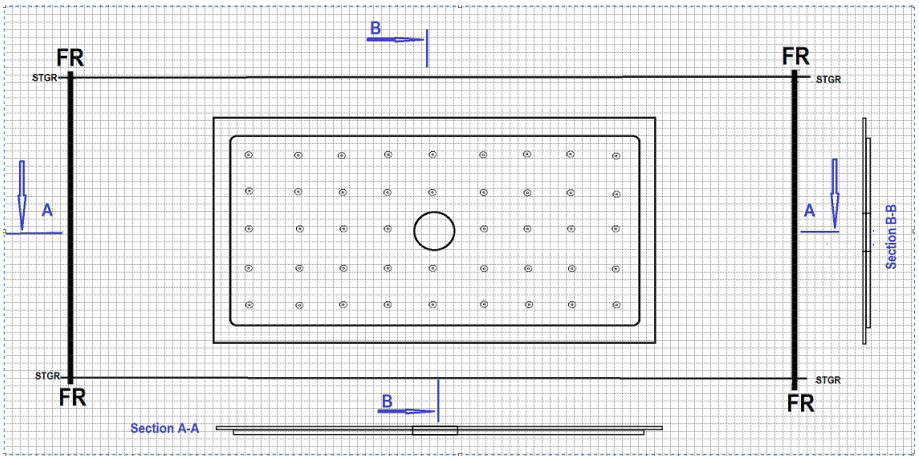

Figure 3.19: Rivets' layout and determination of the number of rivets for the rectangular mounting plate.

FR= Frame: Maintains fuselage shape, transfer shear loads, resists frame bending, provide support for stringer column buckling

STGR= Stringer: Reacts Axial Bending Loads, Resists Skin Buckling, and Resists Frame Rotation

Skin: Reacts Pressure and Bending Loads, Reacts In-Plane tension and compression stress, reacts in-plane shear stresses

3.8.2 For circular mounting plate geometry / shape having diameter of D = 8.00”

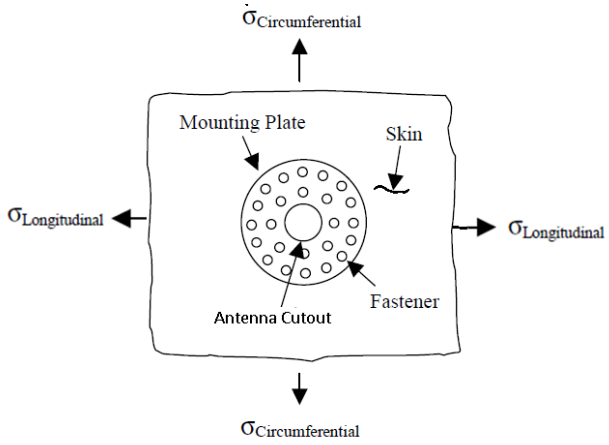

- skin material 2024-T3 [Table 3.1]
- Skin thickness =0.063 inch [1.6mm]
- Mounting plate thkness =0.071 inch [1.8mm]
- Fastener/rivet diameter = 0.25 inch[6.23mm]
- Pich $_{Longitudnal}$ =1.105 inch [28.067mm]
- Pitch $_{Circumfrential}$ =1.105 inch [28.067mm]

Figure 3.20: Rivets layout and determination of number of rivets for circular mounting plate-typical

Number of rivet can be determined using circumference /perimeter of a circle formula

Perimeter-1 = np = pi * (D-2e) =>

n= (pi * (D-2e))/p

n= 19.91

Let n= 20

The new circumferential p becomes 1.1”

Where np= Length of circular mounting plate

n= number of rivet in a single circumference

e= edge margin; e/d=2

d=rivet diameter =0.25”

p= pitch for both longitudinal and circumferential direction = 1.105”

Perimeter-2 =np= pi * (0.5+2d +p’) *2

n= 13

Let n= 13

The new circumferential p becomes1.063”

Perimeter-3 =np= pi * (D-2e) ;n= 6

The new circumferential p becomes 1.047”

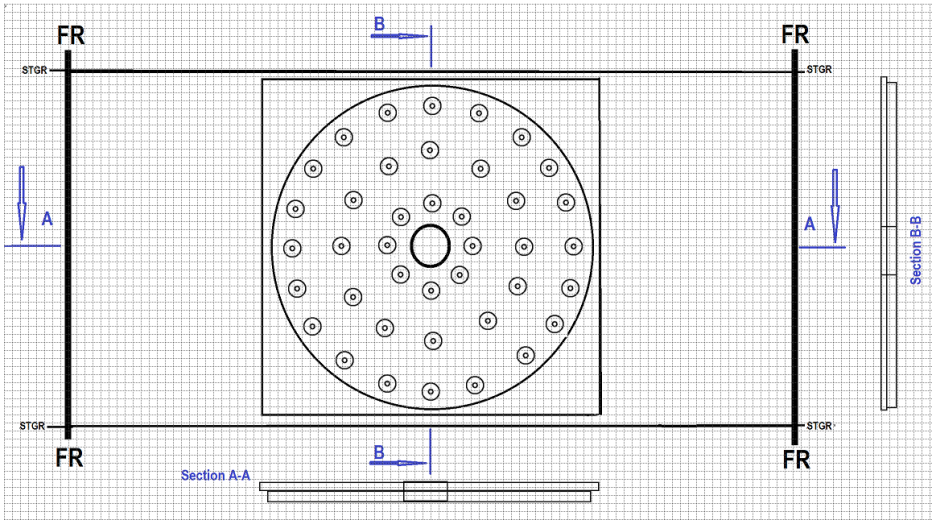

Figure 3.21: Rivets' layout and determination of the number of rivets for the circular mounting plate.

FR= Frame: Maintains fuselage shape, transfer shear loads, resists frame bending, provide support for stringer column buckling

STGR= Stringer: Reacts Axial Bending Loads, Resists Skin Buckling, Resists Frame Rotation

Skin: Reacts Pressure and Bending Loads, Reacts In-Plane tension and compression stress, reacts in-plane shear stresses

3.8.3 For Elliptical Mounting Plate Geometry / Shape Having Diameter

Major diameter = 5.656”

Minor diameter =2.828”

Where: -

L= Perimeter of an ellipse mounting plate
n= number of rivet in a single Perimeter of an ellipse
e= edge margin; e/d=2
d=rivet diameter =0.25”
p= pitch for both longitudinal and circumferential direction = 1.105”

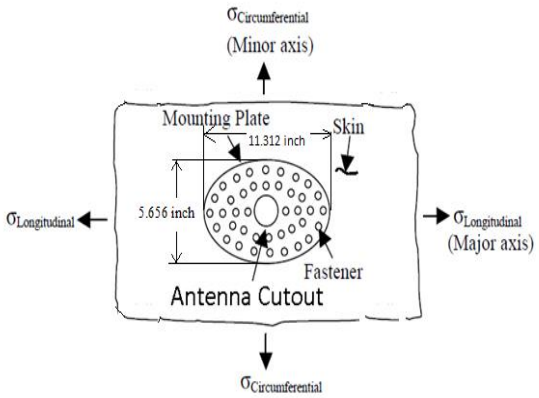

- skin material 2024-T3 [Table 3.1]
- Skin thickness =0.063 inch [1.6mm]
- Mounting plate thkness =0.071 inch [1.8mm]
- Fastener/rivet diameter = 0.25 inch[6.23mm]
- Pich $_{Longitudnal}$ =1.105 inch [28.067mm]
- Pitch $_{Circumfrential}$ =1.105 inch [28.067mm]

Figure 3.22: Rivets' layout and determination of the number of rivets for the elliptical mounting plate - typical.

Perimeter Elliptical geometry with a major axis "a" and a minor axis "b" and "a" and "b" are measured from the centre, like the "radius of a circle". The perimeter of an ellipse is calculated using the below equation.

$$P \approx 2\pi \sqrt{\frac{a^2 + b^2}{2}} \qquad (3.9)$$

Ellipticalperimeter-1

Perimeter-1=n_1P_1; consider perimeter formula (4.2)

Inserting this value of “a” & “b” in the above equation the perimeter1 value becomes =25.13428056 with p_1=1.105

Perimeter1=n_1p_1= 25.13428056

n_1=22.7459

Let n_1=24

The new circumferential p becomes1.047”

EllipticalPerimeter-2

Perimeter-2=n_2p_2, consider perimeter formula (3.9)

a=0.5+2d+0.664” =1.664” b=

2a =3.328”

Inserting this value of a &bin the aboveequationtheperimeter-2 becomes

Perimeter: -2= n_2p_2=16.53115487 and P_2=1.105

n_2=14.9603

Let n2=16

The new circumferential p_2 becomes 1.0331”

EllipticalPerimeter-3

Perimeter-3 =np= pi * (D) =circumference of a circle

n= (pi * (1+1))/ p …. ……. p=1.105”

Inserting this value of a &b intheaboveequationtheperimeter-3 becomes

Perimeter3=n_3p_3= 6.283185307

n_3p_3=6.283185307

n_3= 5.68

Let n= 8

The new circumferential p becomes 0.7854”

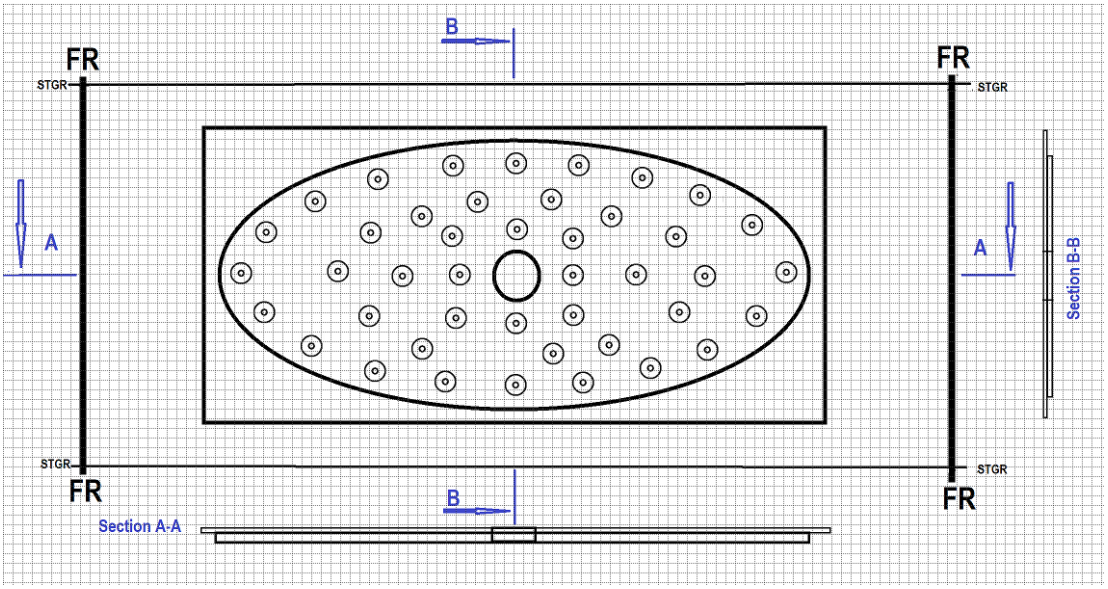

Figure 3.23: Rivets' layout and determination of the number of rivets for the elliptical mounting plate.

The Skin Bay with a physical dimension of 8 inches by 18 inches and for an equal area of mounting plate with geometrical shapes of rectangular, circular, and elliptical. The overall dimensions of the rectangular Mounting Plate, circular Mounting Plates radius, and major and minor diameter of the elliptical Mounting Plates are summarized as indicated in the below table.

Table 3.6: Mounting Plates Geometrical Shape, over all dimension & Number of Rivets used.

Item number	Mounting Plate Shape	Length [inch]	Length [inch]	Number Of Rivet/ Pitch	Pattern
I.	Rectangular	With length a =10”	With width b= 5”	44 Pitch longitudinal Direction =1.125 Pitch Hoop Direction 1.00”	Rectangular
II.	Elliptical	Major diameter 5.656”	Minor diameter =2.828”	44 Perimeter1=1.047” Perimeter2=1.0331” Perimeter3=0.7854”	Elliptical
III.	Circular	Diameter =7.98”	Diameter =7.98”	40 Perimeter1=1.100” Perimeter2=1.063” Perimeter3=1.047”	Circular

3.9 Determination of Pressurization and Bending Loads applied on the fuselage skin.

In order to start detailed analysis of the specific objectives, first we have to determine the fuselage skin internal axial tension stress (i.e., circumferential and longitudinal loads) because of cabin pressurization and bending loads acting on the fuselage skin. This load will be used for the rest of the specific objective analysis to determine the mounting plate allowable and margin of safety, joint stress concentration calculation, damage tolerance analysis.

3.8.1 FAA/SWIFT Method to determine fuselage skin stress

— conservative method to obtain fuselage skin stresses

— fuselage skin stress is a function of inertia loads and cabin pressure loads

— FAA has recommended the following values be used for a typical fatigue stress

Longitudinal: $F_{axial} = 1.5 * F_{1.0g} + \Delta P_a$ (3.10)

circumferential (hoop): $F_{hoop} = 1.5 * \Delta P_h$ (3.11)

$F_{1.0g}$=1.0 g inertia stress at 70% payload

ΔP_a = axial stress due to pressure (cabin differential pressure)

ΔP_h = hoop stress due to pressure (cabin differential pressure)

Since most load data proprietary to the original equipment manufacturer (OEM), the FAA has developed acceptable methods to obtain fuselage skin fatigue stress. The fuselage skin stress is a function of the applied inertia loads and the cabin pressure stress.

For circumferential stress, a value of 1.5 times the cabin pressure stress is acceptable, and for the axial stress, we can use the cabin pressure stress combined with the stress due to $F_{1.0g}$ at 70% payload.

From B767-300 Structural Repair Manual (SRM) chapter 53-00-00-0G-0

P= Maximum cabin differential pressure = 8.6 psi

r=Skin radius = 99.0”

t=Skin thickness (gauge) = 0.063”

First Determine the Pressure Stress:

Axial Stress =$\Delta P_a = P*r/2t$ = (8.6*99)/ (2*.063) =6.757Ksi

Hoop stress$\Delta P_h = P*r/t$ = (8.6*99)/ (0.063) =13.52Ksi

The hoop fatigue stress is simply

$F_{hoop} = 1.5 * \Delta P_h = 1.5 * 13.52 = 20.271$ Ksi

The axial stress determination is more complex. The first step is to calculate the inertia stress at 100% payload, and we start by assuming a zero margin in the skin, such as

With $F_{tu} = 1.5\ F_{lim}$ 14 CFR § 25.303 - Factor of safety

$$F_{lim} = 2.5 * F_{1.0g} + \Delta P_a$$

$F_{1.0g}$= Maximum 1.0 g inertia Longitudinal bending stress at 100% payload [48-49]

Δ Pa = axial stress due to pressure (cabin differential pressure)

Axial Stress $=\Delta P_a = P*r/2t$

with $Ftu = 1.5\ F_{lim}$

Consider that F_{tu} may be lesser of Ftuor$1.5*F_{ty}$

$F_{tu} = 1.5 *(2.5 * F_{1.0g} + \Delta P_a)$

$63000 = 1.5\ (2.5* F_{1.0g}+13520)$

$F_{1.0g=}11.392$ ksi

F_{tu}= 63000;

$1.5* F_{ty}=1.5*47000 = 70{,}500$

This is the one "g" inertia stress assuming 100% pay load. A typical value of 70% pay load is used to calculate a representative fatigue stress

$$F_{1.0g=0.7 *11.392}$$

$$F_{1.0g\ =7.974ksi}$$

The axial fatigue stress is therefore: $F_{axial} = 1.5 * F_{1.0g} + \Delta P_a$

$$F_{axial} = 1.5 * 7.974 + 6.757$$

$$F_{axial} = 18.72ksi$$

The hoop fatigue stress is simply

$$F_{hoop} = 1.5 * \Delta P_h = 1.5 *13.52 = 20.271\ Ksi$$

From the above calculation we can infer the following:

i. Circumferential (hoop) and longitudinal (axial) load act at same time
ii. Circumferential (hoop) stress greater than longitudinal (axial) stress by 7.651%
iii. Load consideration applies the combined Circumferential (hoop) and longitudinal (axial) load or their resultant at certain angle along with the corresponding crack initiation and propagation will be review in the next chapter

Specific objective –I: Theoretical Concepts and Principles.

3.10 Static Strength Analysis

To assess the static strength of the modified skin, three independent criteria are used to evaluate the margin of safety of the mounting plate and fasteners. [48]

I. Mounting plate allowable
II. The joint allowable
III. The shear allowable

3.11 The Mounting Plate Allowable and Margin of Safety

To assess the loss of skin strength due to the antenna connector hole cut-out, the margin of safety of the mounting plate is calculated as

$$\text{Margin of safety} = \frac{\text{Ppu}}{\text{Pp}} - 1 \qquad (3.12)$$

Where P_{pu}, the mounting plate load allowable, is calculated using the equation

$$P_{PU} = F_{tu}(W_P - \text{D})t_p \qquad (3.13)$$

In which F_{tu}, w_p, D, and t_p are the ultimate tensile strength, width, cut-out diameter, and thickness of the mounting plate, respectively.

$$P_P = \sigma_u D \text{t}_s \qquad (3.14)$$

Where σ_u and t_s are the design ultimate tensile stress and thickness of the skin, respectively. σ_u=the lesser of F_{tu} or F_{ty} *1.5

3.12 The Fastener Joint Allowable and Margin of Safety

In the vicinity of an antenna installation on the skin, skin stresses are transferred to the mounting plate through fasteners via fastener shear and hole bearing. The fastener, together with the skin and mounting plate, represents a fastener joint. A joint can only transfer a certain amount of load until it fails. The point at which this fastener joint fails is the joint allowable. The calculation of the joint allowable is based upon two loading conditions: fastener shear and hole bearing.

3.13 Fastener Joint Allowable in Straight Shank Holes

Straight shank holes are used for protruding head fasteners and for mounting plates that have flush head fasteners installed but are not countersunk. The joint allowable is the lower of the shear allowable or the

hole bearing allowable. An allowable is calculated for the skin and mounting plate that the fastener goes through.

The single shear allowable for straight shank holes is calculated using the following equation

$$Psu = Fsu * Af * SCF1 \quad (3.15)$$

The mounting plate double shear allowable for straight shank holes is calculated using the following equation

$$Psu = 2 * Fsu * Af * SCF2 \quad (3.16)$$

In both equations, where

- F_{su} is the ultimate shear strength of the fastener material,
- A_f is the cross-sectional area of each fastener,
- S_{CF1} is the single shear correction factor and
- S_{CF2} is the double shear correction factor.
- S_{CF1} and S_{CF2} are used only for solid rivets and can be found in MIL-Handbook 5F Table 8.1.2.1(b).

The hole bearing allowable for the straight shank hole is calculated using the following equation

$$P_{bru} = F_{bru} * d * t \quad (3.17)$$

In which F_{bru} is the ultimate bearing stress of the plate (skin or mounting plate) material, d is the fastener hole diameter, and t is the thickness. Currently, the F_{bru} is for the case edge distance to hole diameter (e/d) equal to 2.0.

3.14 Fastener Joint Margin of Safety

The fastener joint margin of safety is determined by summing each fastener joint allowable in the skin and mounting plate and this is done for each side of the mounting plate.

$$P_{total} = \sum_{n=1}^{k} (P_{jointl})_n \quad (3.18)$$

In which P_{total} is the total fastener joint load, $(P_{joint})n$ is the fastener joint load for the n^{th} fastener and K is the number of fasteners.

The P_{total} for the skin and mounting are then compared. The smaller of the two is the fastener joint allowable for that side of the mounting plate and is used in determining the margin of safety for the fastener joints.

An applied load is needed to determine a margin of safety. That load is the ultimate applied load to the structure, or if that is not known, then the tensile ultimate strength of the material F_{tu} is used. This applied load $P_{applied}$ is given by

$$P_{applied} = \sigma_u D t_s \quad (3.19)$$

Where: -

σ_u: is either the design ultimate tensile stress or the tensile ultimate skin strength,

t_s: is the skin thickness,

D: is the diameter of antenna connector cut-out hole.

At this point to fix $P_{total} = \sum_{n=1}^{k} (P\ joint)$, we have to have determined the number of fastener for each type of the mounting plate.

3.15 Margin of Safety as a Criterion

The margins of safety (MS) based on the mounting plate allowable and the fastener joint allowable were calculated to determine the adequacy of the antenna installation on the fuselage skin .[48]

MS <0 Antenna installation is statically inadequate

MS=0 Antenna installation is marginally adequate

MS >0 Antenna installation is statically adequate

Antenna installations that are not statically adequate must be redesigned in order to assure antenna installation adequacy.

3.16 The Stiffness Check of the Antenna Installation

The stiffness ratio between the mounting plate and the skin is calculated using the following equation

$$\text{Stiffness Ratio} = \frac{(Et)_p}{(Et)_s} \quad (3.20)$$

The antenna installation is :-

- considered adequate if the ratio is between 1.0 and 1.5.
- The antenna installation is too stiff when the value is greater than 1.5 and
- not stiff enough when it is less than 1.0.

3.17 The Fastener Bending Check

The Fastener Bending Check of the Antenna Installation The fastener bending is checked using the following equation

$$Q = \frac{(ts + tp)}{d} \qquad (3.21)$$

Where d is the fastener diameter, t_s and t_p are the thickness of the skin and mounting plate, respectively. The parameter Q is the fastener bending indicator. For aluminium fasteners, the bending is important. A Q value above 2 may indicate that the aluminium rivet will not fill the hole but instead may buckle in the hole.

3.18 The Inter-Rivet Buckling Guideline

To avoid inter-rivet buckling in the modified skin, the fastener spacing should be four to six times the diameter of the fastener shank diameter.

3.19 The Analytical Modelling for Specific Objective II

Stress concentration factor for antenna cut-out with different geometrical patterns/shapes (i.e., rectangular, circular, and elliptical cut-outs) for biaxial load applied discussed in this topic.

Normally, the stress in a plate is uniform under constant loading. A hole in the plate creates a stress concentration, where the stress at the edge of the hole is several times higher than the gross stress. The gross stress is the far-field stress away from the hole. In-between the hole and the edge of the plate is a stress gradient, which defines the change in stress as the distance from the hole increases. Other changes in cross section, such as notches, tapers, and or thickness changes, can also cause an increase in stress.

To quantify this difference, the stress concentration factor (K_{tg}) is used. It can be defined as $K_{tg} = \sigma_{peak} / \sigma_{gross}$. Values for σ_{peak} are established by test or detailed finite element analysis. K_{tg} can be calculated from the loading test specimen geometry as $\sigma_{peak} = K_{tg} * \sigma_{gross}$.

In general, if the stress level is increased by 20%, the fatigue life is decreased by 50%. The stress concentration factor (K_{tg}) is valid only if the stress gradient is elastic. [49]

Under normal operating loads, stress concentration is a very important factor in determining the fatigue life of a part.

Openings or cut-outs are made into structures in order to satisfy some service requirements, which results in strength degradation. In practice, different shapes of holes are used for different applications. For example, the manhole of any pressure vessel is either circular or elliptical, while the window or door of an airplane is a rectangular hole having a chamfer of some radius at the corners. Various shaped cut-outs are made in aircraft structures to satisfy certain service requirements. This cut-out acts as a stress riser and may lead to catastrophic failure. This chapter of the thesis studies the analytical and finite element method solutions to the stress concentration problem in the mounting plate under biaxial tensile loading for antenna connector hole/ cut-outs having circular, elliptic, and rectangular geometrical shapes subjected to biaxial tensions. Stress concentration factors for biaxial load and geometrical patterns such as circular, rectangular, and elliptical holes can be found in [50].

A representative analysis was simulated using ANSYS software in such a way that the modelling was initially solved by analytical methods [50] and the results were compared with each other for each type of cut out. Finally, stress concentration interims of geometrical shape were compared. Throughout the

analysis, the effect of thickness was ignored and the modelling was taken into account as 2D and in-plane stress stats.

Analytically, stress concentration for the elliptical hole under biaxial loading can be solved by the formula given in 3.29 and 3.30.

3.19.1 Biaxial tension of an obliquely oriented elliptical hole.

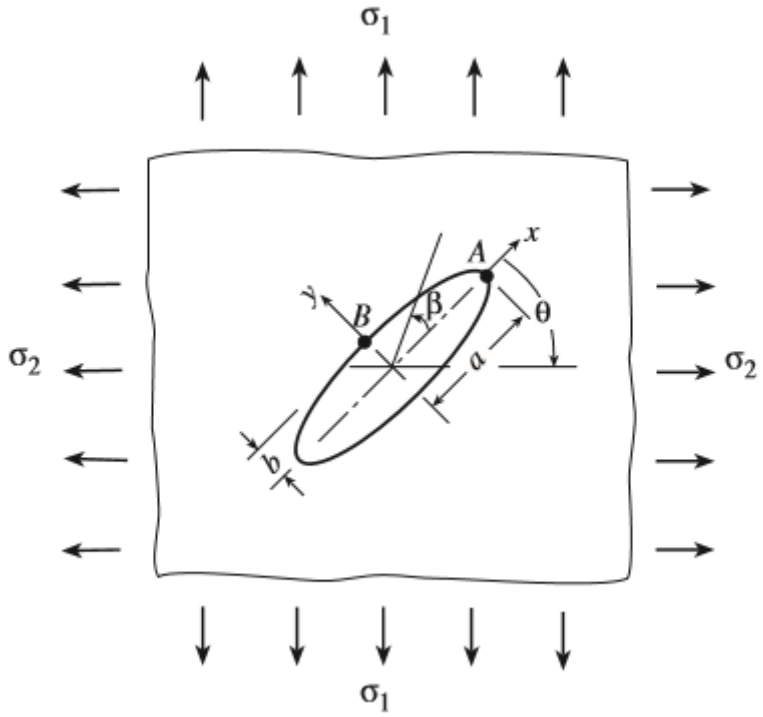

Figure 3.24: Biaxial tension of an obliquely oriented elliptical hole. [50]

Biaxial Tension around an Elliptical Hole Suppose that an element is subjected to tensile stresses σ_1, σ_2 and the direction of σ_2 forms an angle θ with the major axis of the hole, as shown in Fig.3.23. The stress concentration factor at the perimeter of the hole for different angle θ is given by

$$\left(\sigma_\beta\right)_{\alpha_0} = \frac{(\sigma_1+\sigma_2)\sinh 2\alpha_0+(\sigma_2-\sigma_1)\left[\cos 2\theta - e^{2\alpha_0}\cos 2(\beta-\theta)\right]}{\cosh 2\alpha_0 - \cosh 2\beta} \qquad (3.22)$$

Set the derivative of $\left(\sigma_\beta\right)_{\alpha_0}$ with respect to β equal to zero. Then the condition for the maximum stress is

$$(\sigma_2-\sigma_1)[\sin 2\theta(1-\cos 2\beta.\cosh 2\alpha_0)-\cos 2\theta.\sin 2\beta.\sinh 2\alpha_0]$$
$$=(\sigma_2+\sigma_1)\,e^{-2\alpha_0}\sinh 2\alpha_0\,.\sin 2\beta \qquad (3.23)$$

For θ =0and (2) reduces to

$$(\sigma_2-\sigma_1).\sin 2\beta = (\sigma_2+\sigma_1)\,e^{-2\alpha_0}\sin 2\beta \qquad (3.24)$$

The stress concentration factor is which correspond β=0, π/2 to points A and B of Fig.3.24. Thus the extreme values are

$$\sigma_A = \frac{(\sigma_1 + \sigma_2)\sinh 2\alpha_0 + (\sigma_2 - \sigma_1)(1 - e^{-2\alpha_0})}{\cosh 2\,\alpha_0 - 1} \qquad (3.25)$$

$$\sigma_B = \frac{(\sigma_1 + \sigma_2)\sinh 2\alpha_0 + (\sigma_2 - \sigma_1)(1 + e^{-2\alpha_0})}{\cosh 2\,\alpha_0 + 1} \qquad (3.26)$$

let $\tan\alpha_0 = \frac{b}{a}$ so that

$$\cosh\alpha_0 = \frac{a}{\sqrt{a^2 - b^2}}$$

$$\sinh\alpha_0 = \frac{b}{\sqrt{a^2 - b^2}}$$

Substitute $\cosh\alpha_0$ &$\sinh\alpha_0$ into (5.4) and (5.5),

$$\sigma_A = \left(1 + \frac{2a}{b}\right)\sigma_1 - \sigma_2 \qquad (3.27)$$

$$\sigma_B = \left(1 + \frac{2b}{a}\right)\sigma_2 - \sigma_1 \qquad (3.28)$$

With σ_2: as the reference stress, the stress concentration factors are $\sigma_A = (1 + 2a/b)\,\sigma_1 - \sigma_2$

$\sigma_B = (1 + 2b/a)\,\sigma_2 - \sigma_1$

$$K_{tgA} = \left(1 + \frac{2a}{b}\right)\frac{\sigma_1}{\sigma_2} - 1 \qquad (3.29)$$

$$K_{tgB} = \left(1 + \frac{2a}{b}\right) - \frac{\sigma_1}{\sigma_2} \qquad (3.30)$$

3.19.2 Single Circular Hole in an Infinite Thin Element under Biaxial In-Plane Stresses

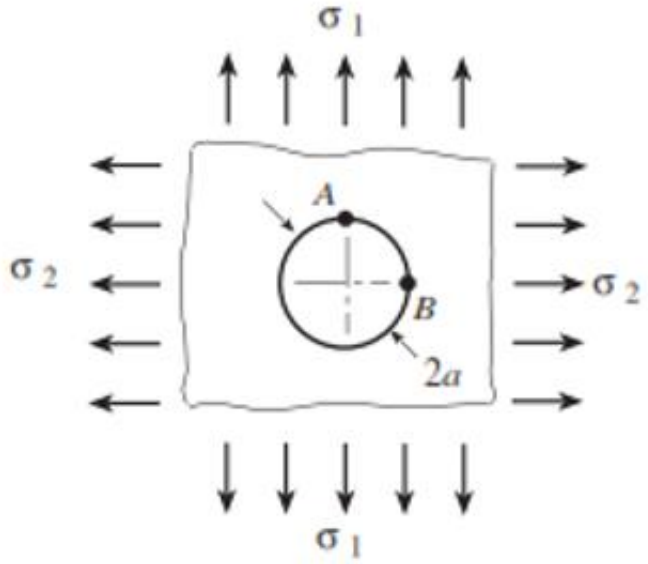

Figure 3.25 Infinite thin element under biaxial tensile in-plane loading. [50]

Let $\frac{\sigma_2}{\sigma_1} = \alpha$=0.857142

$$\sigma_\theta = \sigma_1(1+\alpha) + 2\sigma_1(1-\alpha)\cos 2\theta$$

Assume that $\alpha \leq 1$. Then

$$\sigma_{\theta max} = \sigma_{\theta B} = \sigma_1(3-\alpha)$$

$$\sigma_{\theta min} = \sigma_{\theta A} = \sigma_1(3\alpha - 1)$$

If σ_1 is taken

$$K_{tgA} = \frac{\sigma_{\theta min}}{\sigma_2} = \frac{\sigma_1}{\sigma_2}(3\alpha - 1) = 1.1666(3\alpha - 1)$$

$$K_{tgB} = \frac{\sigma_{\theta max}}{\sigma_1} = \frac{\sigma_1}{\sigma_1}(3-\alpha) = (3-\alpha)$$

3.19.3 Square Cut-Out the Stress Concentration Factors

From Charts 4.62a of "Peterson's stress concentration factors", [50] for r= a third of its width =25.4/3 that means r=25.4/3 = 8.466 = > r/a =8.46/12.71 = 0.667

One might think that a circular opening in a tension panel would have a lower maximum stress than a round-cornered square opening having a width equal to the circle diameter

3.20 Finite Element Method Using ANSYS

3.20.1 Stress-strain Relationship for Isotropic Materials (in Plane Stress condition)

3.20.2 2-Dimensional States of Stress and Strain

$$\{\sigma\} = \begin{Bmatrix} \sigma_x \\ \sigma_y \\ \tau_{xy} \end{Bmatrix} \tag{3.31}$$

$$\{\varepsilon\} = \begin{Bmatrix} \varepsilon_x \\ \epsilon_y \\ \gamma_{xy} \end{Bmatrix} \tag{3.32}$$

$$\varepsilon_x = \frac{\partial u}{\partial x} \tag{3.33}$$

$$\varepsilon_y = \frac{\partial v}{\partial y} \tag{3.34}$$

$$\gamma_{xy} = \frac{\partial u}{\partial y} + \frac{\partial v}{\partial x} \tag{3.35}$$

Stress-strain Relationship for Isotropic Materials (in Plane Stress condition)

$$\{\sigma\} = [D]\{\varepsilon\} \tag{3.36}$$

The matrix D is called the stress-strain matrix or the constitutive matrix

$$[D] = \frac{E}{1-\nu^2}\begin{bmatrix} 1 & \nu & 0 \\ \nu & 1 & 0 \\ 0 & 0 & \left(\frac{1-V}{2}\right) \end{bmatrix} \tag{3.37}$$

E is the modulus of Elasticity

v is the Poisson's ratio

3.20.3 Plane Stress Stiffness Equations

$$\begin{Bmatrix} \sigma_x \\ \sigma_y \\ \tau_{xy} \end{Bmatrix} = \frac{E}{1-\nu^2}\begin{bmatrix} 1 & \nu & 0 \\ \nu & 1 & 0 \\ 0 & 0 & ((1-v)/2) \end{bmatrix}\begin{Bmatrix} \varepsilon_x \\ \epsilon_y \\ \gamma_{xy} \end{Bmatrix} \tag{3.38}$$

From the physical dimensions of the aircraft crown area where the antenna is installed, we found the following overall dimension:

From Frame to frame = 18 inch

Stringer to stringer = 8 inch

Pitch $_{long}$ = 1.105 inch

Pitch $_{circum}$ = 1.105 inch

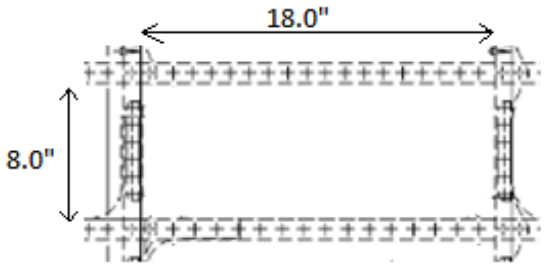

Figure 3.26: Skin Bay (Area between 2 Adjacent Frames and Stringers) physical dimension

In this topics , for an equal area of rectangular, circular, and elliptical mounting plates, the static strength of the mounting plate will be analyzed.

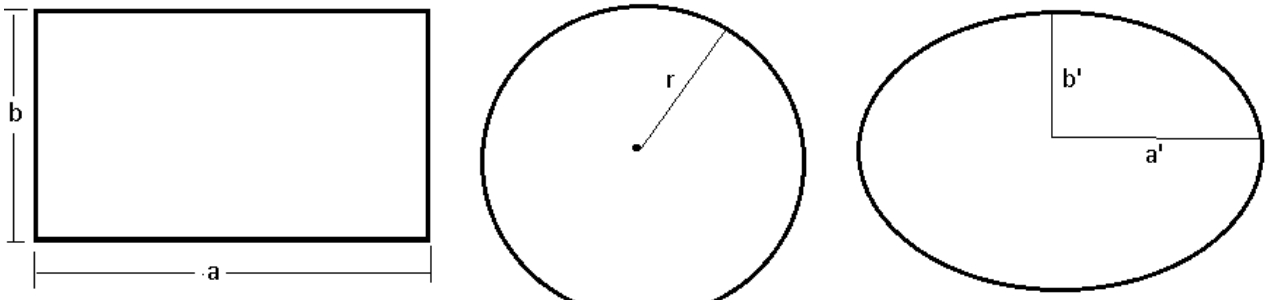

A= a*b …..assume a=2b

$A = \pi r^2$

$A = \pi$ ∗a'*b' ..assume a'=2b'

Item number	Mounting Plate Shape	Length [inch]	Length [inch]
I.	Rectangular	With length a =10"	With width b= 5"
II.	Elliptical	Major diameter 5.656"	Minor diameter =2.828"
III.	Circular	Diameter =7.98"	Diameter =7.98"

Figure 3.27: Skin Bay (Area between 2 Adjacent Frames and Stringers) physical dimension

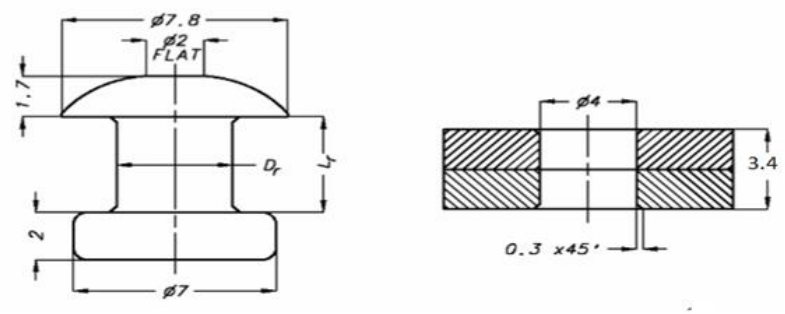

Figure 3.28: Geometries of deformed rivet and rivet hole on the plates

3.21 The Finite Element modelling of antenna mounting plates

The finite element method (FEM) is a powerful numerical technique for finding approximate solutions of complex problems in structural mechanics. Meshing is a vital step of the finite element method. Choosing appropriate element type and size is a trade-off between accuracy and time required for the analysis. Therefore, element types are selected accordingly and local mesh refinement was applied at locations where they are necessary [50-51]. Refer to Appendix-VI.

Three-dimensional finite element models of the antenna mounting plate and fuselage skin joined by permanent fasteners (rivets) are prepared by using ANSYS. The geometry, boundary conditions, and material properties of the respective models are depicted in figures 4.5 to 4.11.

Three-dimensional 20 node structural solid elements (SOLID186) are used for creating the model, and three-dimensional 8 node surface-to-surface contact (CONTA174) and three-dimensional target segment (TARGE170) elements are internally generated for modelling the surface-to-surface contact.

SOLID186 is a higher-order 3-D 20-node solid element that exhibits quadratic displacement behaviour. The element is defined by 20 nodes having three degrees of freedom per node: translations in the nodal x, y, and z directions. The element supports plasticity, hyper elasticity, creep, stress stiffening, large deflection, and large strain capabilities. SOLID186 is a newer version of Solid95.has mixed formulation capability for simulating deformations of nearly incompressible elastoplastic materials and fully incompressible hyperelastic materials.

CONTA174 is used to represent contact and sliding between 3-D target surfaces (TARGE170) and a deformable surface. This element is located on the surfaces of 3-D solid elements (here, SOLID186) with midsize nodes. It has the same geometric characteristics as the solid element face to which it is connected. Contact occurs when the element surface penetrates one of the target segment elements (TARGE170) on a specified target surface. Coulomb and shear stress friction is allowed.

TARGE170 is used to represent various 3-D target surfaces for the associated contact elements (CONTA174). The contact elements themselves overlay the solid, shell, or line elements describing the boundary of a deformable body and are potentially in contact with the target surface. This target surface is discredited by a set of target segment elements (TARGE170) and is paired with its associated contact surface via a shared real constant set.

PLANE182 Element Description PLANE182 is used for 2-D modelling of solid structures. The element can be used as either a plane element (plane stress, plane strain, or generalized plane strain) or an axisymmetric element. It is defined by four nodes having two degrees of freedom at each node: translations in the nodal x and y directions. The element has plasticity, hyper elasticity, stress stiffening, large deflection, and large strain capabilities. It also has a mixed formulation capability for simulating deformations of nearly incompressible elastoplastic materials and fully incompressible hyper elastic materials.

Table 3.7: Element Type, Graphic Pictorials and output application area

Elements	Graphic Pictorials	Element Output Data
SOLID186 3-D 20-Node Structural Solid 20 nodes 3-D space;DOF: UX, UY, UZ	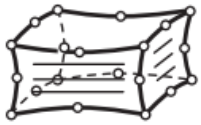	The element supports plasticity, hyper elasticity, creep, stress stiffening, large deflection, and large strain capabilities
CONTA174 3-D 8-Node Surface-to-Surface Contact 8 nodes 3-D space DOF: UX, UY, UZ, TEMP, VOLT, MAG	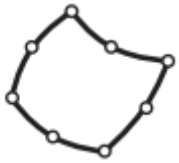	The element is used to represent contact and sliding between 3-D target surfaces and a deformable surface
TARGE170 Contact 3-D Target Segment 8 nodes 3-D space DOF: UX, UY, UZ, TEMP	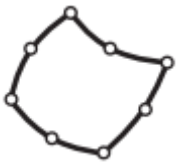	The element is used to represent various 3-D target surfaces for the associated contact elements
PLANE182 2-D 4-Node Structural Solid 4 nodes 2-D space DOF: UX, UY	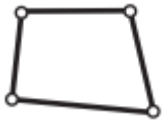	Either a plane element (plane stress, plane strain or generalized plane strain) or an axisymmetric element
PLANE183 2-D 8-Node Structural Solid 8 nodes 2-D space DOF: UX, UY	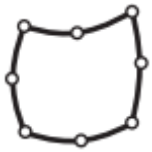	The element may be used as a plane element (plane stress, plane strain and generalized plane strain) or as an axisymmetric element.

3.21.1 Symmetry

Due to the double symmetry of the geometry and the stress applied to the skin, the analysis is performed on one quarter of the respective mounting plate and skin.

One fourth (¼) of the geometry can be modelled and the symmetry condition can be employed along both x and y (Figure (3.29,3.30 & 3.31)).

3.21.2 Loading and Boundary Conditions

The boundary conditions applied on each model is in such a way that the load is entered as a uniform tensile stress of in the hoop and longitudinal direction on two transversal aspects along x & y. In order to prevent motion of rigid body, movement and rotation from a point of sample got constrained.

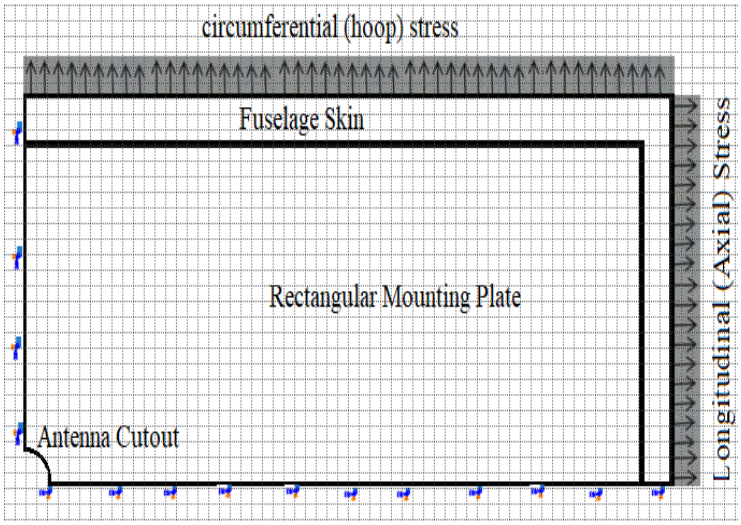

Figure 3.29: Loading and boundary conditions fuselage skin and rectangular mounting plate.

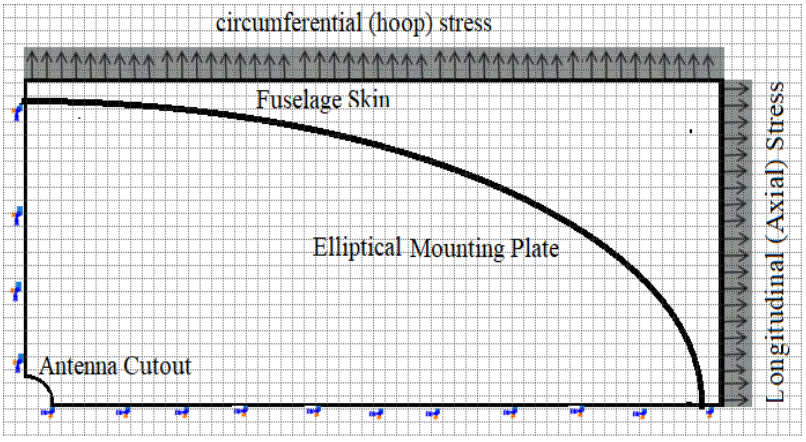

Figure 3.30: Loading and boundary conditions fuselage skin and an elliptical mounting plate.

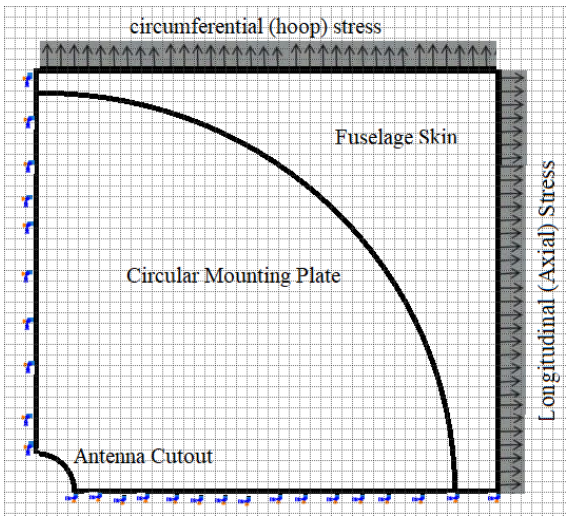

Figure 3.31: Loading and boundary conditions the fuselage skin and circular mounting plate.

4.7 Mesh convergence/ optimization

A method for verifying adequate mesh size is to perform a convergence check. This is performed by refining the mesh and evaluating the results (stress, deformation, strain etc.) until convergence occurs.

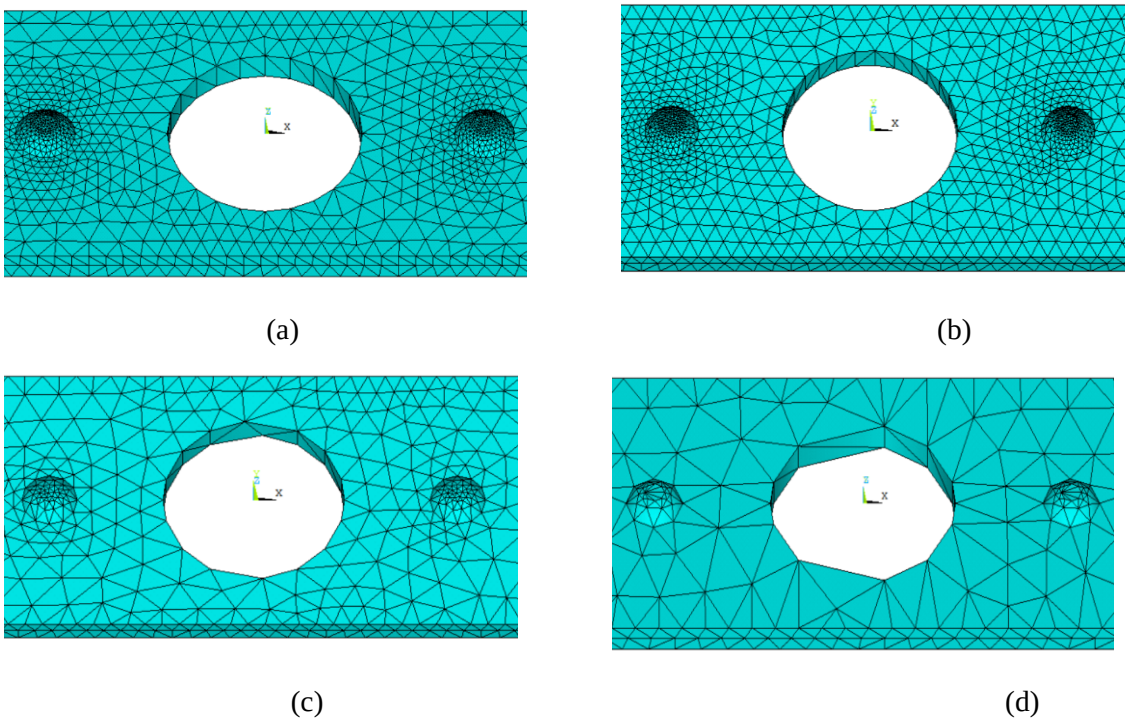

(a) (b)

(c) (d)

Figure 3.32: Close-up views of different mesh densities (a) very fine mesh (b) fine mesh (c) medium mesh (d) coarse mesh and Mesh Influence on Hole Representation

Table 3.8 Results of mesh refinement Number of Nodes, The Number of Elements and Mesh Densities for a strap of Mounting Plate, Skin Rivets Assembly

Mesh densities	Number Of Element	Number Of Node	SEVQ	Displacement Vector Sum	Total Mechanical Strain
Coarse	3854	7709	72.2436	13.5819	0.001447
Medium	8414	16358	73.7321	13.708	0.001508
Fine	29014	47291	74.177	13.7578	0.001499
Very fin	52010	81763	74.153	13.7749	0.001415

Table 3.9 Comparisons for different mesh densities for Von Mises Stress, displacement vector sum and total mechanical strain values

Mesh densities	**Von Mises stress**	**DISPLACEMENT VECTOR SUM**	**TOTAL MECHANICAL STRAIN**
Coarse	72.2436	13.5819	0.001447
Medium	73.7321	13.708	0.001508
Average	72.98785	13.64495	0.0014775
Maximum Difference	1.4885	0.1261	6.1E-05
Medium	73.7321	13.708	0.001508
Fine	74.177	13.7578	0.001499
Average	73.95455	13.7329	0.0015035
Maximum Difference	0.4449	0.0498	-9E-06
Fine	74.177	13.7578	0.001499
Very fin	74.153	13.7749	0.001415
Average	74.165	13.76635	0.001457
Maximum Difference	-0.024	0.0171	-8.4E-05

A chosen Von Mises stress, displacement vector sum, and total mechanical strain values at a specified point are compared for different mesh densities. The values of each parameter are converging to a single value as the mesh densities vary from coarse to medium, from medium to fine, and from fine to very fine.

Table 3.9 summarizes the average and maximum differences in stress values for different mesh densities. Changing mesh density from course to medium results in a 72.98785 MPa average and a 1.4885 MPa maximum difference in von Mises equivalent stress. Medium to fine mesh density shifting results in a 73.95455 MPa average and a 0.4449 MPa maximum difference. The fine to very fine mesh density transition results in a 74.165 MPa average and a 0.024 MPa maximum difference. 0.024 MPa corresponds to less than 1% of the average stress. The same is true for displacement vector sum and total

mechanical strain. The differences in fine to very fine mesh density transition are relatively small compared to the others. Therefore, it is needless to use very fine mesh densities, keeping in mind the computation time needed for the analysis. Thus, fine mesh density is utilized throughout the study.

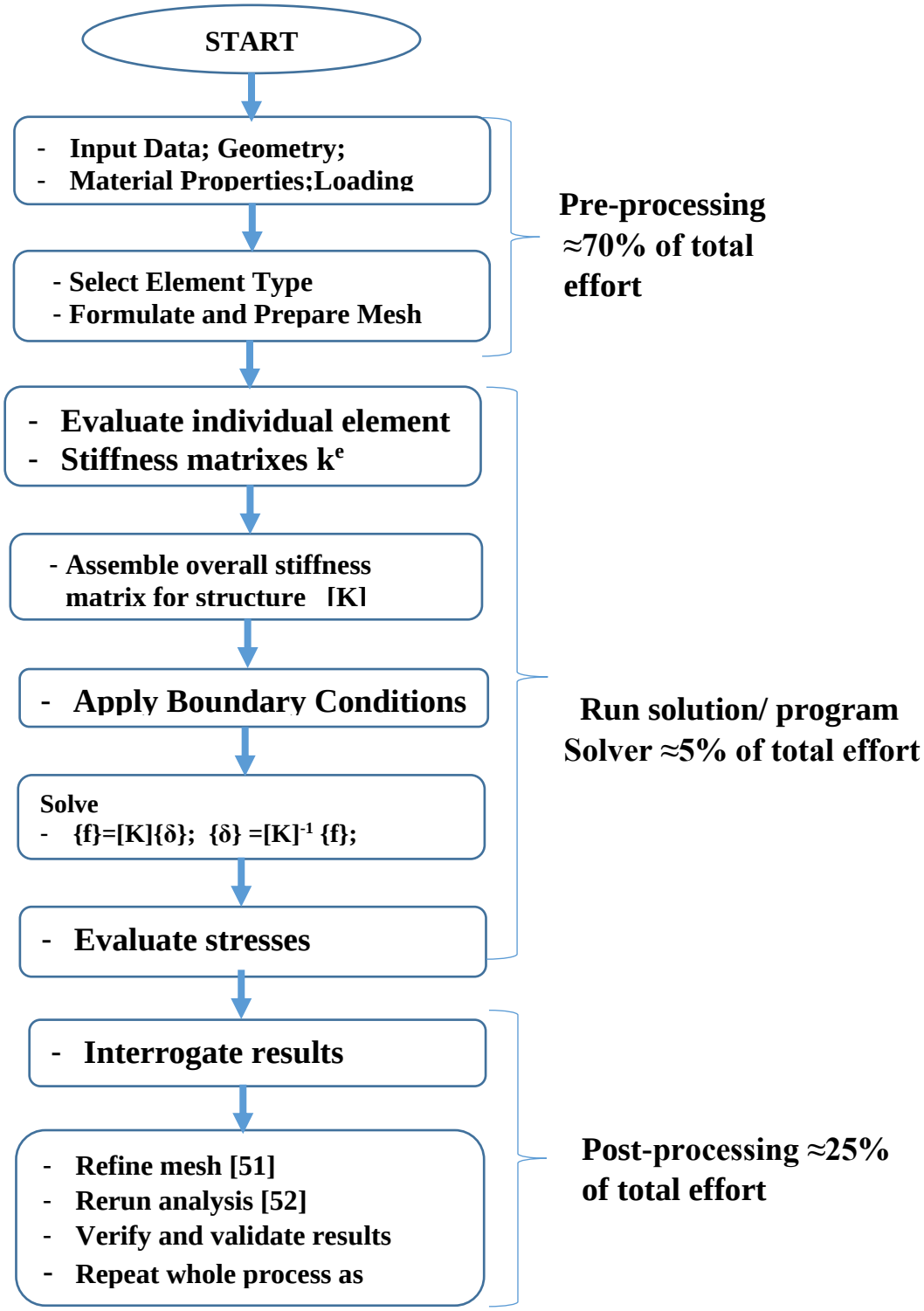

Figure 3.33: FEM steps analysis process –Mounting plate structural simulation

3.22 The Analytical Modelling for Specific Objective III

3.22.1 Damage tolerance analysis for Antenna installation and establishing inspection type and inspection threshold (Damage Detection)

3.22.2 Crack Tip Stresses

3.22.3 Crack Extension Modes

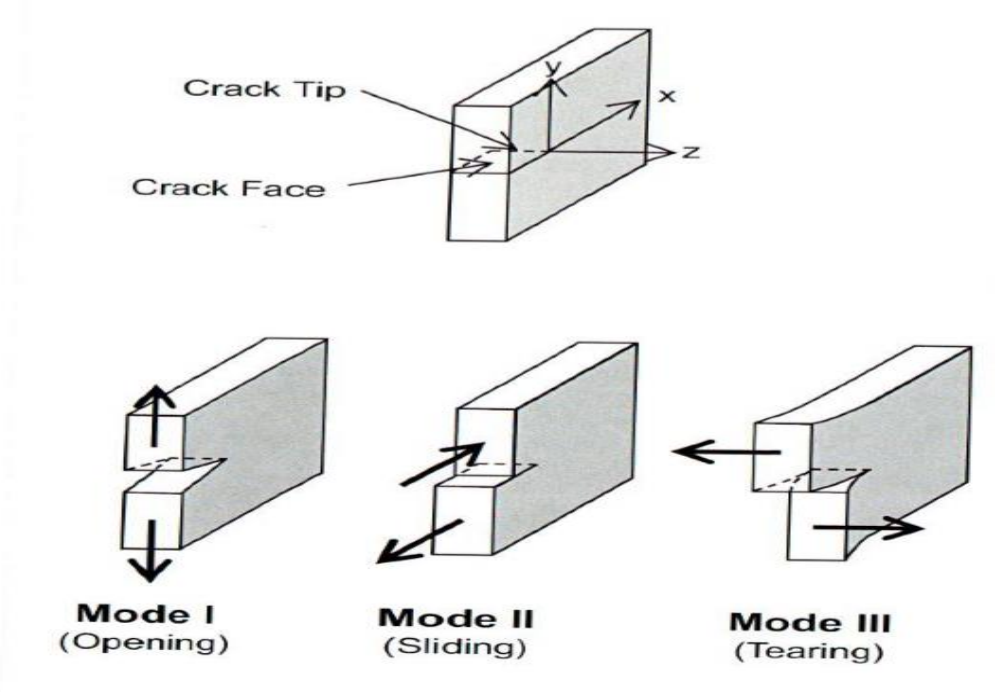

Figure 3.34 Fracture Mechanics Crack Extension Modes [53-55]

3.22.4 Mode I Crack Tip Stress Distribution

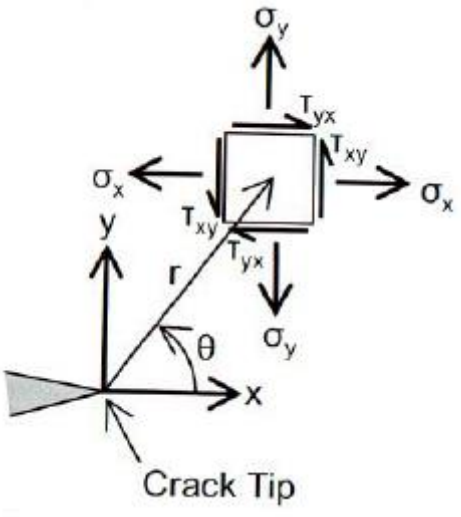

$$\sigma_x = \frac{K}{\sqrt{2\pi r}}\cos\left(\frac{\theta}{2}\right)\left[1 - \sin\left(\frac{\theta}{2}\right)\sin\left(\frac{3\theta}{2}\right)\right] \quad (3.39)$$

$$\sigma_y = \frac{K}{\sqrt{2\pi r}}\cos\left(\frac{\theta}{2}\right)\left[1 + \sin\left(\frac{\theta}{2}\right)\sin\left(\frac{3\theta}{2}\right)\right] \quad (3.40)$$

$$\tau_{xy} = \frac{K}{\sqrt{2\pi r}}\sin\left(\frac{\theta}{2}\right)\left[\cos\left(\frac{\theta}{2}\right)\cos\left(\frac{3\theta}{2}\right)\right] \quad (3.41)$$

Where: r= distance from a right hand crack tip (in.)

θ =Angle from the horizontal axis (degrees)

K=Stress intensity factor (ksi√in)

3.22.5 Linear Elastic Fracture Mechanics

During the crack initiation phase, crack growth was dependent on surface effects and localized stress concentrations, $\mathbf{K_t}$. During the crack growth phase, the crack tip is essentially a notch with a zero radius. Calculating the $\mathbf{K_t}$ for such a notch would result in an infinite stress concentration factor. This is also apparent from the equation for stress near the crack tip; as r approaches zero, stress increases inversely with the square root of r [56-59]

Stresses at the crack tip are high but not infinite. There is a plastic zone surrounding the crack tip, but the size of that zone compared to the size of the part is typically small. The stress intensity factor, K, has

been developed to define the stresses in the area near a crack tip. Prediction of fatigue crack growth using the stress intensity factor is referred to as "Linear Elastic Fracture Mechanics," or LEFM.

3.22.6 Stress Intensity Factor

Griffith was the first to recognize there was a linear relationship between stress near a crack tip and the far field stress times the square root of the crack length and specific material properties. The product was related to the strain energy release rate. Irwin developed the stress intensity factor as a parameter that quantified the crack tip driving force, which was directly related to Griffith's strain energy release rate. These two gentlemen are considered the father of fracture mechanics. [60-62].

The commonly used formula for the stress intensity factor is:

$$K = \beta * \sigma * \sqrt{(\pi * a)} \qquad (3.42)$$

Units are ksi $in.^{1/2}$

Where:

β = Geometric constant (unit-less)

σ =Far filed stress (ksi)

a =Crack length (in) (2a used for centre cracks, a for edge cracks)

The geometry factor is dependent on loading crack location (centre or edge cracks) and panel configuration. Some panel configurations include

- An infinite plane with a single centre crack
- An infinite panel with an infinite row of collinear cracks
- A semi-infinite plate with a single edge cracks
- A finite panel with a single centre crack
- A finite panel with a single edge crack
- A finite panel with cracks on both edges

Geometry factors are typically a function of panel configuration, crack configuration and location loading, and possibly crack length. Some, like the semi-infinite plate with a single edge crack, are constant.

3.22.7 Residual strength

The tension statistic strength of a simple structural element is defined as stress times net area (F_{tu}* A_{net}). This definition is not valid when a crack exists in the structure. The stress intensity produced by the crack reduced the load caring capability more than would be expected due to the net area loss alone. Tension load caring capability of a partial cracked metallic structure can be derived by:

$$P = K * \frac{A_{gross}}{[\beta * \sqrt{\pi * a}]} \quad (3.43)$$

The remaining load-caring capability of the structure with damage present is known as its residual strength capability.

The residual strength requirement is the lowest strength capability allowed that will meet fail-safe load requirements for a given crack size. Typically, the requirement for residual strength is at or above the designer's limit loads. Residual strength requirements can be higher depending on the controlling agency.

3.22.8 Resistance to Fatigue

Fracture toughness (K_c) is a mechanical property that measures a material's resistance to fracture. K_c characterizes the stress intensity at the crack tip when rapid crack growth takes place, the point at which the crack is exhibiting unstable growth to failure. Fracture toughness can vary depending on the temperature and applied load.

3.22.9 Critical Crack Length

The stress intensity factor can be used along with Fracture toughness (Kc) to determine critical crack length. The formula previously given for stress intensity is rearranged to solve for the critical stress σ associated with a crack length producing.

$$\sigma_{RS} = \frac{K_C}{[\beta * \sqrt{\pi * a}]} \quad (3.44)$$

This equation can be used, with an appropriate geometry factor, to plot a curve of stress versus crack size. Such a curve can then be used by the analyst to determine either a critical length for specific stress level.

It should be noted that the critical crack length formula is not the only value that should be consider when determining residual strength. Material yield stress should also be considered.

3.22.10 Crack Growth Assessment

Paris' law (also known as the Paris–Erdogan equation) is a crack growth equation that gives the rate of growth of a fatigue crack. The stress intensity factor K characterizes the load around a crack tip and the rate of crack growth is experimentally shown to be a function of the range of stress intensity ΔK seen in a loading cycle. The Paris equation is

$$\frac{da}{dN} = C(\Delta K)^m \qquad (3.45)$$

Where a is the crack length and da/dN is the fatigue crack growth for a load cycle N. The material coefficients c and m are obtained experimentally and also depend on environment, frequency, temperature and stress ratio. [49-62] The stress intensity factor range has been found to correlate the rate of crack growth from a variety of different conditions and is the difference between the maximum and minimum stress intensity factors in a load cycle and is defined as

$$\Delta K = K_{max} - K_{min} \qquad (3.46)$$

Being a power law relationship between the crack growth rate during cyclic loading and the range of the stress intensity factor. The Paris–Erdogan equation can be visualized as a linear graph on a log-log plot, where the x-axis is denoted by the range of the stress intensity factor and the y-axis is denoted by the crack growth rate (see Figure 3.30).

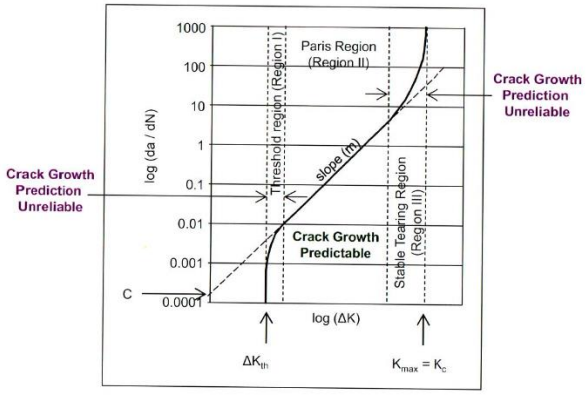

Figure 3.35: A typical plot of crack growth rate with respect to the stress intensity range where the Paris–Erdogan equation fits the central, linear region of Regime B. [62]

Paris–Erdogan equation can only approximate one linear segment for a serious of material crack growth curves and incorrectly implies the same da/dN for different mean stress.

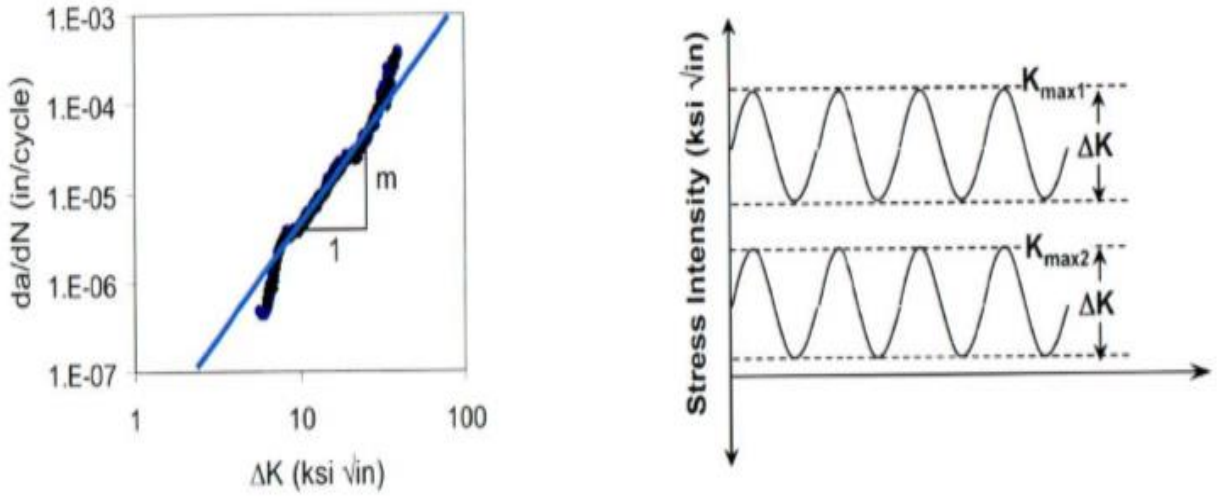

Figure 3.36 Fracture Mechanics Crack Extension Modes. [53-62]

Walker Equation

In 1970, K. Walker published a modified version of the Paris equation that accounts for increasing crack growth rate with increasing stress ratio, R

The Walker equation is a generalization of the Paris equation to account for the effect of stress ratio R on crack growth rate. The Walker equation takes the following form:

$$\frac{da}{dN} = C\left[\frac{\Delta K}{(1-R)^{(1-n)}}\right]^m \tag{3.47}$$

The walker equation can also be defining as

$$\frac{da}{dN} = C[(1-R)^n . K_{max}]^m \tag{3.48}$$

The Walker equation, like the Paris equation, can approximate the linear segment of material crack growth curves. It also includes stress ratio effects to account for different mean stress levels. It can, therefore, approximate several linear segments of crack growth curves based on R. If R = 0, the Walker equation becomes the Paris equation.

$$R = \frac{K_{min}}{K_{max}} \tag{3.49}$$

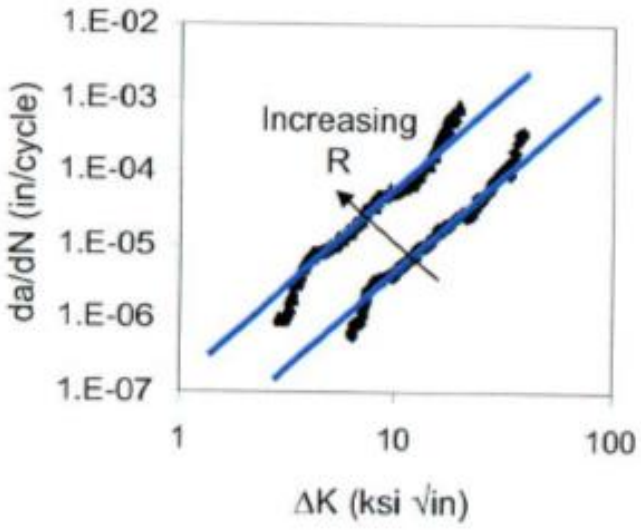

Figure 3.37 Fracture Mechanics Crack Extension Modes. [56]

Recall that the stress intensity factor is a function of geometry and applied stress:

$$= \beta * \sigma * \sqrt{\pi * a} \qquad (3.50)$$

Where σ is the applied stress, 'a' is the crack size, and β is a dimensionless geometry factor that is dependent on the geometry of the crack, the geometry of the part, and the loading configuration.

The values "β" and "a" are dependent on geometry, so for a specified crack and part geometry, the stress intensity factor is proportional to the applied stress. Therefore, we can define the following:

Table 3.10: Shows Maximum Stress Intensity, Minimum Stress Intensity, Stress Intensity Range, and Stress Ratio for Fatigue Life Analysis.

Maximum stress intensity:	$K_{max} = \beta\sigma_{max}\sqrt{\pi * a}$
Minimum stress intensity:	$K_{min} = \beta\sigma_{min}\sqrt{\pi * a}$
Stress intensity range:	$\Delta K = K_{max} - K_{min}$
Stress ratio (R-ratio):	$R=K_{min}/K_{max}$

Note that: if the definitions for maximum and minimum stress intensity are substituted into the definition for the stress intensity range, a new, useful definition for the stress intensity range can be obtained: Another useful relationship can be derived by combining the equations for stress intensity range and R-ratio:

$$\triangle K = K_{min}(1 - R) \qquad (3.51)$$

Chapter Four

4. The Mathematical Modelling for Specific Objectives

4.1 The Analytical Modelling for Specific Objective I

4.1.1 Elliptical antenna mounting-plate compare with circular and rectangular MP.

Three common types of antenna installation are considered. They differ only in the shapes of their mounting plates: rectangular, circular, and elliptical, as shown in Figure 4.1, and they have the same area. The mounting plates are mechanically fastened to the skin around the cut-out using rivets.

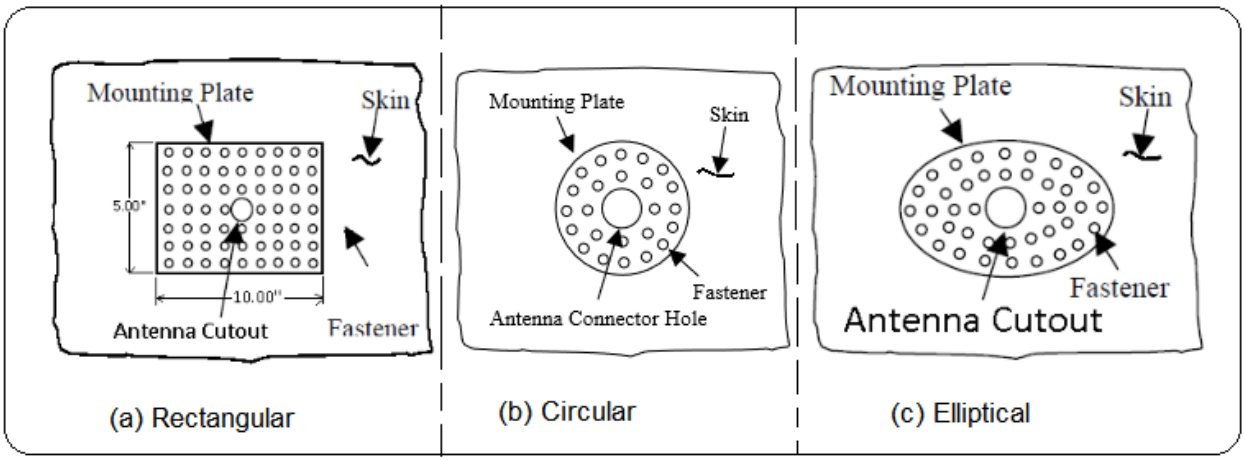

Figure 4.1: Three Types of Antenna Installation

Static Strength Analysis

P_{pu}= 17,892 lb rectangular mounting plate

P_{pu} = 20,826.54lb for elliptical

P_{pu}=31,311lb for circular

The skin internal force, P_p, is calculated using the equation

$$P_p=\sigma_U D t_s$$

Where σ_U and t_s are the design ultimate tensile stress and thickness of the skin, respectively. σ_U = the lesser of F_{tu} or F_{ty} *1.5

P_p = 63000*1*0.063

= 3969lb

$$\text{Margin of safety} = \frac{\text{Ppu}}{\text{Pp}} - 1$$

Margin of safety = (17,892/3969)-1 = 4.51 -1 = 3.51

Margin of safety based on mounting plate

= 3.51 for rectangular mounting plate

=6.88 for circular mounting plate

= 4.23 for elliptical mounting plate

The Fastener Joint Allowable and Margin of Safety and Fastener Joint Allowable in Straight Shank Holes. using equation 3.13 and 3.14 at page 31 calculated as follow.

- For Rectangular mounting plate P_{su}=1874.2*44=82465Lbs
- For Elliptical circular mounting plate
- For Circular mounting plate P_{su}=1874.2*40=74968.22 Lbs
- For solid protruding head rivets having diameter of d=0.025” $Psu = Fsu * Af * SCF1$

  = 39000*pi*0.25” ^{2}*0.979/4

  =1874.2 lbs/Rivet.

The hole bearing allowable for the straight shank hole is calculated using the following equation

$$P_{bru} = F_{bru} * d * t$$

In which F_{bru} is the ultimate bearing stress of the plate (skin or mounting plate) material, d is the fastener hole diameter, and t is the thickness. Currently, the F_{bru} is for the case edge distance to hole diameter (e/d) equal to 2.0.

F_{bru}=the lesser of F_{bru} or F_{bry} *1.5

114 or 1.5*79 =118.5

P_{bru} = 114 *0.25*0.063

P_{bru} = 1795.5 lb.

- For Rectangular mounting plate P_{bru} =1795.5 *44=79,002.00 Lbs
- For Elliptical circular mounting plate
- For Circular mounting plate P_{bru} =1795.5 *40=71820.00 Lbs.
- For solid protruding head rivets having diameter of d=0.25” F_{bru}=the lesser of F_{bru} or F_{bry} *1.5

  114 or 1.5*79 =118.5

  P_{bru} = 114*0.25*0.063

  = 1795.5 lb / rivet

P_{su}: single shear allowable for straight shank holes =1874.2 lbs.

P_{bru}: hole bearing allowable for the straight shank =1795.5 lbs.

The joint allowable for a given joint is the lower of P_{su} or P_{bru} denoted by P_{joint} in this case P_{bru} is less than $P_{su.}$ Therefore, the joint allowable P_{joint}=1795.5 lbs.

Fastener Joint Margin of Safety

The fastener joint margin of safety is determined by using equation (3.16) & (3.17)

F_{bru}=the lesser of F_{bru} or F_{bry} *1.5

114 or 1.5*79 =118.5

P_{total} = $P_{bru\ for\ skin}$ = 114 *0.25*0.063

= 1795.5 lb

P_{total} =$P_{bru\ for\ mounting\ plate}$ = 114 *0.25*0.071

= 2023.5 lb.

An applied load is needed to determine a margin of safety. That load is the ultimate applied load to the structure, or if that is not known, then the tensile ultimate strength of the material F_{tu} is used. This applied load $P_{applied}$ is given by

$$P_{applied} = \sigma_u * D*t_s$$

Where: -

σ_u: Lesser of F_{tu}=63000 or F_{ty}*1.5 =47,000 *1.5= 70500.00

t_s: is the skin thickness,

D: is the diameter of antenna connector cut-out hole.

- For rectangular mounting plate
- For elliptical mounting plate
- For circular mounting plate
- D: is the diameter of antenna connector cutout hole D=1”

$P_{applied} = \sigma_u * D*t_s$

= 63000*1” *0.063

= 3969lbs.

$$\text{Fastener Joint Margin of safety} = \frac{\text{Ptotal}}{\text{Papplied}} - 1$$

Fastener Joint Margin of Safety

- For rectangular mounting plate 18.899
- For elliptical mounting plate
- For circular mounting plate 17.09

Table 4.1: Analytical comparison of the mounting plate with each other

	Independent Criteria	Rectangular Mounting Plate	Circular Mounting Plate	Elliptical Mounting Plate
1	The Mounting Plate Allowable and Margin of Safety MS*	3.51	6.88	4.23
2	The Fastener Joint Allowable	79,002.00 lbs	71,820.00 lbs	79,002.00 lbs
3	Fastener Joint Margin of Safety MS*	18.899	17.09	18.899
4	The Shear Margin of Safety MS*	0.1269	0.1269	0.1269
5	Stiffness Ratio **	1.1269	1.1269	1.1269
6	The fastener bending(Q)***	0.536	0.536	0.536
7	Number of rivets used for same area	44	40	44

*The margins of safety (MS) based on the mounting plate allowable and the fastener joint allowable were calculated to determine the adequacy of the antenna installation on fuselage skin.

- MS < 0 Antenna installation is statically inadequate
- MS = 0 Antenna installation is marginally adequate
- MS > 0 Antenna installation is statically adequate

**The antenna installation is considered adequate if the ratio is between 1.0 and 1.5. The antenna installation is too stiff when the value is greater than 1.5 and not stiff enough when it is less than 1.0.

***For aluminium fasteners, the bending is important. A Q value above 2 may indicate that the aluminium rivet will not fill the hole but instead may buckle in the hole

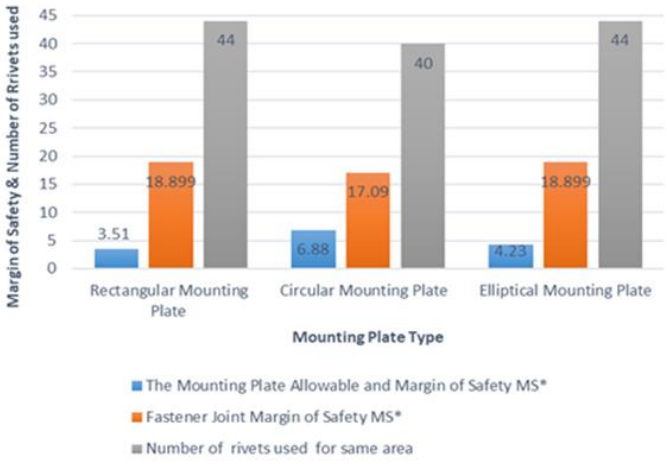

Figure 4.2: Graphical Representation of mounting plate allowable margin of safety fastener joint margin of safety and number of rivet utilized

Inference:

1. The mounting plate allowable for circular mounting plate is the highest compared with rectangular and circular mounting plate.
2. Fastener joint margin of safety influenced by number of rivets not by mounting plate shape
3. Number of rivets' used for the same area with different shape of mounting plate circular mounting plates has less than the other two.
4. Fastener joint margin of safety for rectangular and elliptical mounting plate are same value and higher than circular mounting plate.
5. Using mounting plate with shape rectangular or elliptical obliged usage of additional four (4) rivets which means additional material and maintenance cost and direct impact increasing stress concentration on the fuselage skin.
6. Fastener joint margin of safety for rectangular and elliptical mounting plate compare with rectangular mounting plate, the percentage of error Is less than 10%(i.e. 0.095)
7. Stiffness Ratio for same material it is a function of sheet metal thickness i.e. skin thickness t_s and mounting plate thickness-$t_{mp.}$
8. The Shear Margin of Safety, The Fastener Joint Allowable and Stiffness Ratio for same material mounting plate and fastener the result is same therefore special attention should be given for mounting plate allowable & Fastener joint margin of safety.
9. From preparation of the mounting plate and rivet pattern rectangular mounting plate is relatively easy compare with circular and elliptical mounting plate.
10. **Circular mounting plate relatively better than that of rectangular mounting plate and elliptical mounting plate.**

4.2 The Analytical Modelling for Specific Objective II

4.2.1 Gross Area Stress Concentration Factor for MP with different antenna cut out compared.

Table 4.2: Analytical result of K_{tg}: for different geometrical cut-out

Cutout Type	σ Peak stress [Mpa]	σ Remote OR (Far-Field) Uniform Stress[Mpa]	K_{tg}: Gross Area Stress Concentration factor
Horizontal Ellipse	580.00	140	4.8333
Lateral Ellipse	340.00	120	3.8333
Square	420.00	140	2.5500
Circular	300.0	140	2.1428

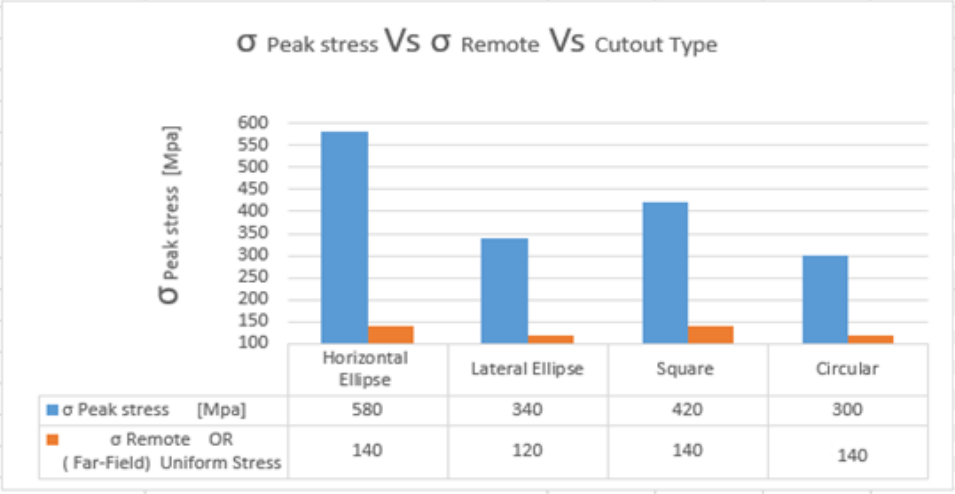

Figure 4.3: σ Remote - (Far-Field) Uniform Stress, peak stress Vs Antenna Cut-out Type

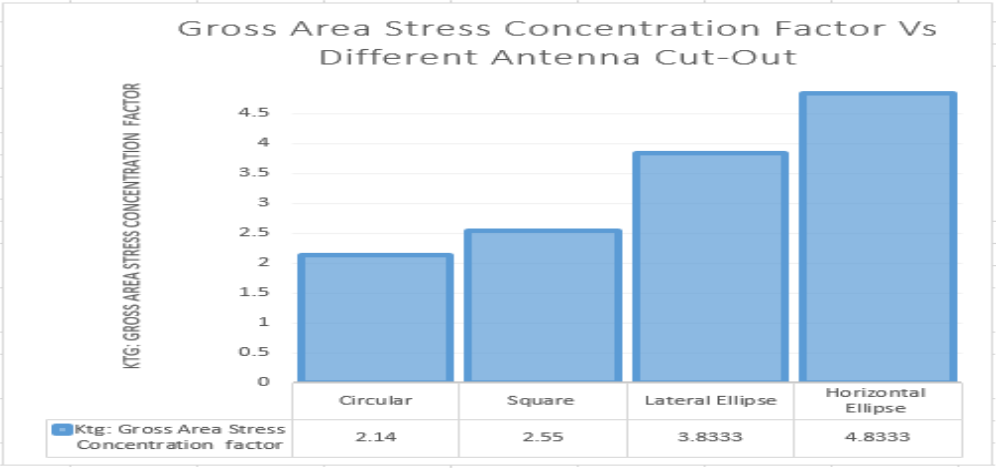

Figure 4.4: Gross Area Stress Concentration Factor Vs Different Antenna Cut-Out

Inference:

i. For a given biaxial load applied on the plate, the Gross Area Stress Concentration factor for different geometries of cut out was compared and found to vary from 2.14 for circular cut out, 2.55 for square cut out, 3.833 for lateral elliptical cut out, and finally 4.833 for elliptical horizontal cut out.

ii. An antenna cut out with shape of a circular cut out has a relatively lower Ktg: Gross Area Stress Concentration factor

iii. In line with the maximum loading Ktg: Gross Area Stress Concentration factor, which is relatively minimized, consider cut out with a horizontal ellipse (major axis aligned along the longitudal axis) and a lateral ellipse (major axis aligned along the radial/hoop direction).

iv. Cut out with its maximum direction is perbendicular to the maximum crosswise loading has maximum K_{tg}: Gross Area Stress Concentration factor.

v. Considering Figure **3.23** ,Resultant force /stress i.e.$\sqrt[2]{{\sigma_1}^2 + {\sigma_2}^2}$ and its direction $\theta = \tan^{-1}\frac{\sigma_1}{\sigma_2}$ that means the segment length of the cut out along which the resultant vector cover directly affect the value of K_{tg}: Gross Area Stress Concentration factor for horizontal ellipse (majore axis aligne along the longitudal axis) and lateral ellipse (majore axis aligne along the radial /hoop direction).

vi. square cut out with a side length equal to the diameter of a circular cut out, which is less than or equal to 1 inch, and with a fillet radius of the square is one third of the length of the side of the square. Ktg: The Gross Area Stress Concentration factor is between circular and elliptical cutouts with lateral direction.

vii. Analytically, an antenna cut out with a geometrically circular cut out is selected because of the biaxial load; the circular cut out has a relatively low K_{tg}: Gross Area Stress Concentration factor.

4.2.2 The Finite Element modelling of antenna mounting plates

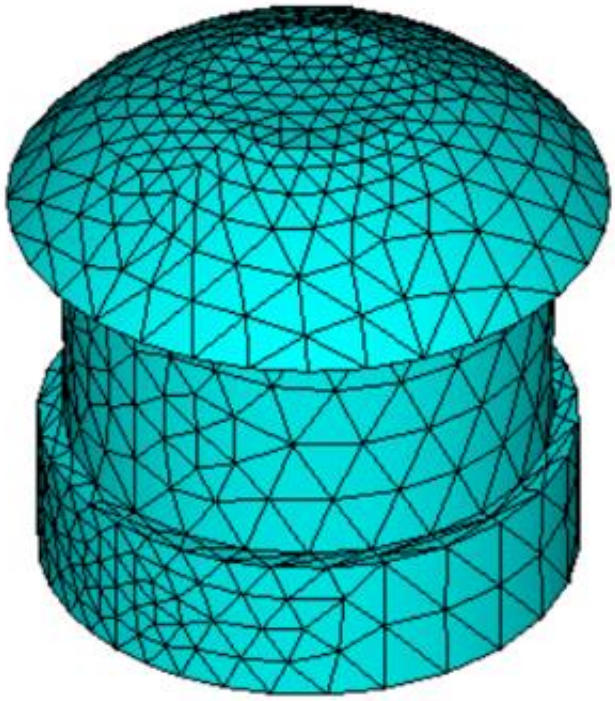

Figure 4.5: Finite element model of rivet

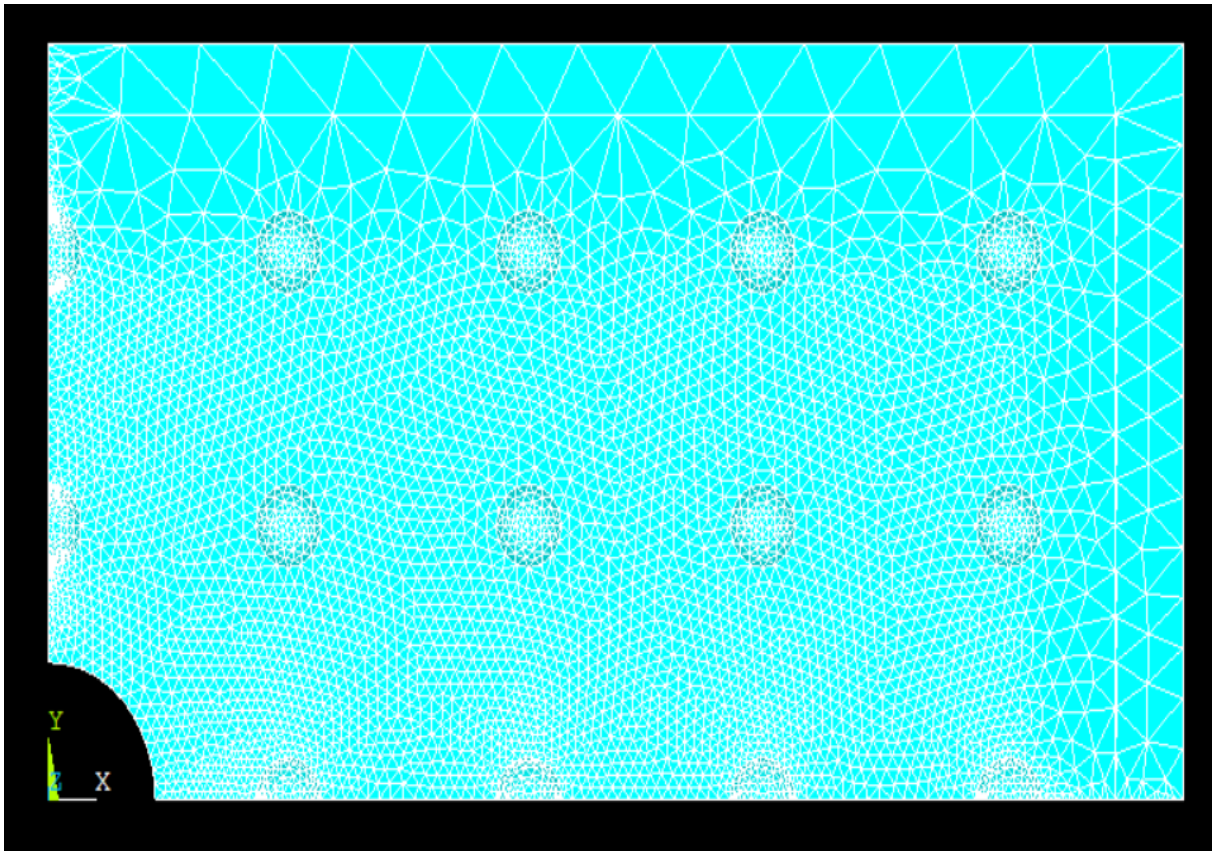

Figure 4.6: Rectangular Mounting Plate with 2D

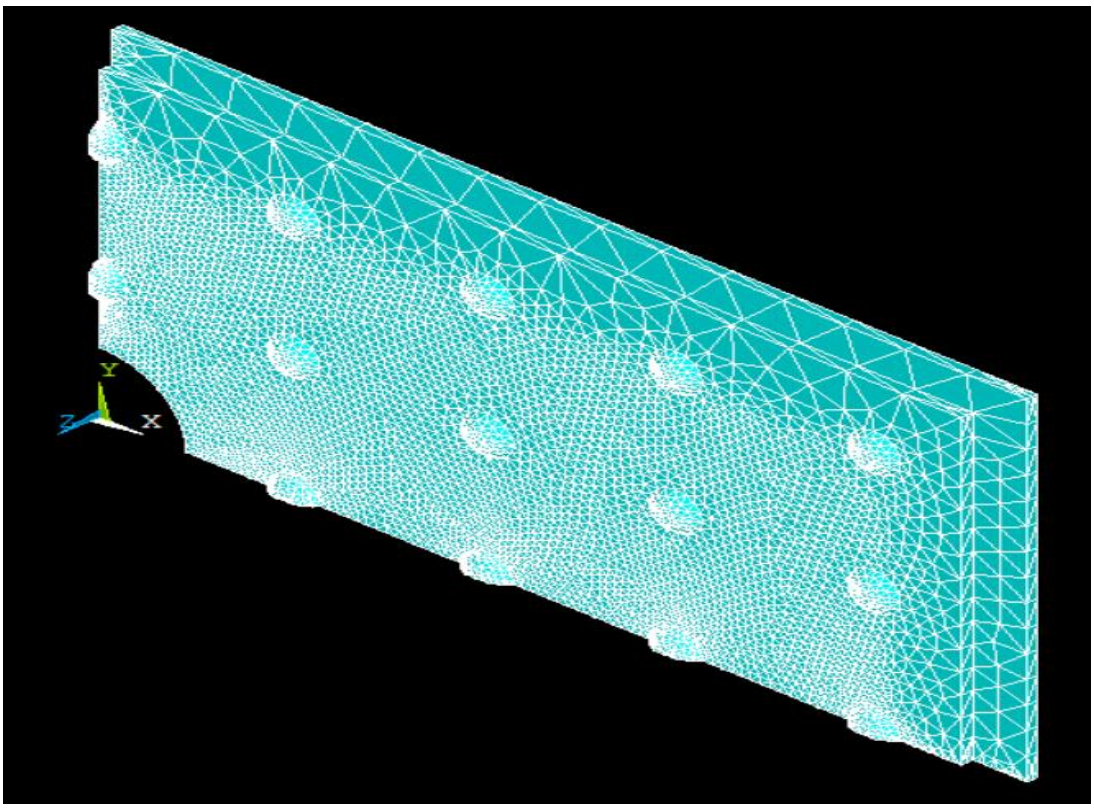

Figure 4.7: Rectangular mounting plate with 3D

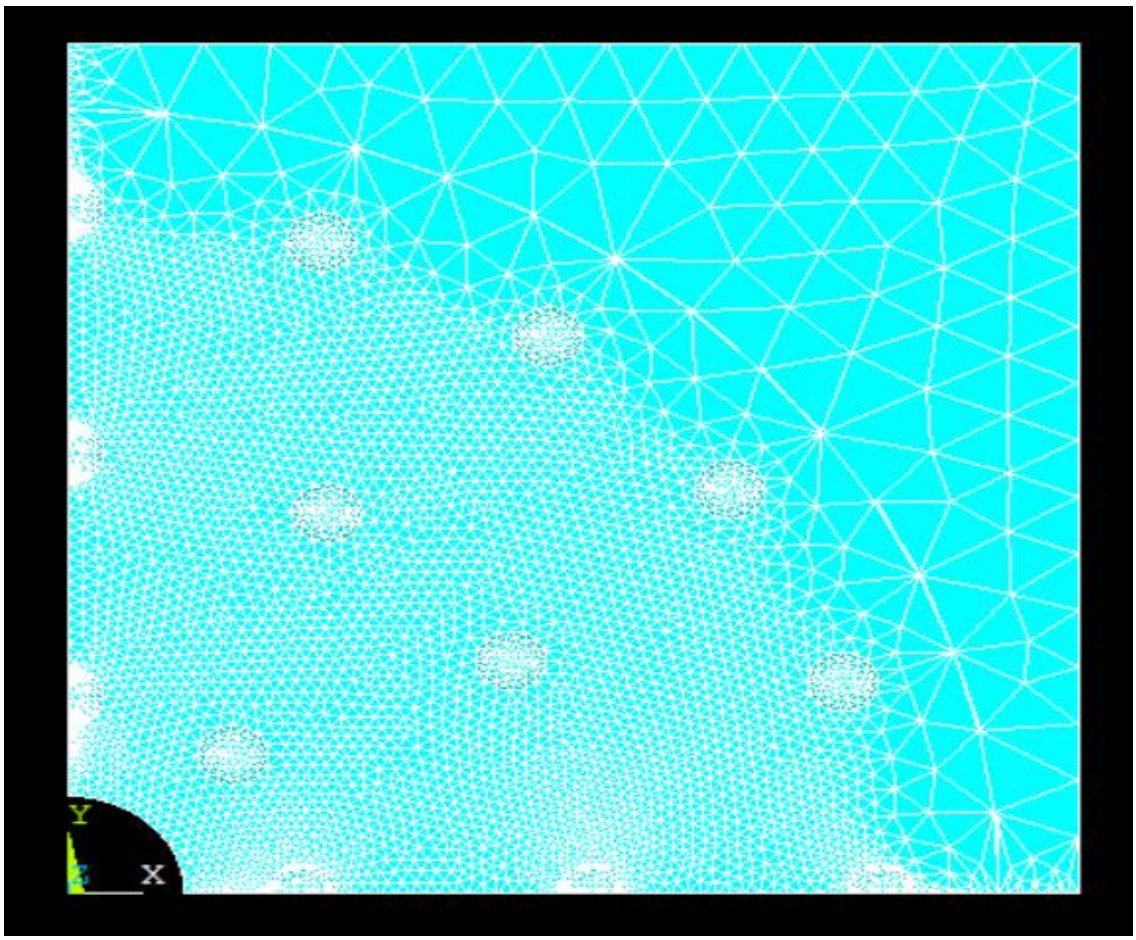

Figure 4.8: Circular mounting plate with 2D

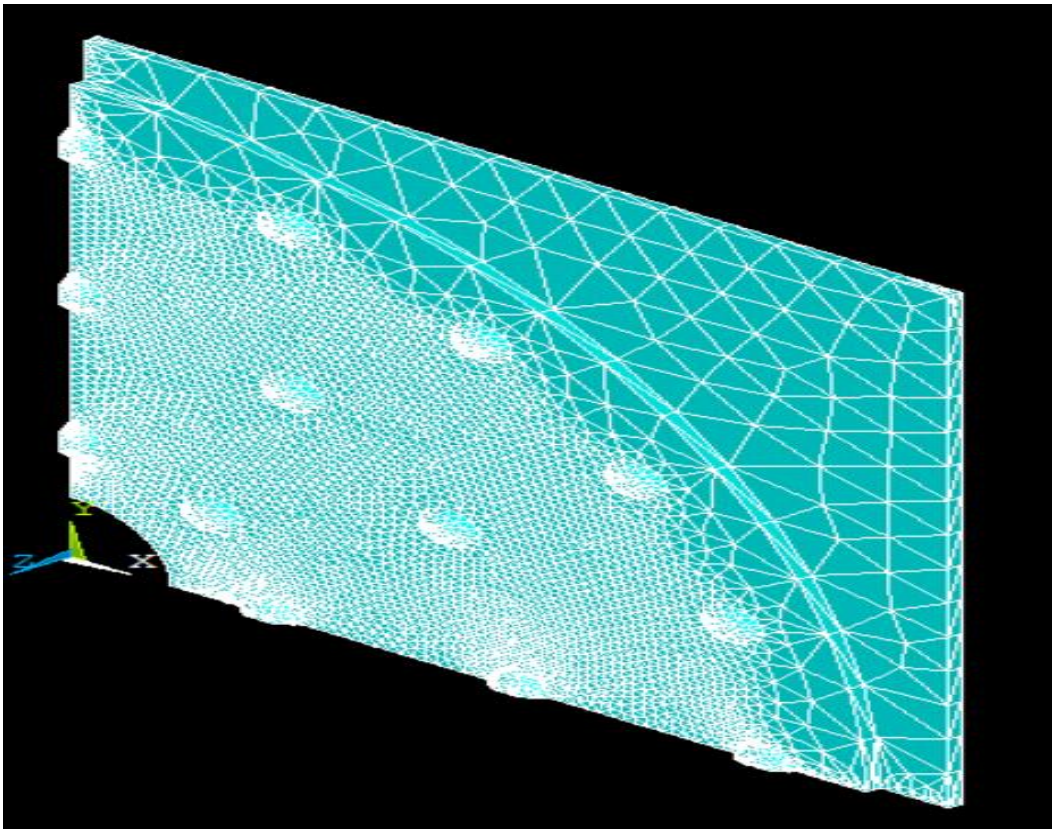

Figure 4.9: Circular mounting plate with 3D

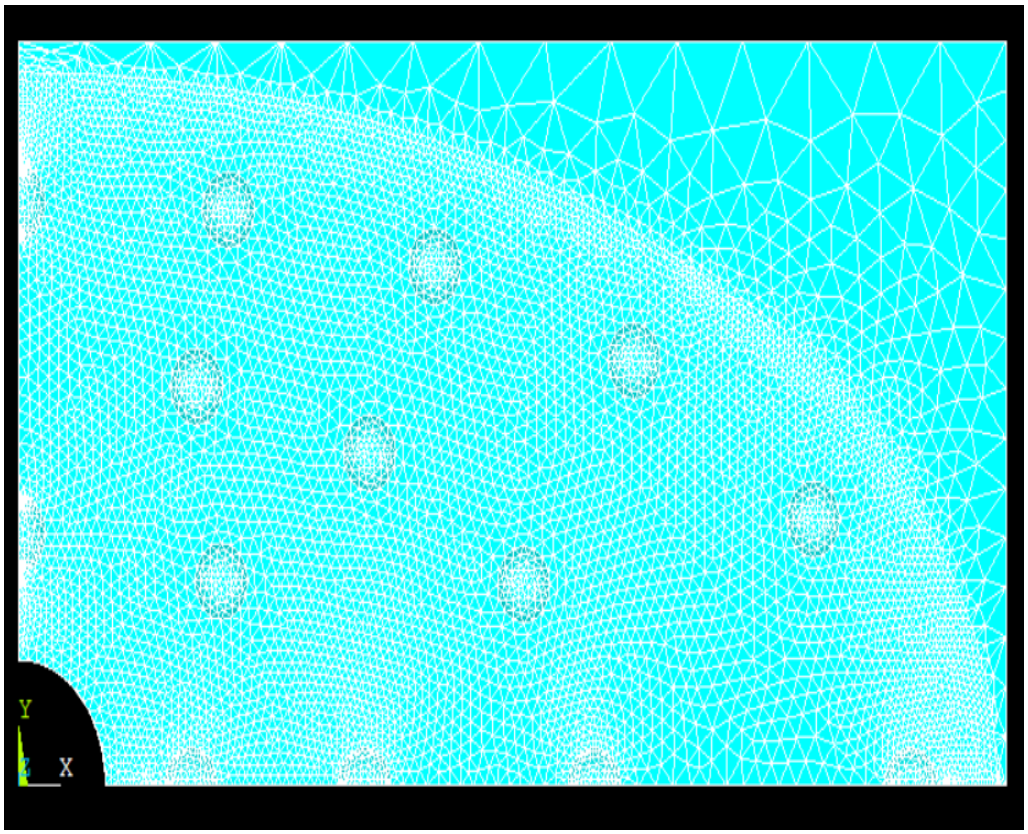

Figure 4.10: Elliptical mounting plate with 2D

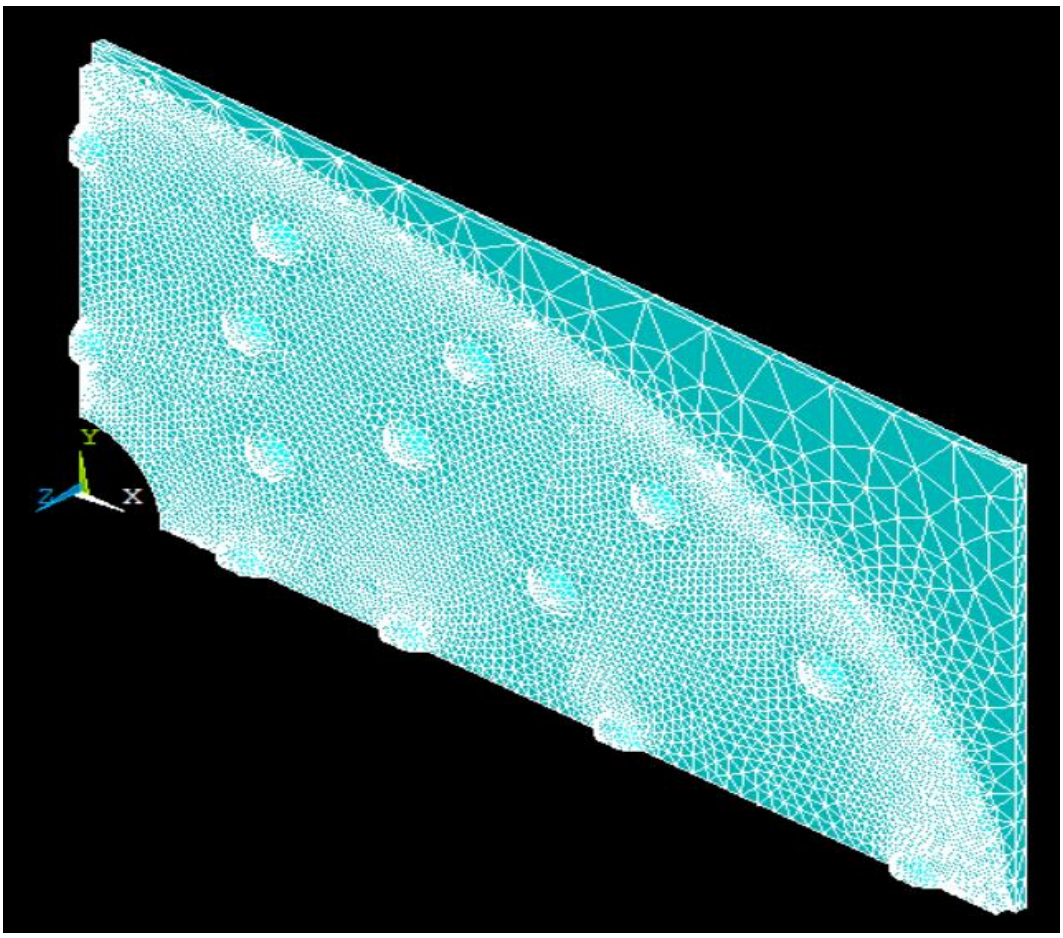

Figure 4.11: Elliptical mounting plate with 3D

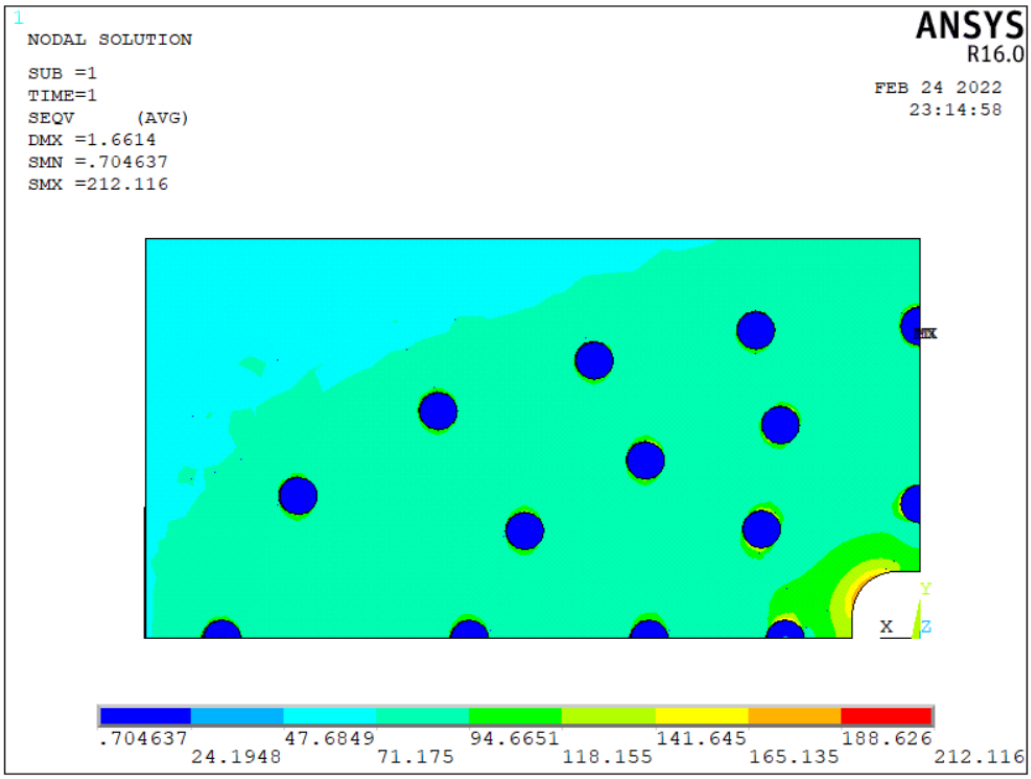

Figure 4.12: Nodal solution for Von Mises Stress distribution [MPa] of an elliptical mounting plate with a square cut-out.

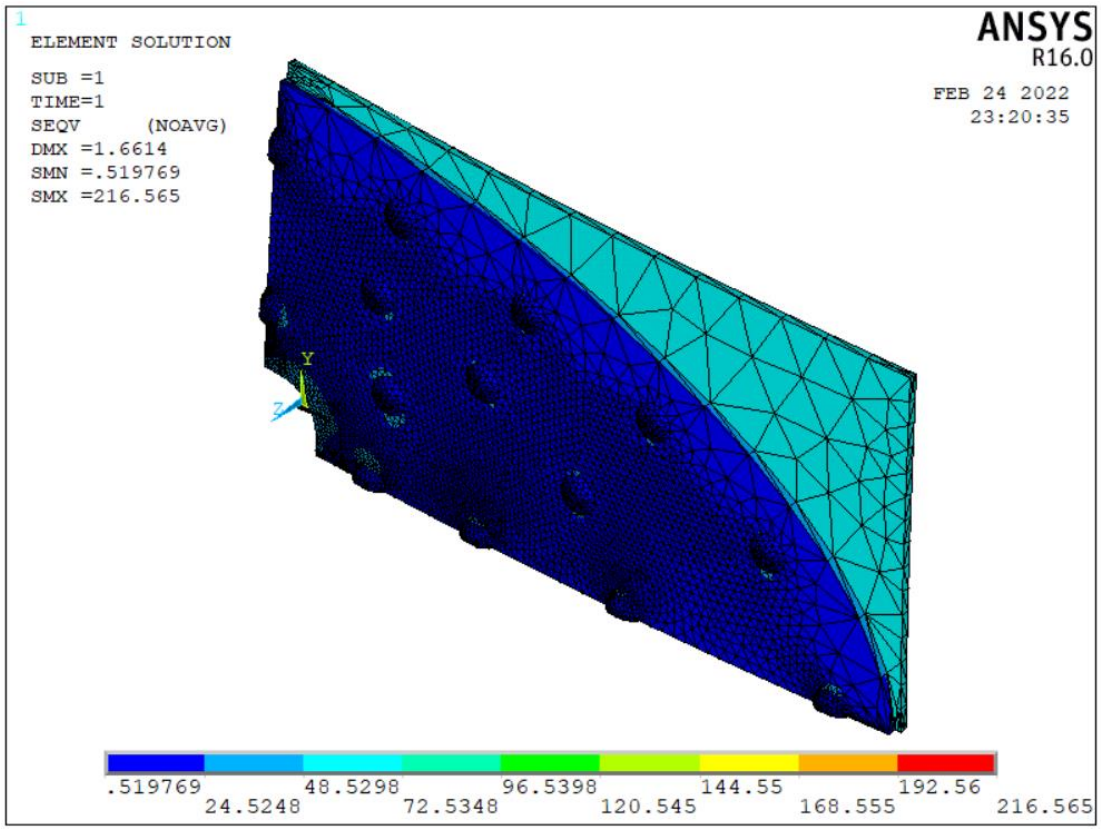

Figure 4.13: Element solution for Von Mises Stress distribution [MPa] of an elliptical mounting plate with a square cut-out.

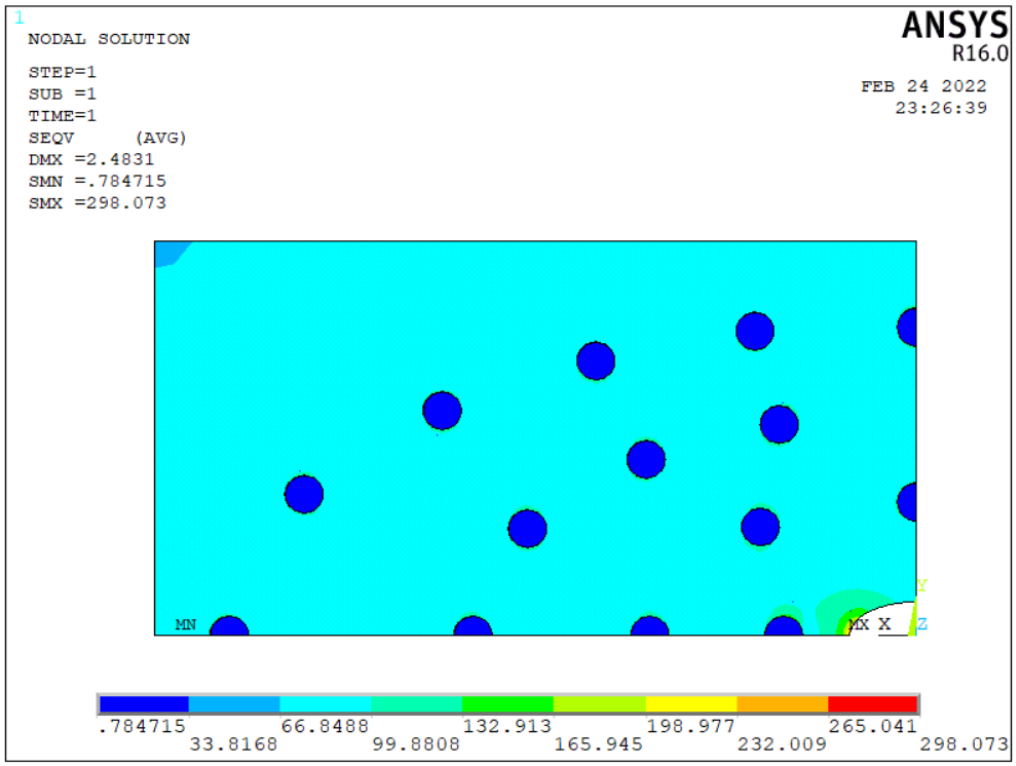

Figure 4.14: Nodal solution for Von Mises Stress distribution [MPa] of an elliptical mounting plate with an elliptical cut out along the longitudinal axis, i.e., the major diameter tip of the elliptical cut out along the longitudinal axis,

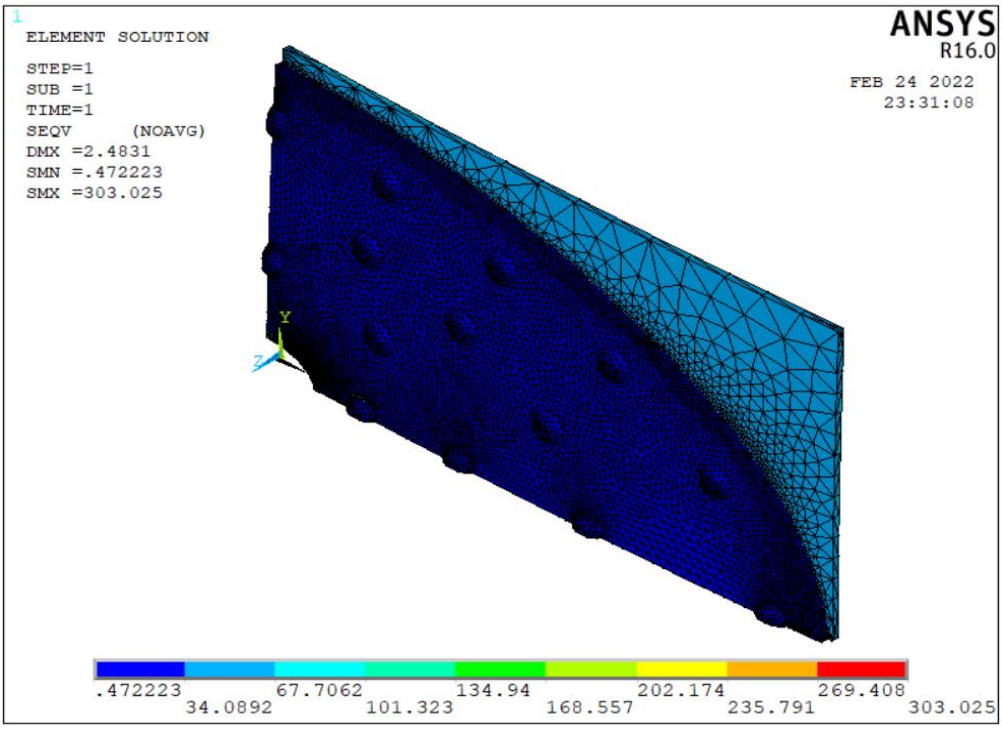

Figure 4.15: Element solution for Von Mises Stress distribution [MPa] of an elliptical mounting plate with an elliptical cut out along the longitudinal axis, i.e., the major diameter tip of the elliptical cut out along the longitudinal axis.

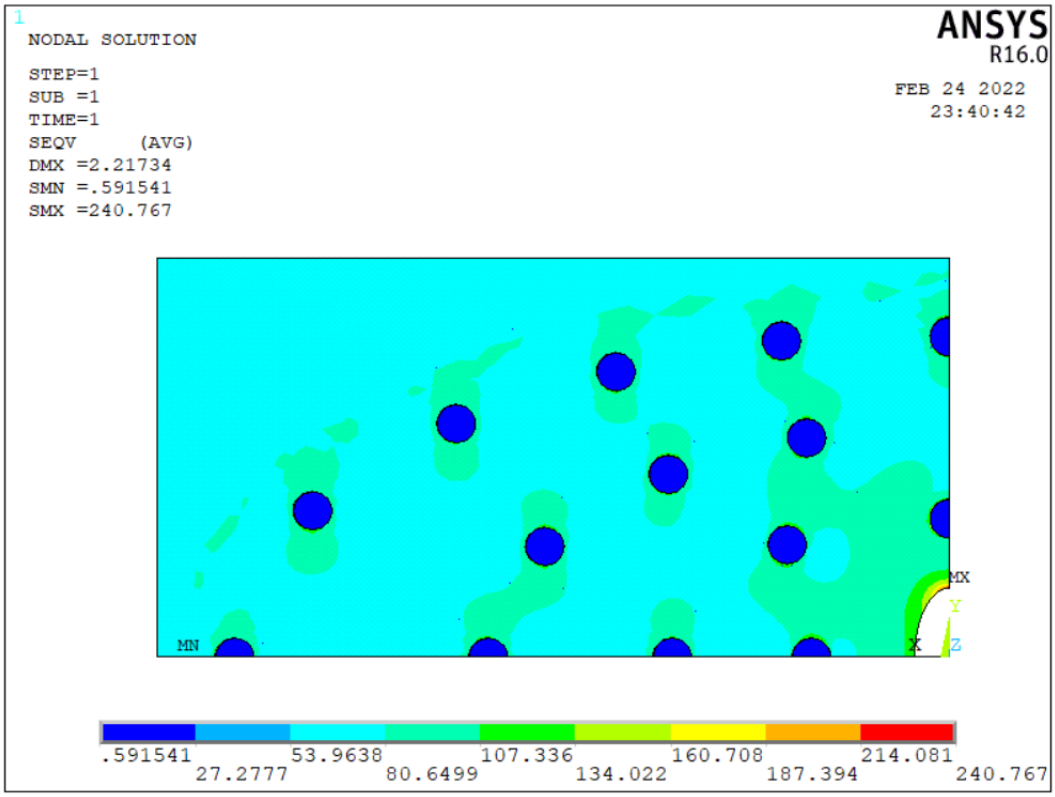

Figure 4.16: Nodal solution for Von Mises Stress distribution [MPa] of an elliptical mounting plate with an elliptical cut-out along the lateral axis, i.e., the major diameter tip of the elliptical cut out along the lateral axis,

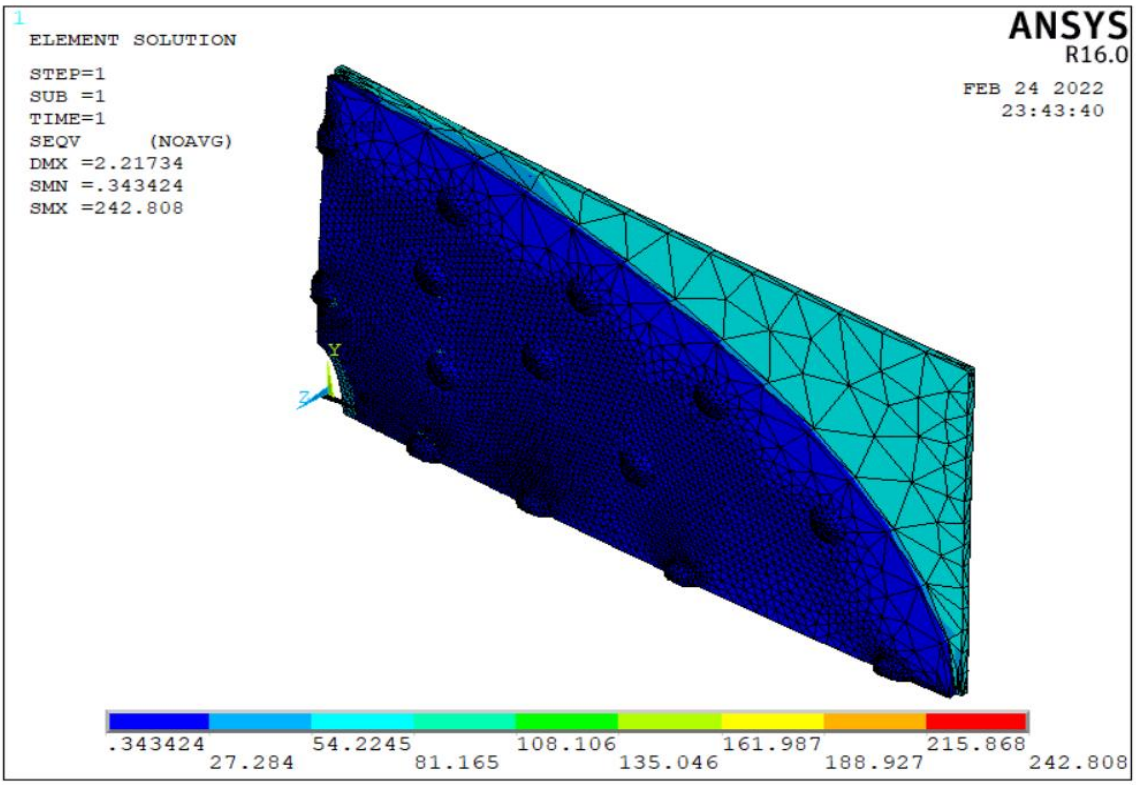

Figure 4.17: Element solution for Von Mises Stress distribution [MPa] of an elliptical mounting plate with an elliptical cut-out along the lateral axis, i.e., the major diameter tip of the elliptical cut out along the lateral axis.

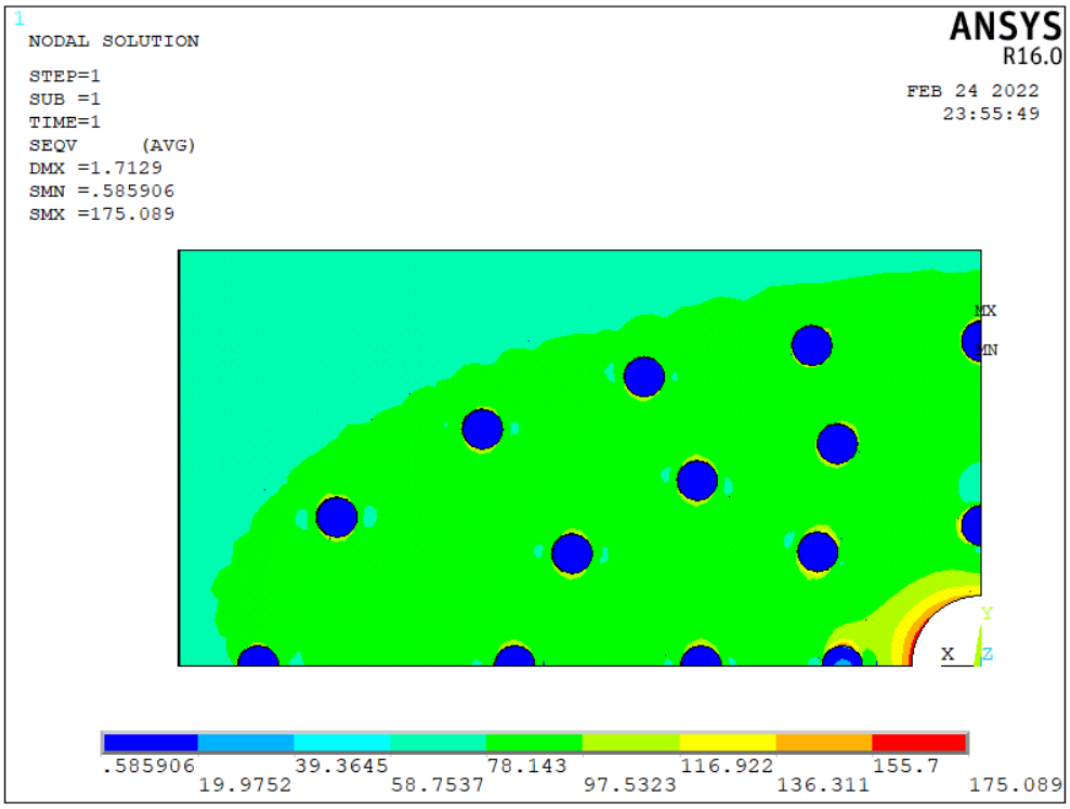

Figure 4.18: Nodal solution for Von Mises Stress distribution [MPa] of an elliptical mounting plate with circular cut-out.

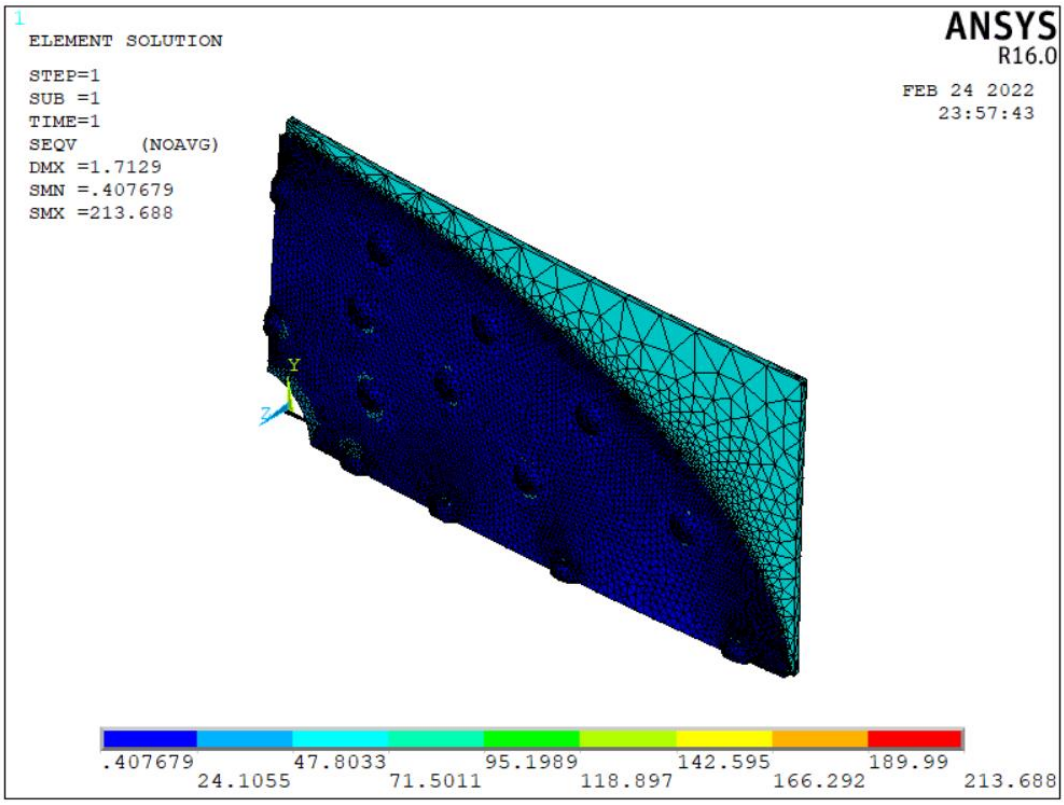

Figure 4.19: Element solution for Von Mises Stress distribution [MPa] of an elliptical mounting plate with circular cut-out.

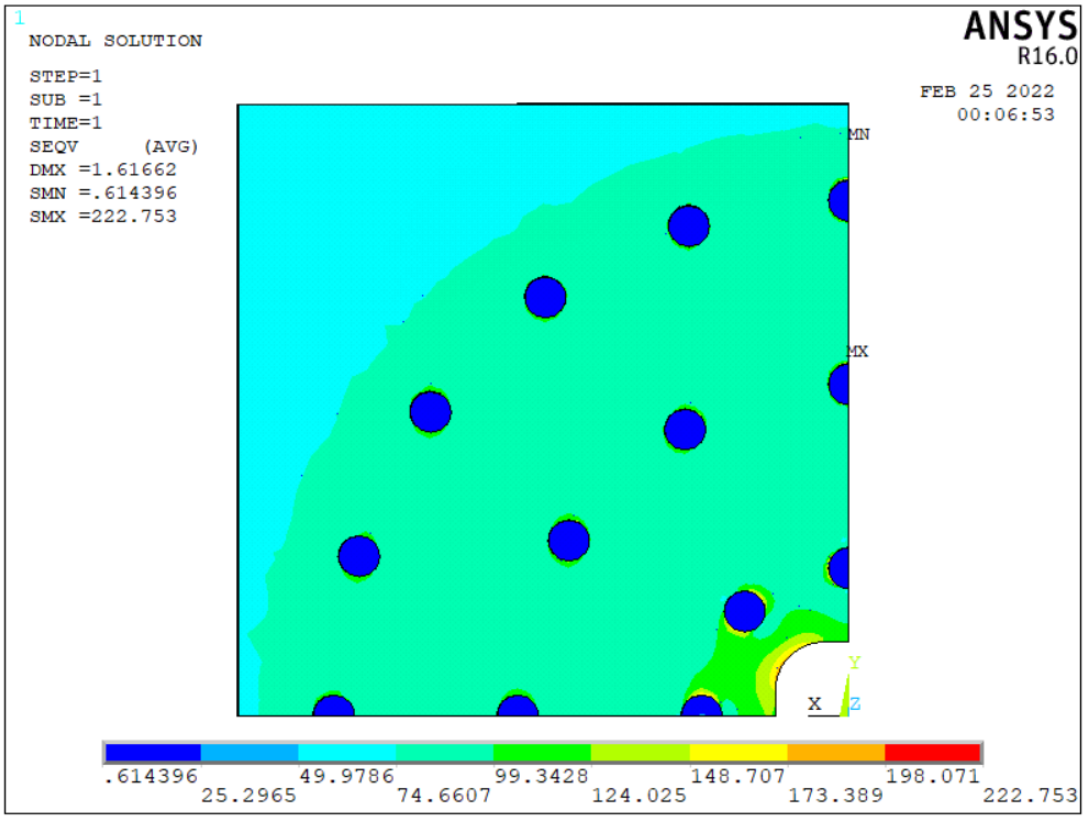

Figure 4.20: Nodal solution for Von Mises Stress distribution [MPa] of a circular mounting plate with a square cut-out.

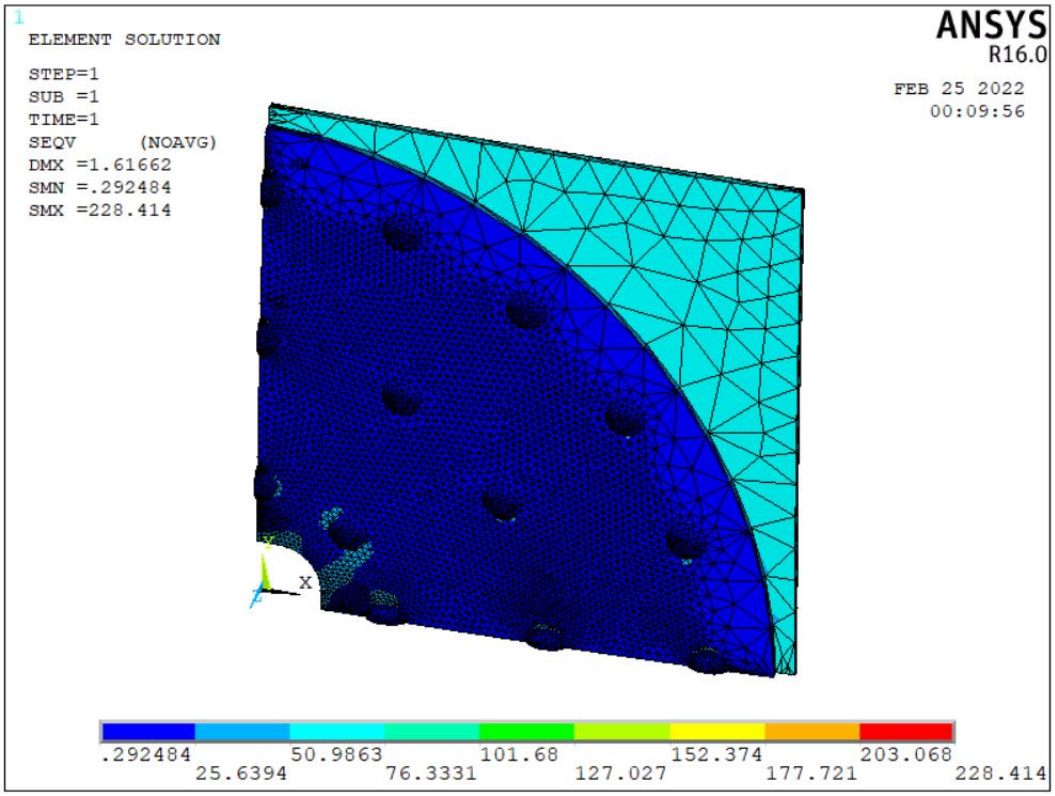

Figure 4.21: Element solution for Von Mises Stress distribution [MPa] of a circular mounting plate with a square cut-out.

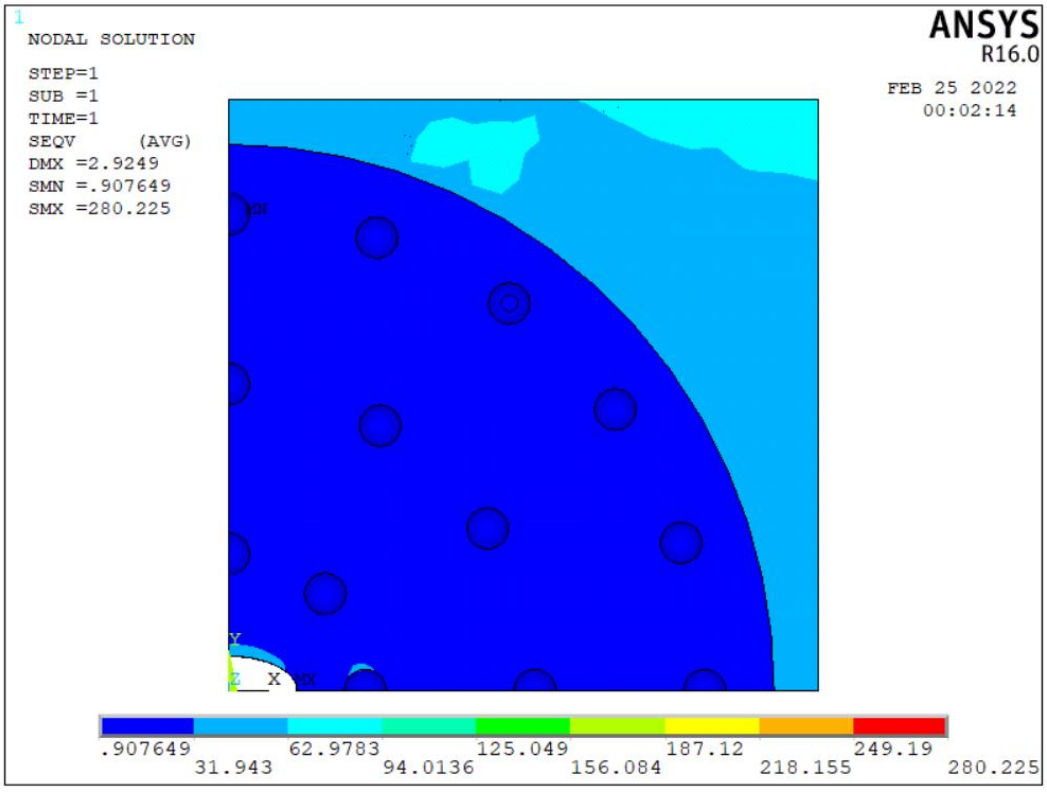

Figure 4.22: Nodal solution for Von Mises Stress distribution [MPa] of circular mounting plate with an elliptical cut out along the longitudinal axis, i.e., the major diameter tip of the elliptical cut out along the longitudinal axis.

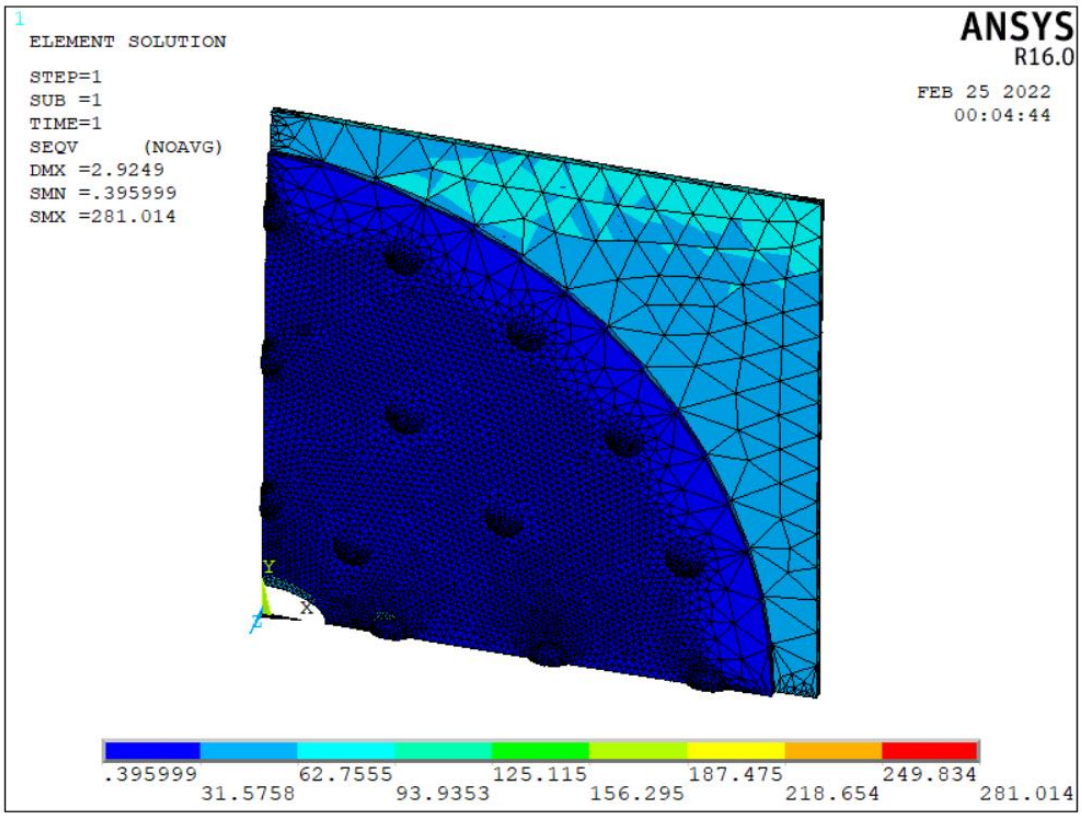

Figure 4.23: Element solution for Von Mises Stress distribution [MPa] of circular mounting plate with an elliptical cut out along the longitudinal axis, i.e., the major diameter tip of the elliptical cut out along the longitudinal axis.

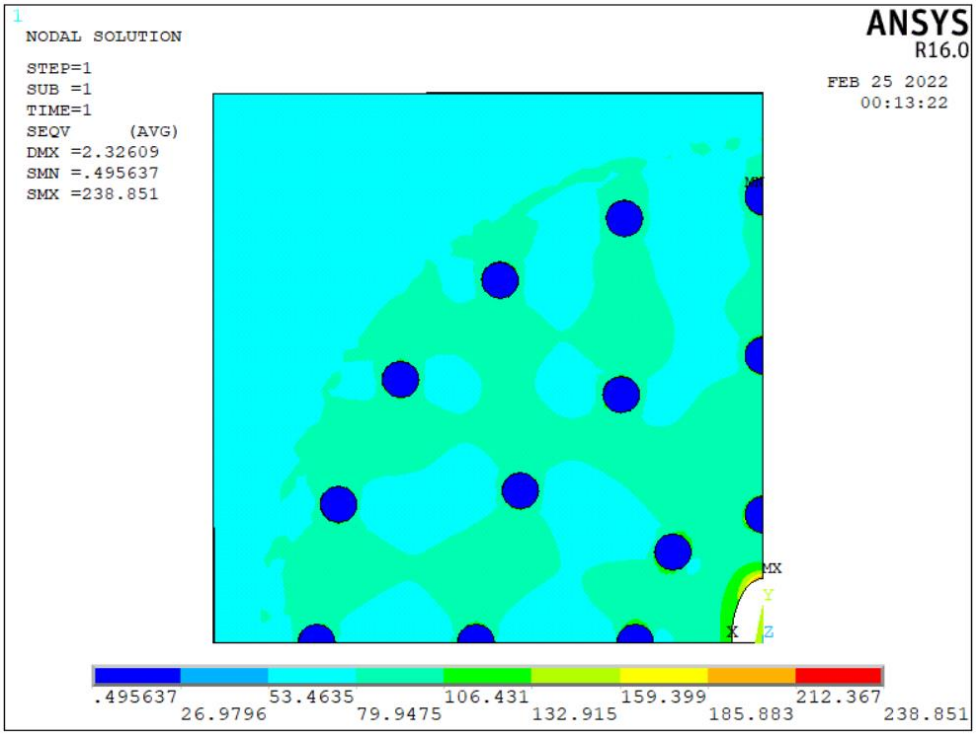

Figure 4.24: Nodal solution for Von Mises Stress distribution [MPa] of circular mounting plate with an elliptical cut-out along the lateral axis, i.e., the major diameter tip of the elliptical cut out along the lateral axis.

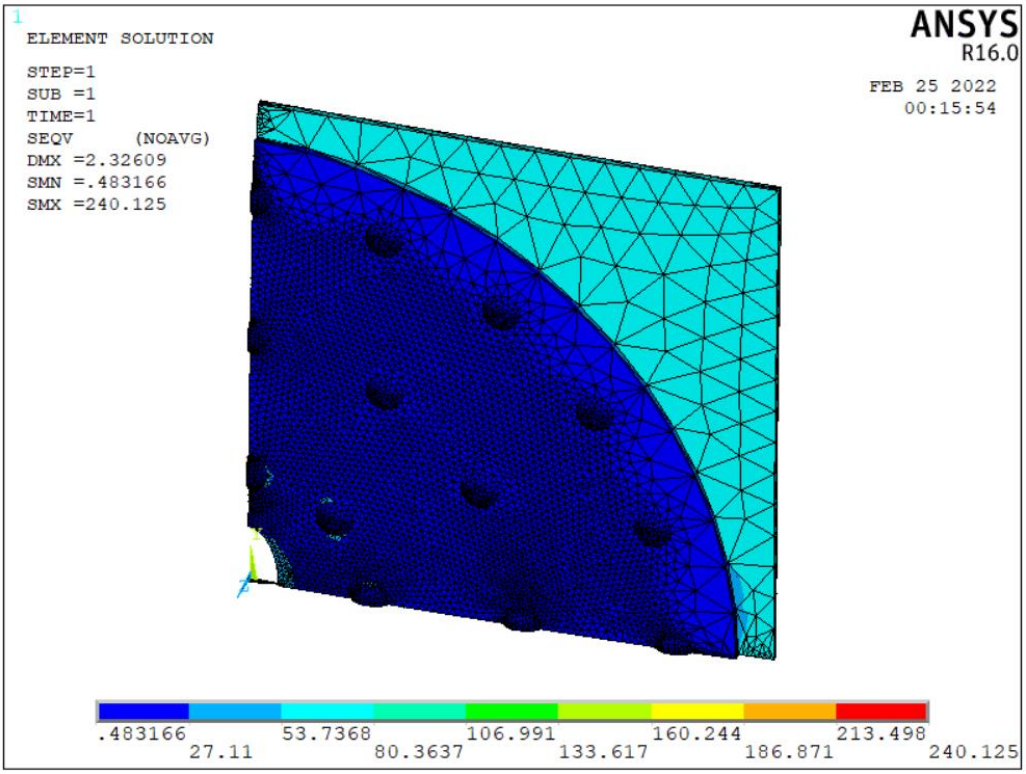

Figure: 4.25: Element solution for Von Mises Stress distribution [MPa] of circular mounting plate with an elliptical cut-out along the lateral axis, i.e., the major diameter tip of the elliptical cut out along the lateral axis.

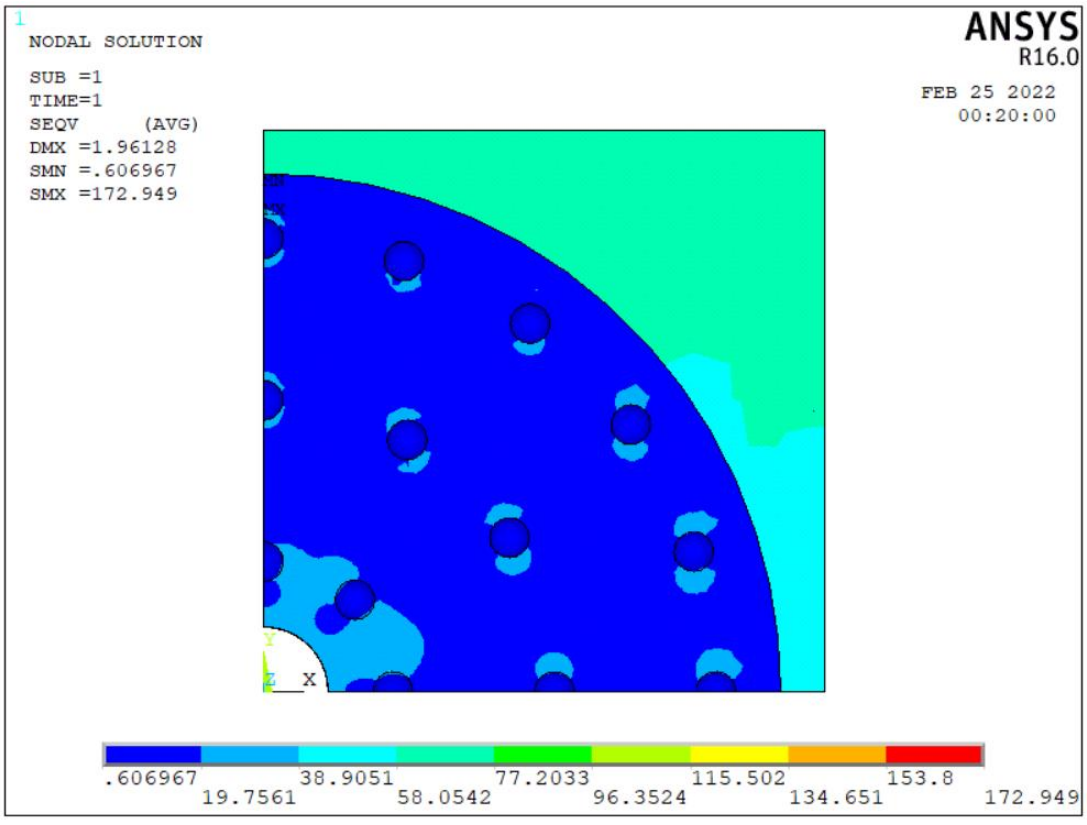

Figure 4.26: Nodal solution for Von Mises Stress distribution [MPa] of circular mounting plate with circular cut out cut-out.

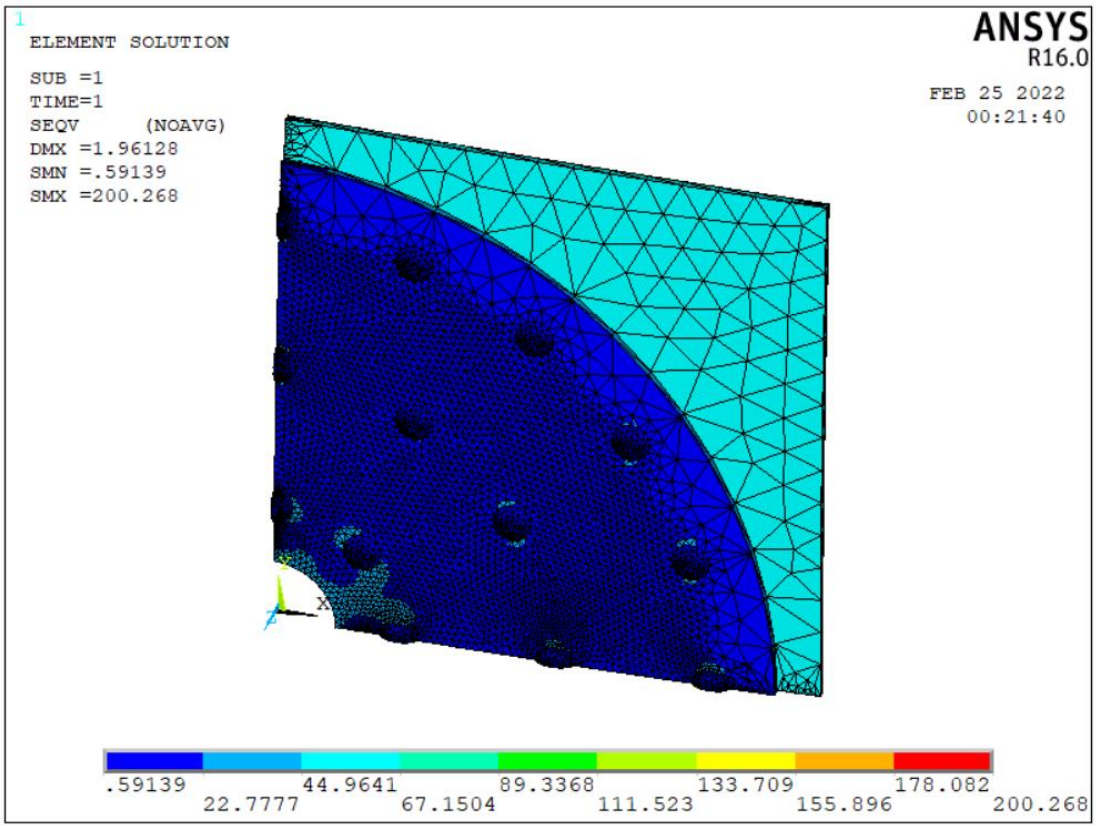

Figure 4.27: Element solution for Von Mises Stress distribution [MPa] of circular mounting plate with circular cut out cut-out.

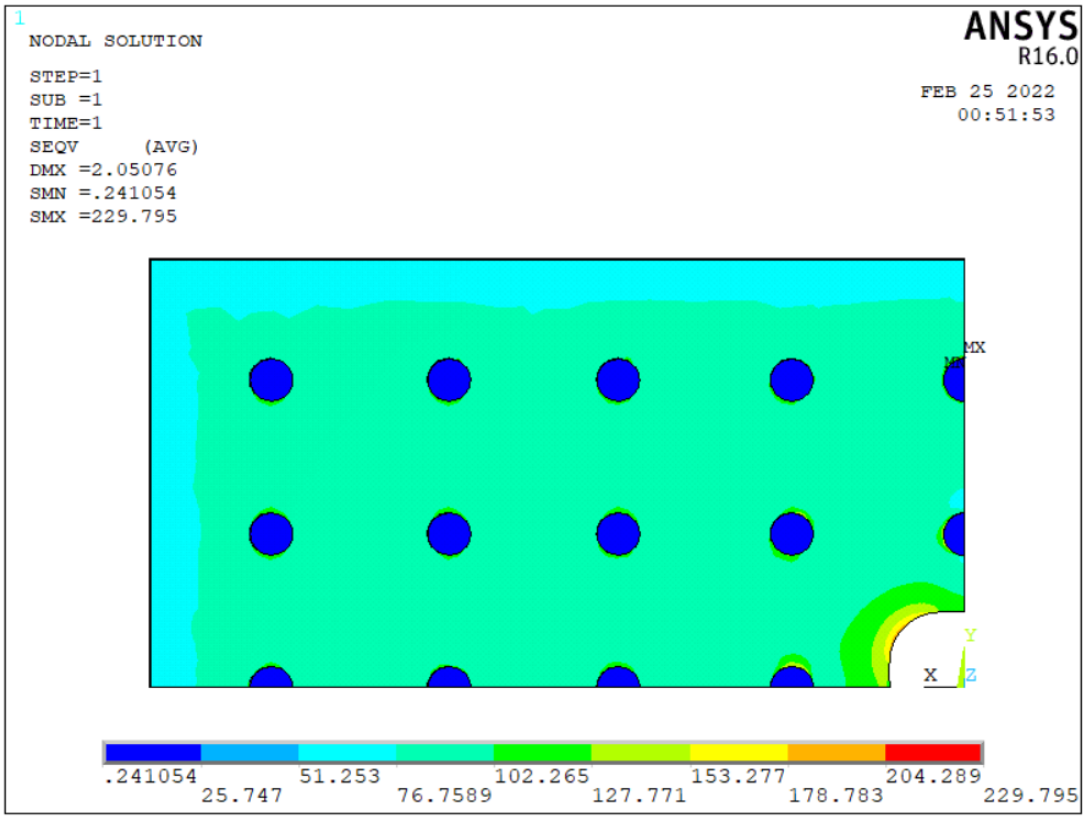

Figure 4.28: Nodal solution for Von Mises Stress distribution [MPa] of rectangular mounting plate with square cut-out.

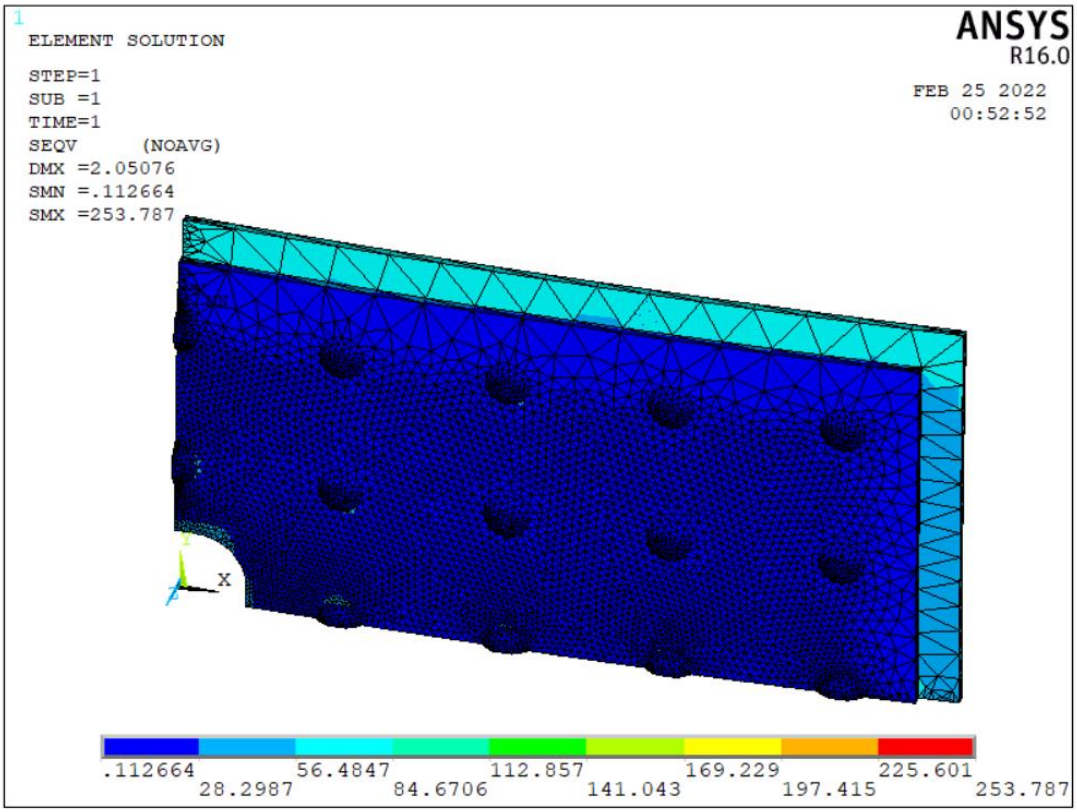

Figure 4.29: Element solution for Von Mises Stress distribution [MPa] of rectangular mounting plate with square cut-out.

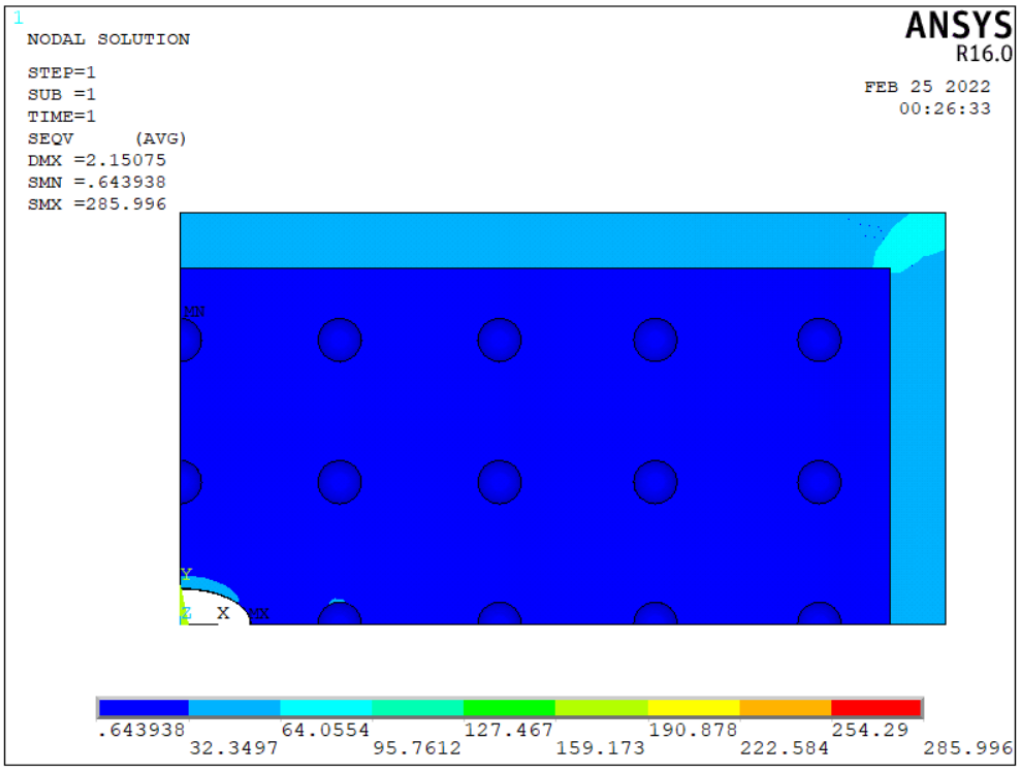

Figure 4.30: Nodal solution for Von Mises Stress distribution [MPa] of Rectangular mounting plate with elliptical cut out along the longitudinal axis, i.e., the major diameter tip of the elliptical cut out along the longitudinal axis.

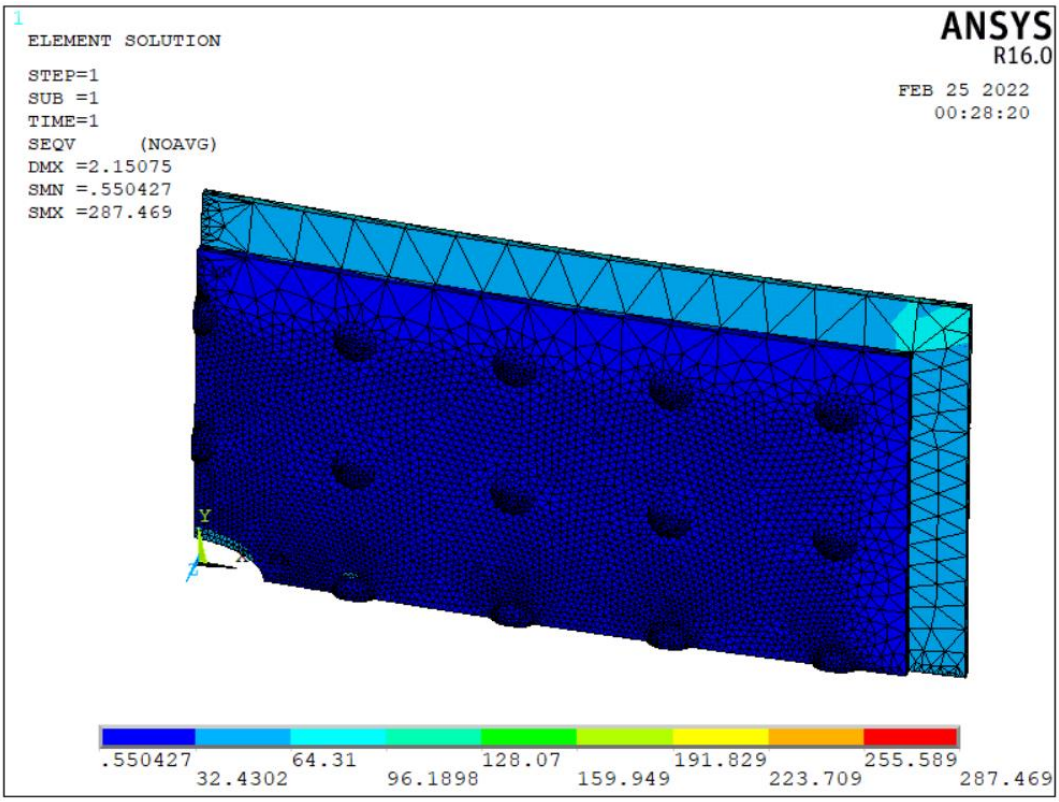

Figure 4.31: Element solution for Von Mises Stress distribution [MPa] of Rectangular mounting plate with elliptical cut out along the longitudinal axis, i.e., the major diameter tip of the elliptical cut out along the longitudinal axis.

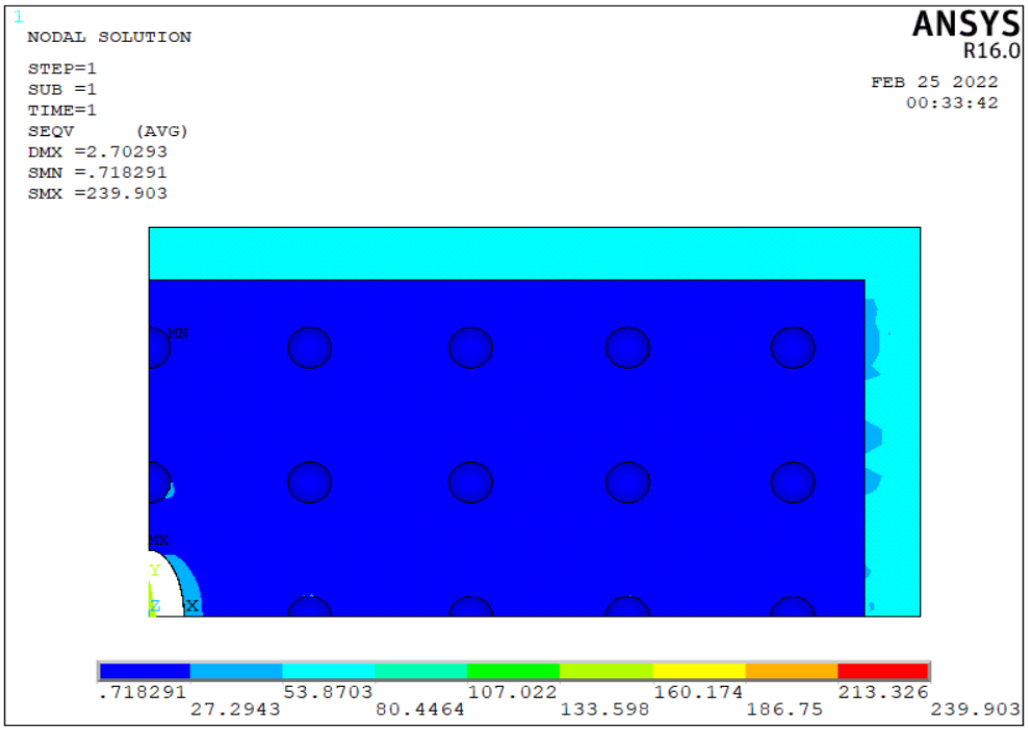

Figure: 4.32: Von Mises Stress distribution [MPa] Nodal solution for rectangular mounting plate with elliptical cut out along the lateral axis, i.e. major diameter tip of the elliptical cut out along the lateral axis.

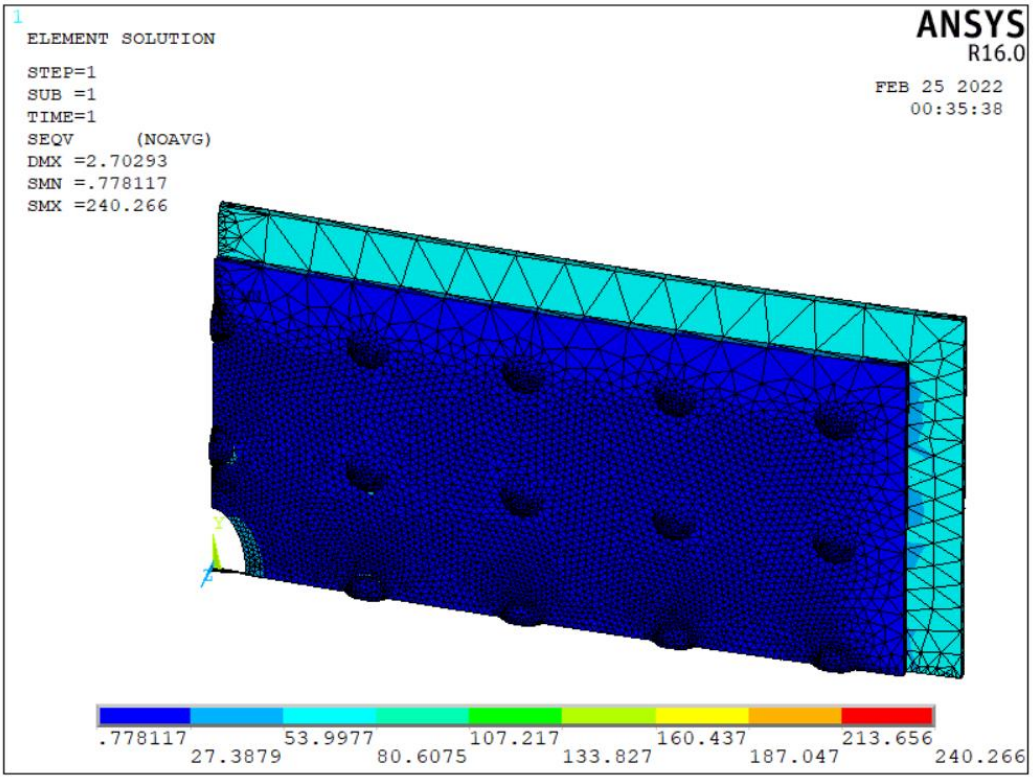

Figure: 4.33: Von Mises Stress distribution [MPa] Element solution for rectangular mounting plate with an elliptical cut out along the lateral axis, i.e., the major diameter tip of the elliptical cut out along the lateral axis.

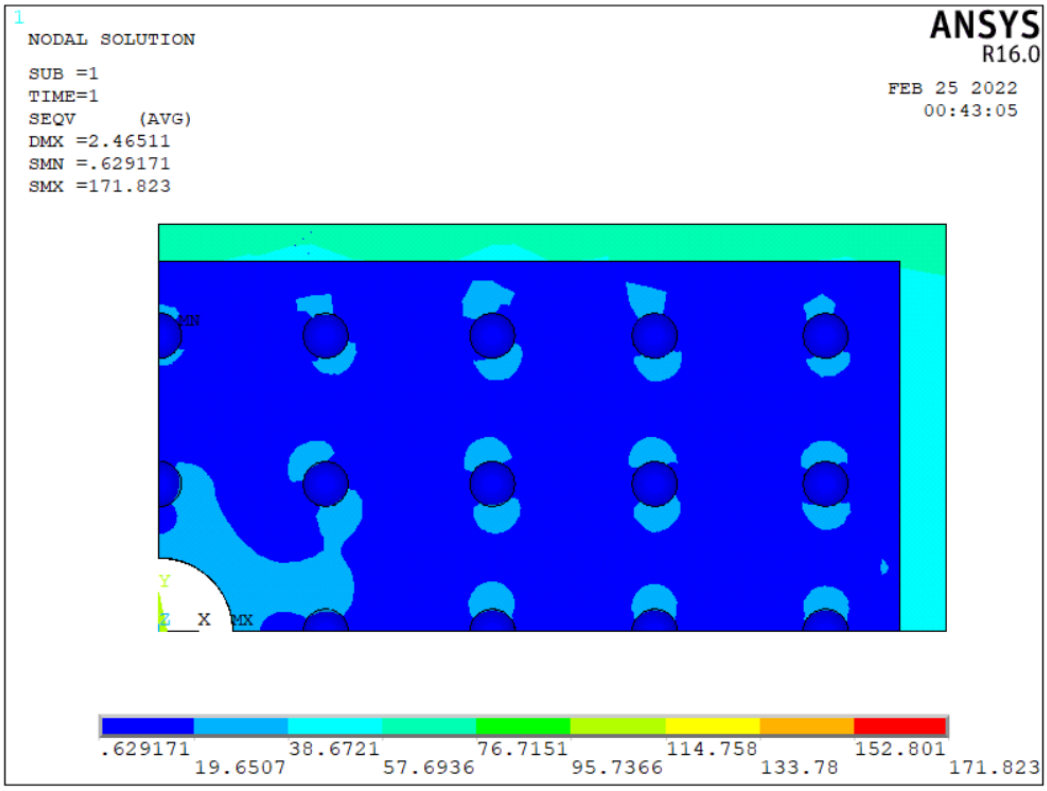

Figure 4.34: Von Mises Stress distribution [MPa] Nodal solution for rectangular mounting plate with circular cut out.

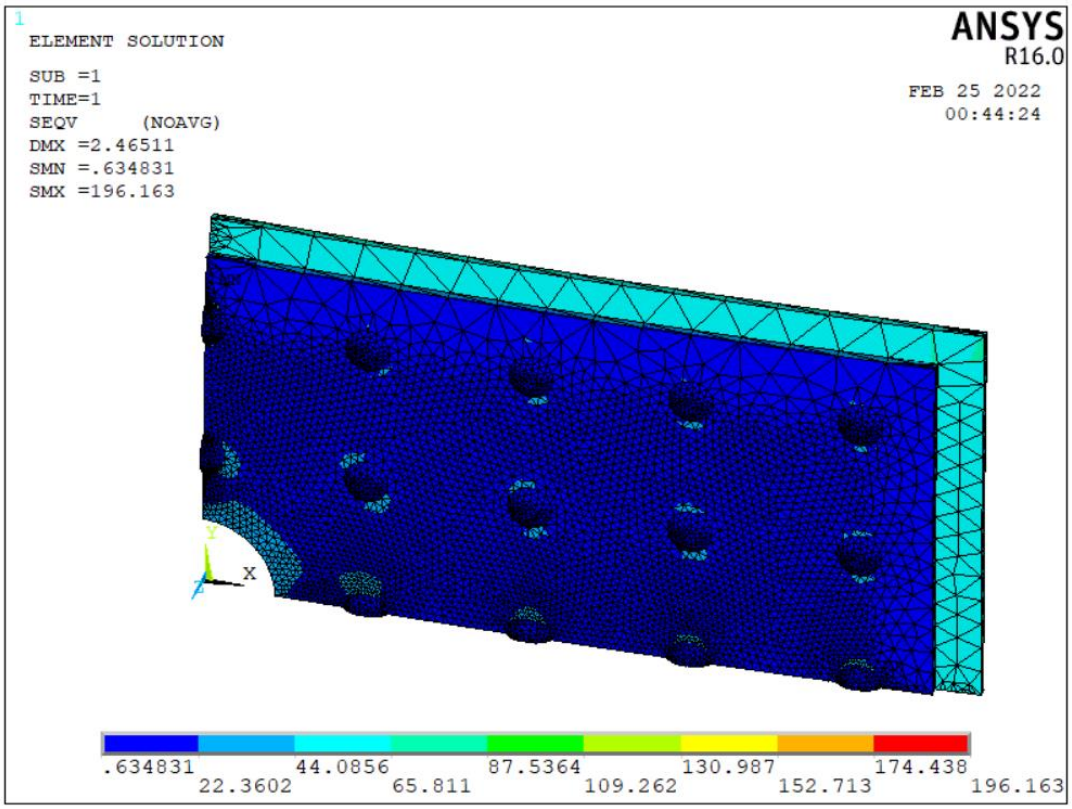

Figure 4.35: Von Mises Stress distribution [MPa] element solution for rectangular mounting plate with circular cut out.

ANSYS RESULT:

Mounting Plate FEA Result

Table 4.3: ANSYS Result Summarized for Different Parameters of rectangular, circular, and elliptical mounting plates with circular cut-out.

Parameter Reviewed	Max. value of the indicated parameter		
	Rectangular MP With Circular Cut-out	circular MP with circular cut-out	elliptical MP with circular cut-out
X-component of stress[MPa]	38.8427	36.7847	40.4768
Y-component of stress[MPa]	49.2091	55.9224	50.7084
1st -principal stress[MPa]	54.2679	61.9774	62.0413
2nd -principal stress[MPa]	24.5155	26.4679	26.8357
3rd -principal stress[MPa]	9.40915	14.3191	12.2359
Von Mises Stress[MPa]	**171.823**	172.949	175.089
X-component of total mechanical strain [mm]	0.060748	0.000765	0.000757
Y-component of total mechanical strain [mm]	0.036655	0.000634	0.000637
Z-component of total mechanical strain [mm]	0.463101	0.001101	0.00104
Von Mises total mechanical strain [mm]	**0.002379**	0.002464	0.002553
DOF Solution / Displacement vector sum	2.46511	1.96128	**1.7129**
Number of Rivet	44	**40**	44

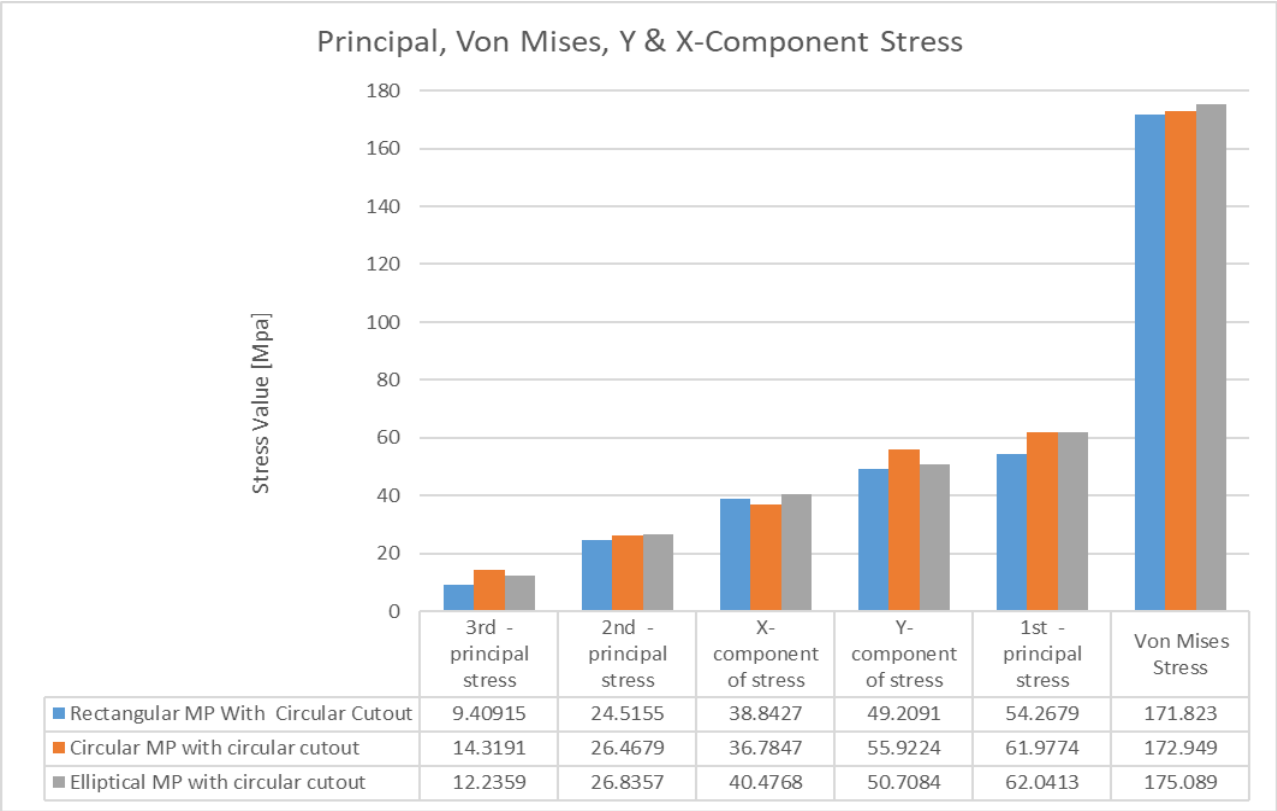

	3rd - principal stress	2nd - principal stress	X-component of stress	Y-component of stress	1st - principal stress	Von Mises Stress
Rectangular MP With Circular Cutout	9.40915	24.5155	38.8427	49.2091	54.2679	171.823
Circular MP with circular cutout	14.3191	26.4679	36.7847	55.9224	61.9774	172.949
Elliptical MP with circular cutout	12.2359	26.8357	40.4768	50.7084	62.0413	175.089

Figure 4.36: Principal, Von Mises, Y & X-Component Stress

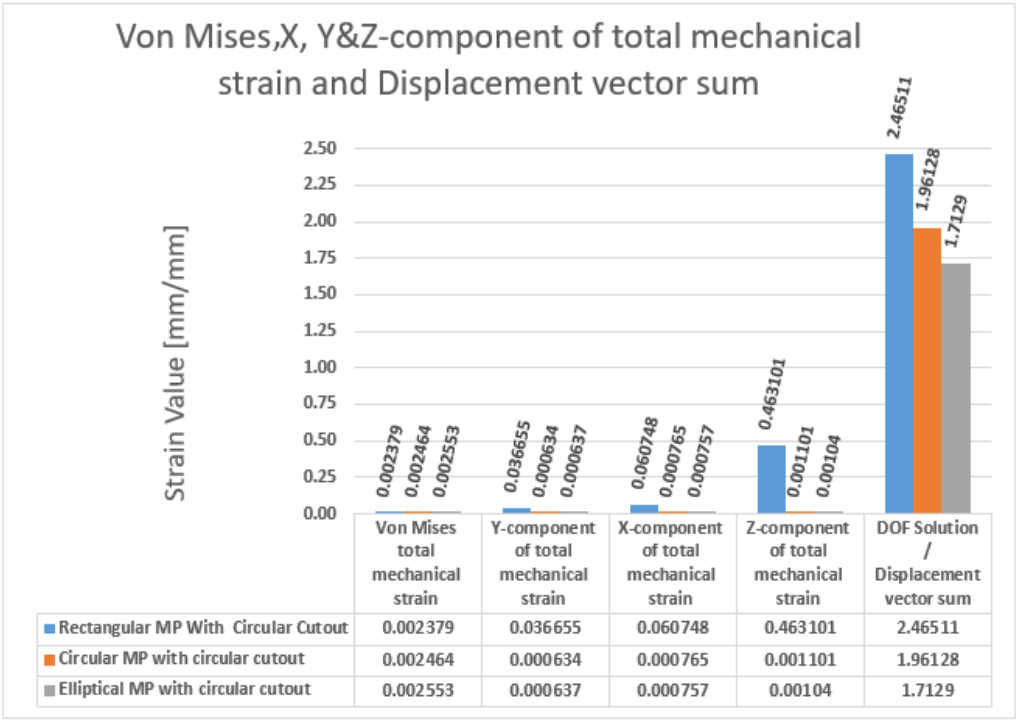

	Von Mises total mechanical strain	Y-component of total mechanical strain	X-component of total mechanical strain	Z-component of total mechanical strain	DOF Solution / Displacement vector sum
Rectangular MP With Circular Cutout	0.002379	0.036655	0.060748	0.463101	2.46511
Circular MP with circular cutout	0.002464	0.000634	0.000765	0.001101	1.96128
Elliptical MP with circular cutout	0.002553	0.000637	0.000757	0.00104	1.7129

Figure 4.37: Von Mises X, Y&Z-component of total mechanical strain and Displacement vector sum.

From Table 4.3 and Figures 4.12 to 4.37, different stress levels are considered, primarily principal, Von Mises, and X and Y-Component Stress for each of the mounting plates as depicted in the above figure.

Then strains such as Von Mises, X, Y, and Z-component of total mechanical strain and displacement vector sum are considered.

From Table 4.3 and Figure Figures 4.12 to 4.37, we can conclude that:

1. Stress results for the respective mounting plates are considered. mounting plate with the minimum stress has been reliable during the in-service life of the aircraft.
2. From stress results, the rectangular mounting plate is the best one compared with circular and elliptical mounting plates, and the circular mounting plate is better than the elliptical mounting plate.
3. von mises total mechanical strain for each of the mounting plate is almost same
4. The y-component of total mechanical strain, i.e., in the hoop/circumferential direction of the fuselage, The rectangular mounting plate is higher than the circular and elliptical mounting plates.
5. The x-component of total mechanical strain, i.e., in the longitudinal direction of the fuselage. The rectangular mounting plate is higher than the circular and elliptical mounting plates.
6. The z-component of total mechanical strain, i.e. in the vertical direction, i.e., across the thickness direction of the skin/sheet metal fuselage. The rectangular mounting plate is higher than the circular and elliptical mounting plates.
7. The displacement vector sum for the rectangular mounting plate is higher than the circular and elliptical mounting plates. From a strain point of view, an elliptical mounting plate is more acceptable relative to a circular mounting plate, and a circular mounting plate has less displacement than a rectangular mounting plate.
8. The size and shape of the mounting plate determine the number of rivets / fasteners required to perform the modification /repair.
9. The determination of the number of rivets/fasteners, rivet pattern, and pitch of the 1st, 2nd, and 3rd row or annulus circles contour for the circular mounting plate is somewhat tiresome compared with the rectangular mounting plate (i.e. preparation of the rectangular mounting plate is the easiest one) and, relatively, it needs less effort compared with the elliptical mounting plate (preparation of the elliptical mounting plate is the most tiresome compared with the circular and rectangular mounting plates).
10. **In this study, by taking the effect of stress and strain on the mounting plate, a stress and strain value of the medium was selected, i.e., in this case, a circular mounting plate. For rectangular and elliptical mounting plates, the maximum and minimum values of stress and strain are not selected.**

4.3 FEA Stress Concentration Result –II

Table 4.4: ANSYS result of K_{tg}: Gross Area Stress Concentration factor for different geometrical cutout

Mounting Plate Type	Mounting Plate Type – cut out geometry	Ktg: Gross Area Stress Concentration factor Analytical	Ktg: gross area stress concentration By FEM	The Smallest K_{tg}
Elliptical Mounting Plate	E-HE	4.8333	4.32857	2.68571
	E-LE	3.8333	4.03333	
	E-SQ	2.55	2.68571	
	E-C	2.5	3.04286	
Rectangular Mounting Plate	R-HE	4.8333	4.1	2.8
	R-LE	3.8333	4	
	R-SQ	2.55	2.91429	
	R-C	2.5	2.8	
Circular Mounting Plate	C-HE	4.8333	4.01429	2.82857
	C-LE	3.8333	4	
	C-SQ	2.55	2.82857	
	C-C	2.5	2.85714	

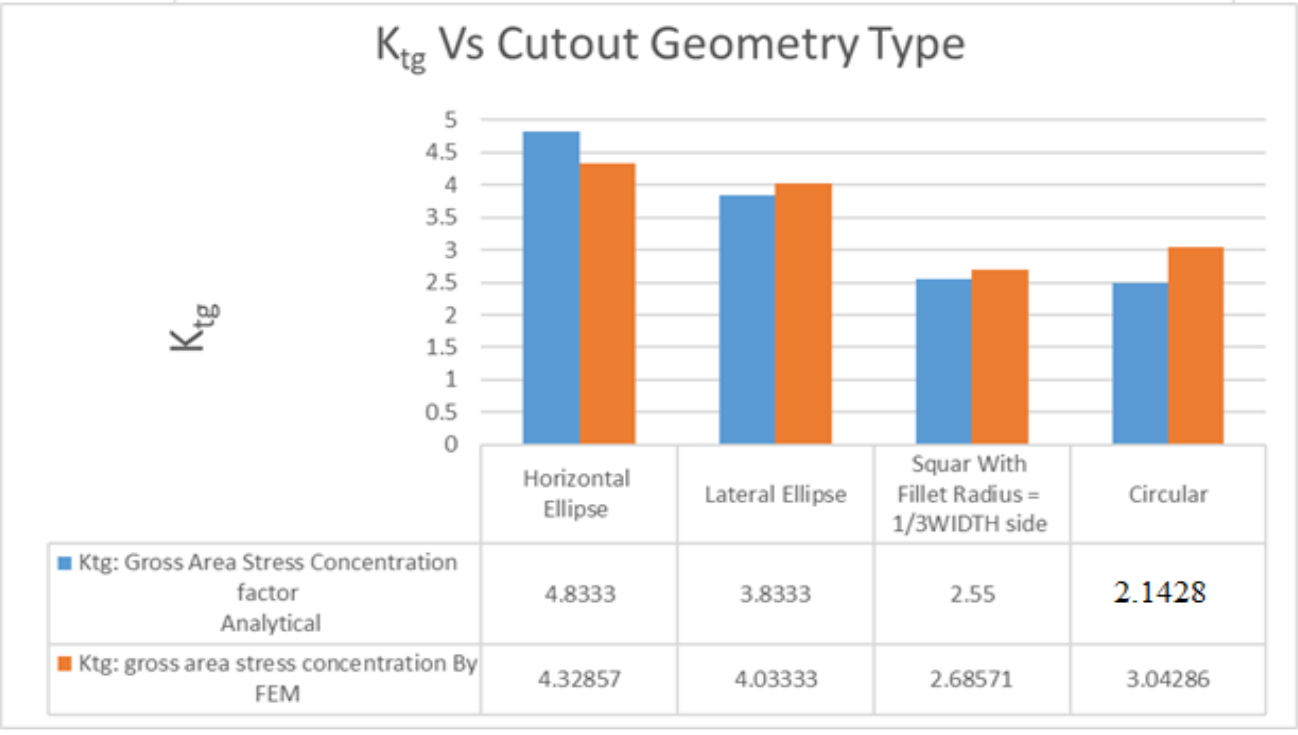

Figure 4.38: Stress Concentration Factor Analytical vs. Ansys Results for Cut-out Geometry Type for Elliptical Mounting Plate.

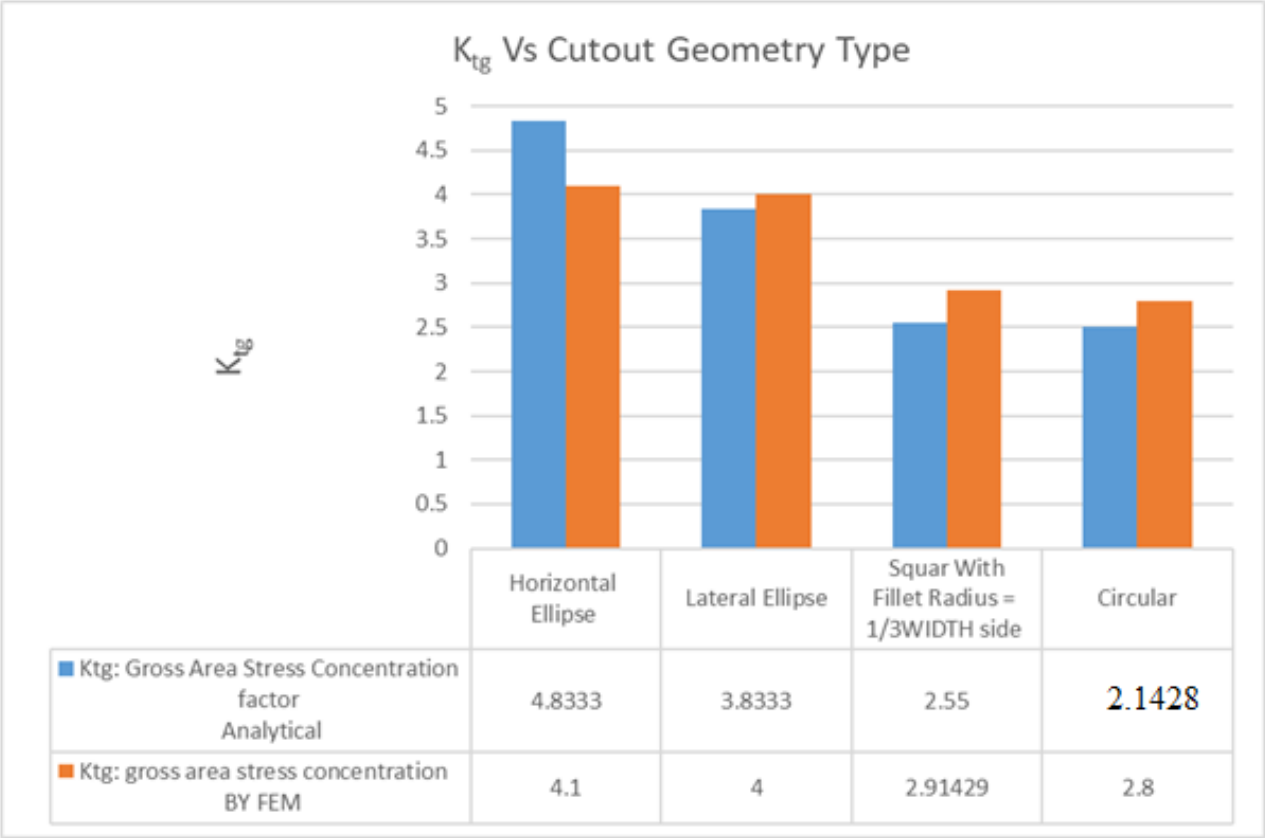

Figure 4.39: Stress Concentration Factor **Analytical vs. Ansys Results for Different Cut**-out Geometry Type for Rectangular Mounting Plate

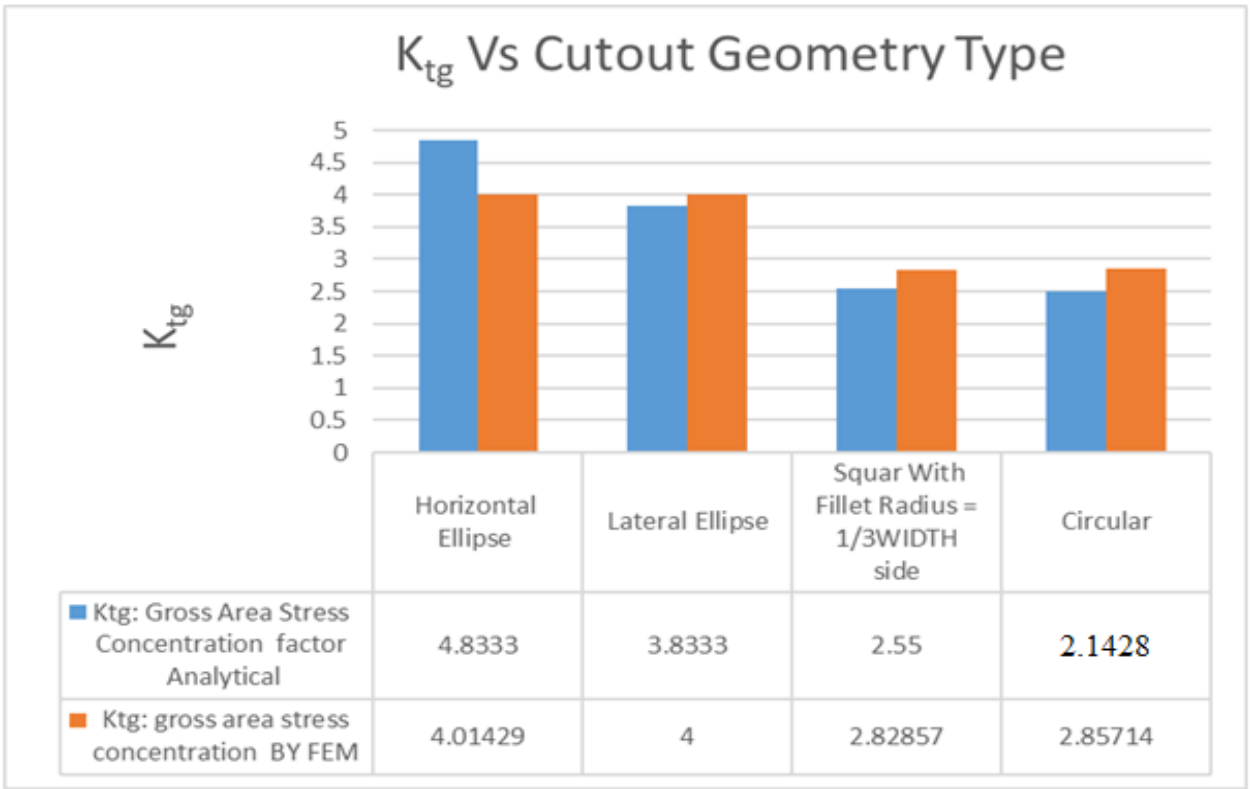

Figure 4.40: Stress Concentration Factor: Analytical vs. Ansys Results for Different Cut-out Geometry for Circular Mounting Plate.

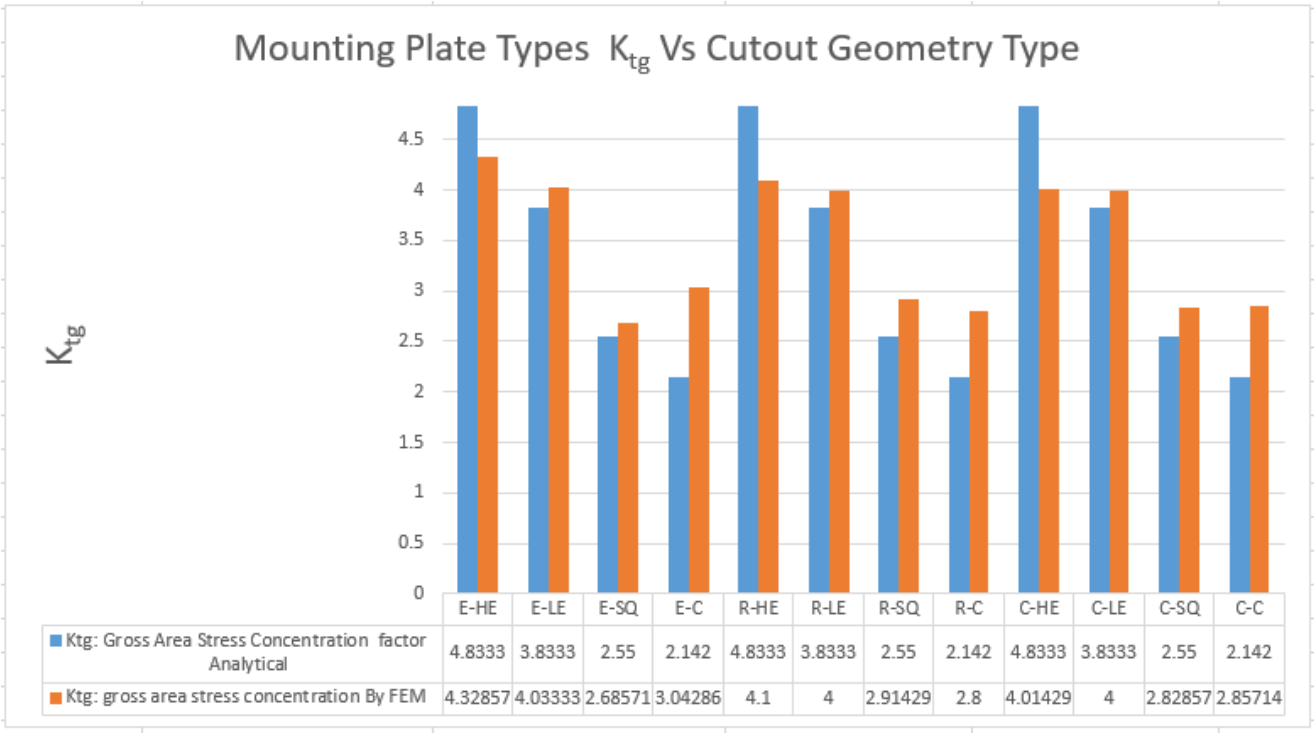

	E-HE	E-LE	E-SQ	E-C	R-HE	R-LE	R-SQ	R-C	C-HE	C-LE	C-SQ	C-C
Ktg: Gross Area Stress Concentration factor Analytical	4.8333	3.8333	2.55	2.142	4.8333	3.8333	2.55	2.142	4.8333	3.8333	2.55	2.142
Ktg: gross area stress concentration By FEM	4.32857	4.03333	2.68571	3.04286	4.1	4	2.91429	2.8	4.01429	4	2.82857	2.85714

Figure 4.41: Stress Concentration Factor: Analytical vs. Ansys Results for Different Cut-out Mounting Plate Types Vs Cut-out Geometry Type

Where:

For Elliptical Mounting Plate

[E-HE]=>Elliptical Mounting Plate (E)-Horizontal Ellipse (HE)

[E-LE]=>Elliptical Mounting Plate (E)-Lateral Ellipse (LE)

[E-SQ]=>Elliptical Mounting Plate (E)-Square with Fillet Radius = 1/3WIDTH side (SQ)

[E-C] =>Elliptical Mounting Plate (E)-Circular(C)

For Rectangular Mounting Plate:

[R-HE]=>Rectangular Mounting Plate(R)-Horizontal Ellipse (HE)

[R-LE]=>Rectangular Mounting Plate (R)-Lateral Ellipse (LE)

[R-SQ] =>Rectangular Mounting Plate (R)-Square with Fillet Radius = 1/3WIDTH side (SQ)

[R-C]=>Rectangular Mounting Plate (R)-Circular(C)

For Circular Mounting Plate

[C-HE]=>Circular Mounting Plate (C)-Horizontal Ellipse (HE)

[C-LE] =>Circular Mounting Plate (C)-Lateral Ellipse (LE)

[C-SQ]=>Circular Mounting Plate (C)-Square with Fillet Radius = 1/3WIDTH side (SQ)

[C-C]=>Circular Mounting Plate (C)-Circular(C)

Inference:

- In this FEA, stress concentration for different mounting plates such as elliptical mounting plates, rectangular mounting plates, and circular mounting plates with different cut outs such as Horizontal Ellipse (HE), Lateral Ellipse (LE), Square with Fillet Radius = 1/3width side (SQ), and Circular (C) was compared and concluded that:
- An elliptical mounting plate with a square cut-out has a lower stress concentration factor than those of the same mounting plate with other types of cut-out.
- Rectangular mounting plate with circular cut-out has a lower stress concentration factor than those of the same mounting plates with other types of cut-outs.
- An antenna cut out with circular geometry has a relatively lower gain than other cut-out types. Therefore, from specific objective one (1), a circular mounting plate with circular geometry is selected, and from specific objective two (2), for the next chapter, i.e., a DTA-section antenna amounting plate with circular geometry and circular cut-out is considered.
- The rectangular mounting plate provides a good concentration of rivets within a critical stress area, eliminates dangerous stress concentrations, and is very simple to prepare the layout. The rectangular mounting plate area may extend beyond the nearest frame and stringer based on the condition of the repair.

- Elliptical Mounting Plate (E)-Square cut out and with Fillet Radius = 1/3width side (SQ) provides a good concentration of rivets within a critical stress area, eliminating dangerous stress concentration, but is difficult to fabricate and install with the indicated pattern.

- Elliptical Mounting Plate (E)-Square with Fillet Radius = 1/3width side (SQ), Determine the number of fasteners or rivets, rivet pattern, fixing relative/spacing of the 1st, 2nd, and 3rd rows or annuluses elliptical contour for the elliptical mounting plate. This is somewhat tiresome compared with the rectangular mounting plate and circular mounting plate.
- **A circular mounting plate with a circular cut-out has a lower stress concentration factor than those of the same mounting plate with other types of cut-out.**

4.4 The FEM Modelling for Specific Objective III

Table 4.5: Crack Length –a_i and corresponding stress intensity factors (K_I)

Item Number a_i	Crack Length –a_i a (mm)	Stress Intensity Factor, K_I (MPa.m½)
1	1.25	24.375
2	2	28.492
3	3	32.321
4	4	34.69
5	5	35.494
6	6	36.367
7	6.47	36.879
8	7	37.7
9	8	37.897
10	9	38.626
11	9.53	38.631

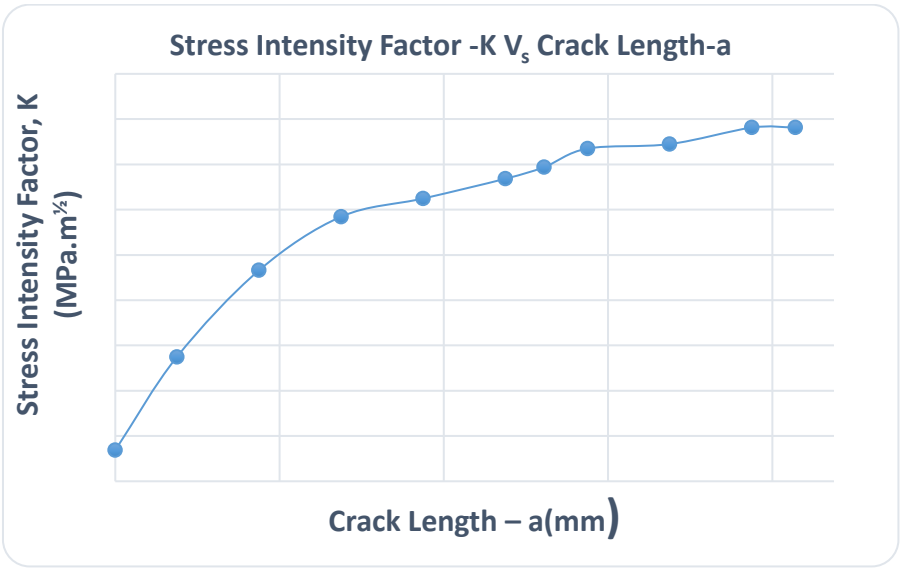

Figure 4.42. Stress Intensity Factor -K Vs Crack Length-a

4.5 FEA Crack Initiation and Propagation Critical Fastener Location

Damage tolerance analysis of modified skin by postulating the initial flaws at the critical locations. For circular installation, the critical location is identified at the point where Von Mises stress is the highest, which is at the top or bottom fastener in the outermost ring and at the antenna connector hole cut-out. Due to the double symmetry of the geometry and the stress applied to the skin, the analysis is performed on one quarter of the repaired skin.

Table 4.6: ANSYS solution for K_I vs. Crack Length $–a_i$ (mm)

Item Number a_i	Crack Length $–a_i$&a (mm)	Stress Intensity Factor, K [MPa.m½]
1	1.25	24.375
2	2	28.492
3	3	32.321
4	4	34.69
5	5	35.494
6	6	36.367
6.1	6.47	36.879
7	7	37.7
8	8	37.897
9	9	38.626
10	9.53	38.631

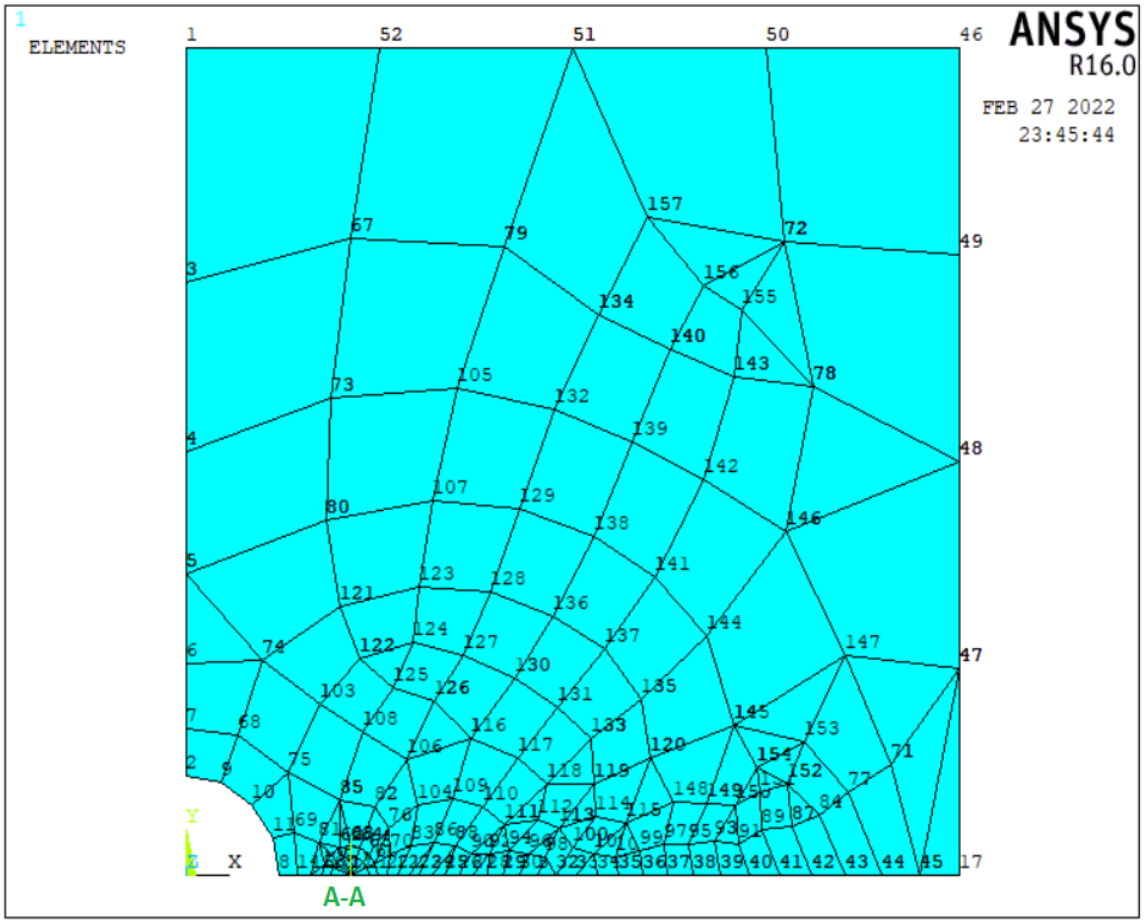

Figure 4.43: The mesh element of a skin is used to model crack length and fix the stress intensity factor for the given crack length.

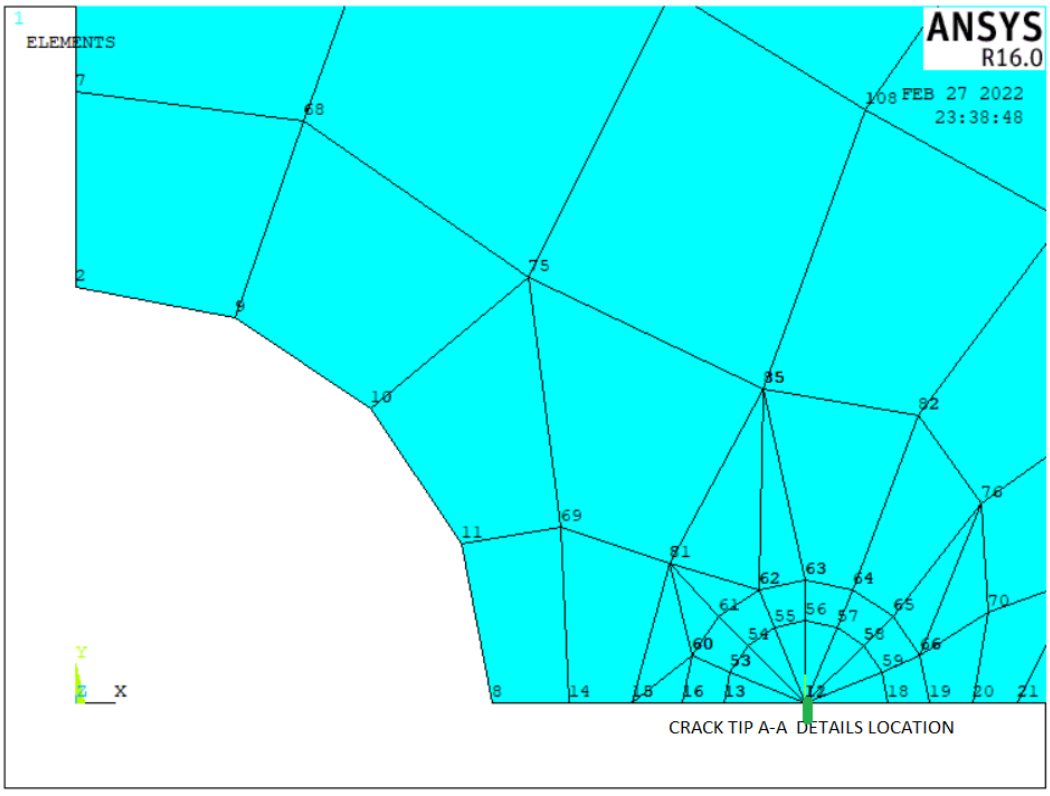

Figure 4.44: A-A Details of crack tip location

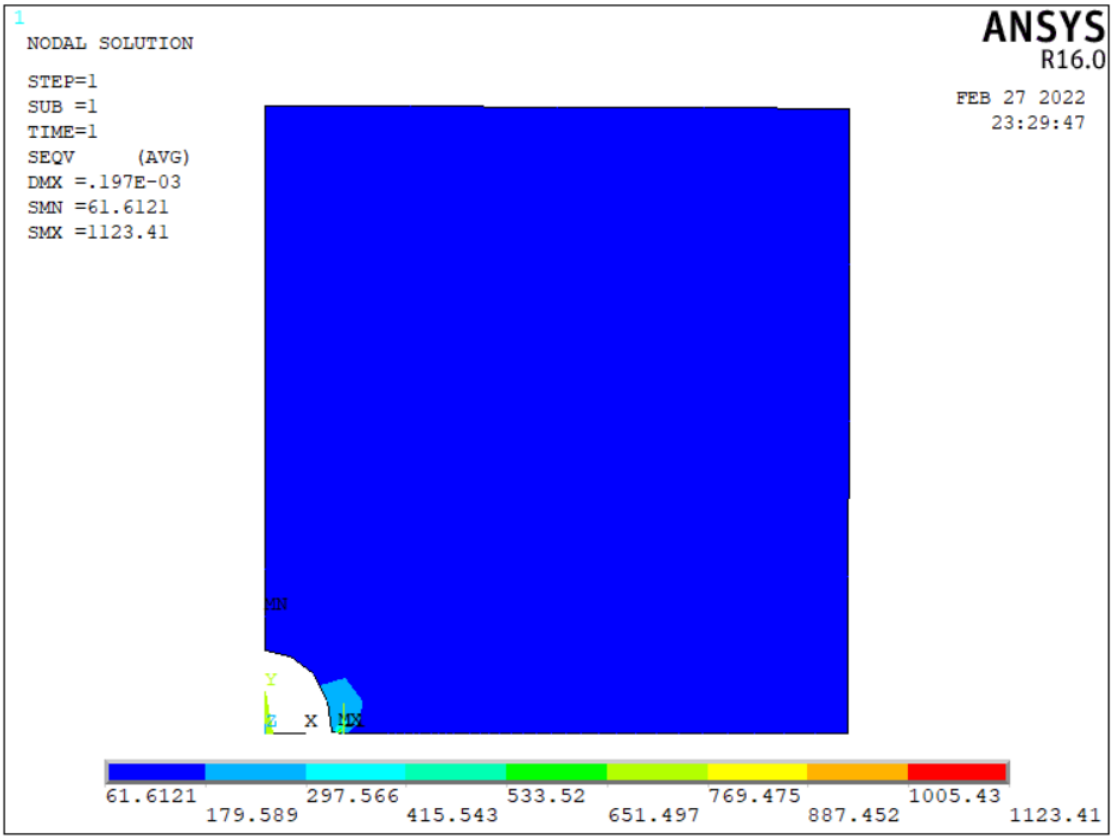

Figure 4.45: Von Mises Stress distribution at the tip of the crack due to tension stress in the hoop direction when the longitudinal crack length a = 1.25 mm.

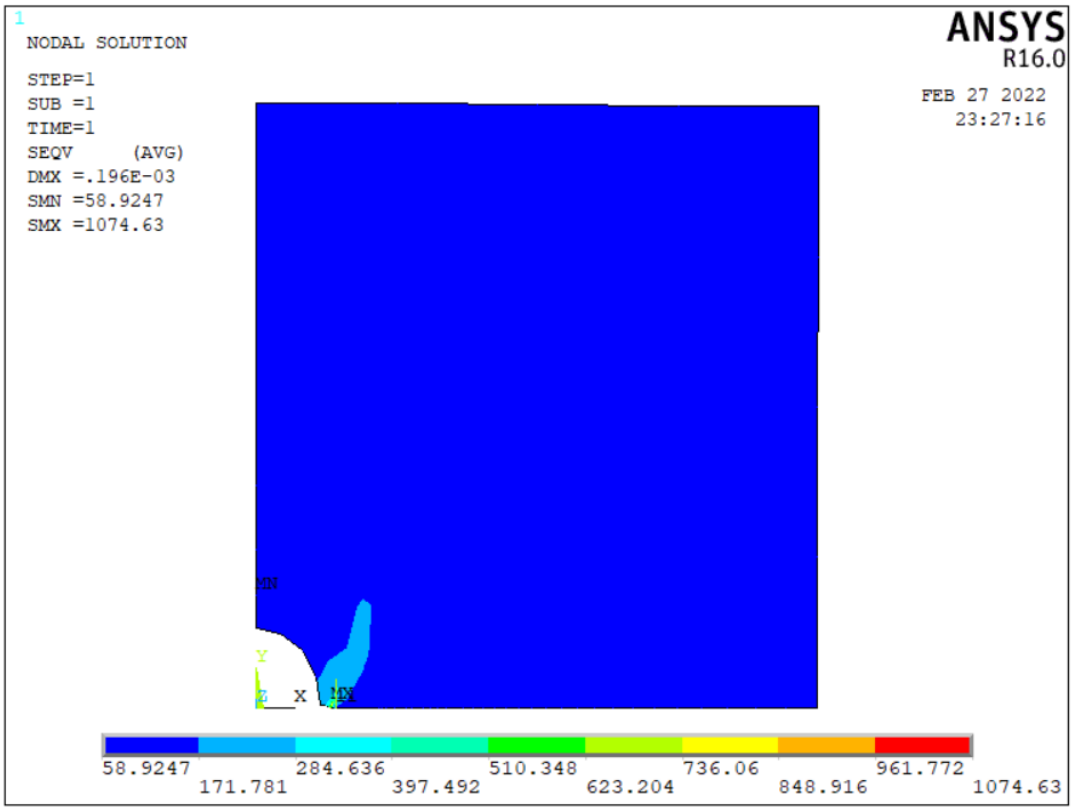

Figure 4.46: Von Mises stress distribution at the tip of the crack due to tension stress in the hoop direction when the longitudinal crack length a = 2 mm.

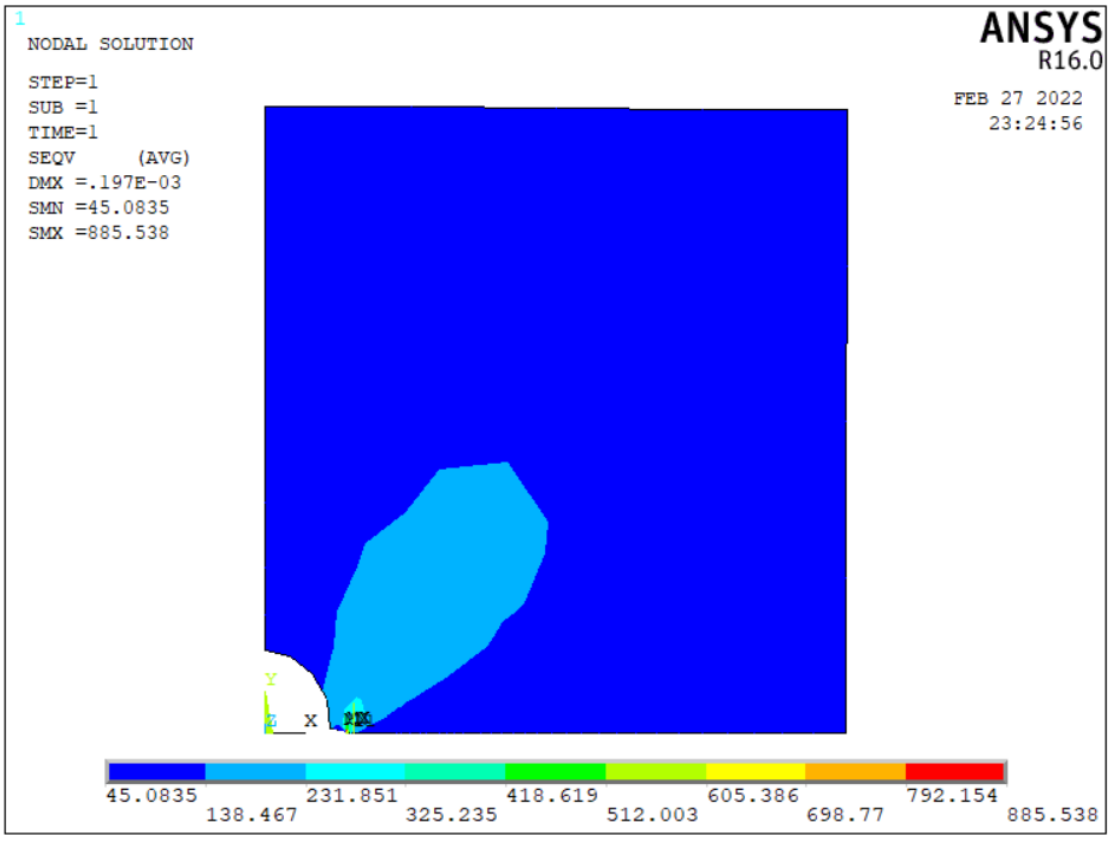

Figure 4.47: Von Mises Stress distribution at the tip of the crack due to tension stress in the hoop direction when the longitudinal crack length a = 3 mm.

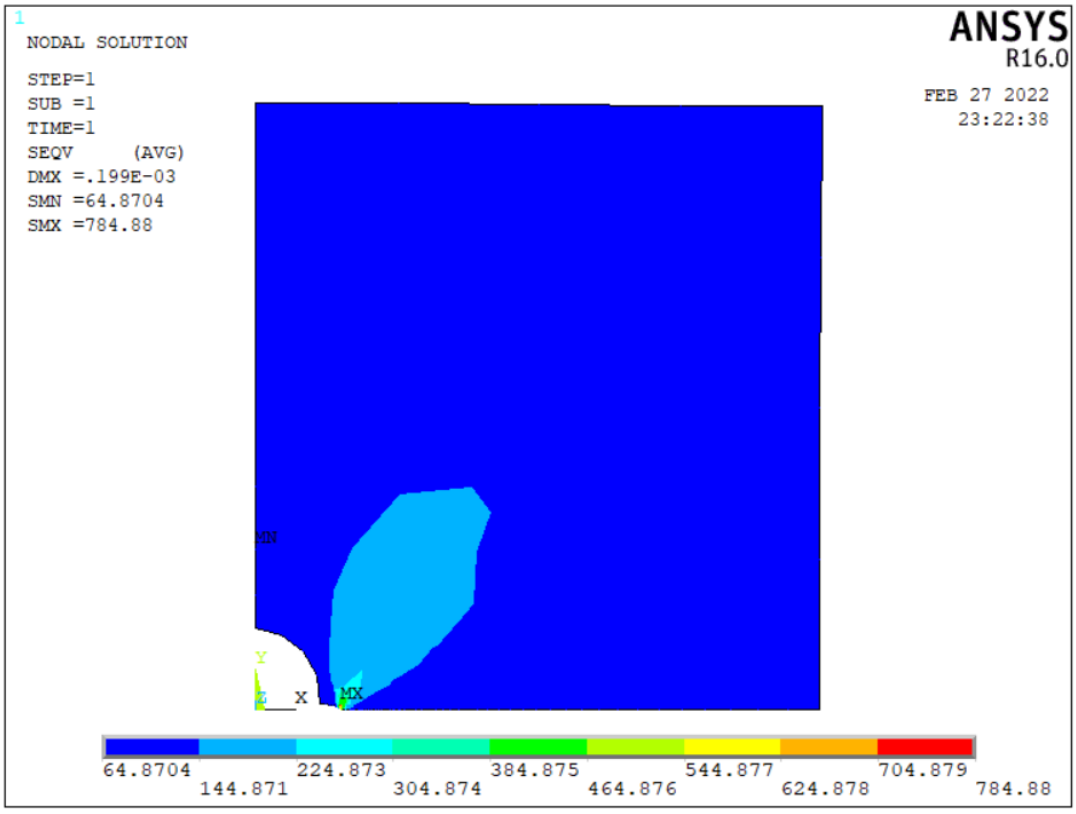

Figure 4.48: Von Mises stress distribution at the tip of the crack due to tension stress in the hoop direction when the longitudinal crack length a = 4 mm.

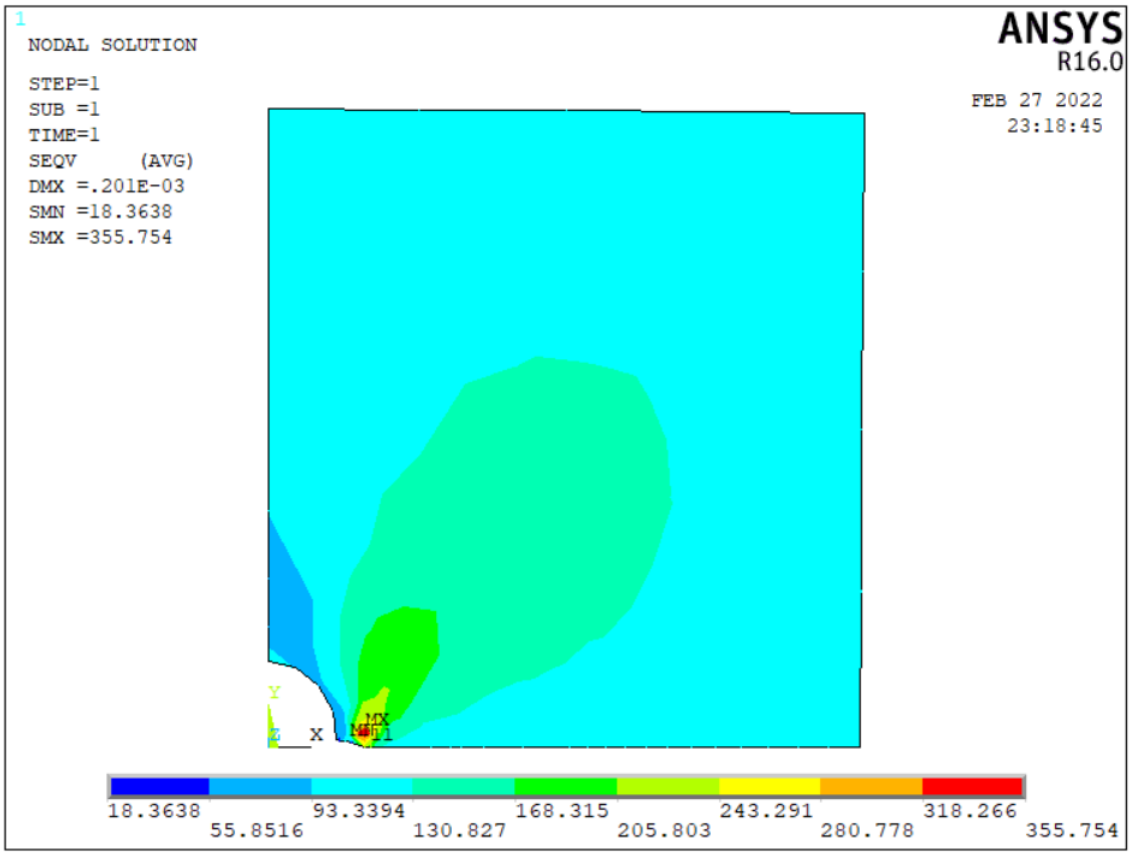

Figure 4.49: Von Mises stress distribution at the tip of the crack due to tension stress in the hoop direction when the longitudinal crack length a = 5 mm.

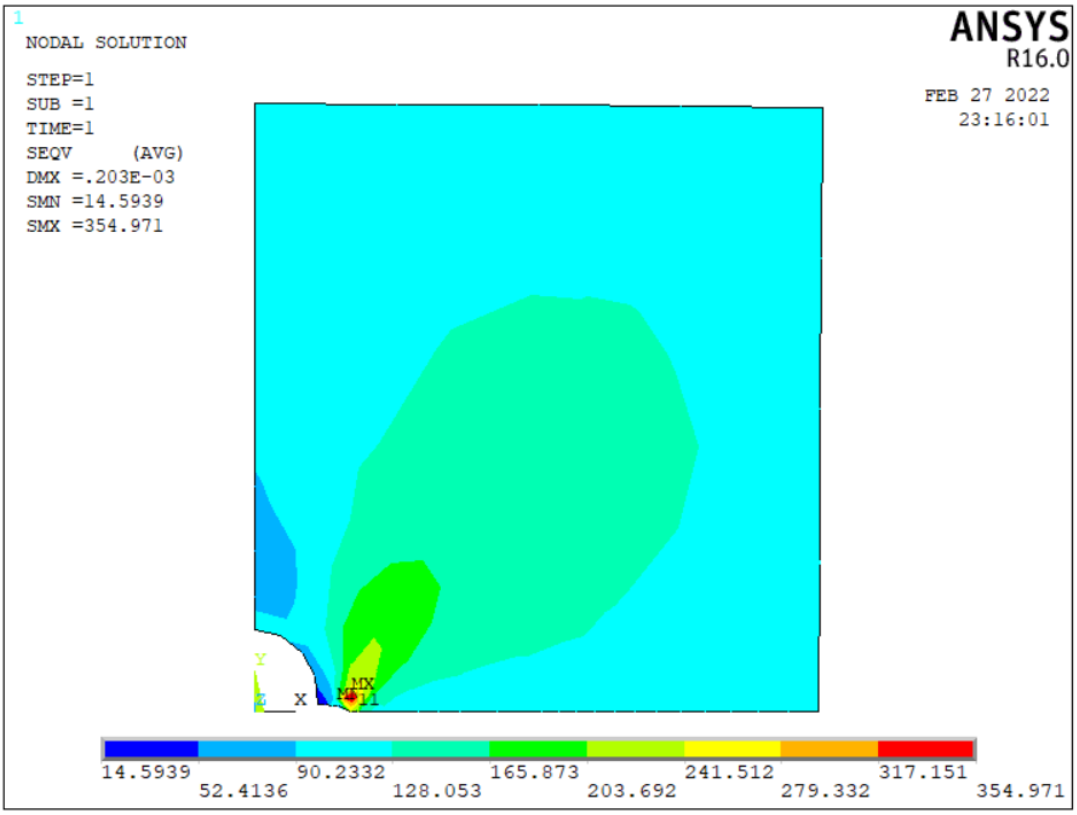

Figure 4.50: Von Mises Stress distribution at the tip of the crack due to tension stress in the hoop direction when the longitudinal crack length a = 6 mm.

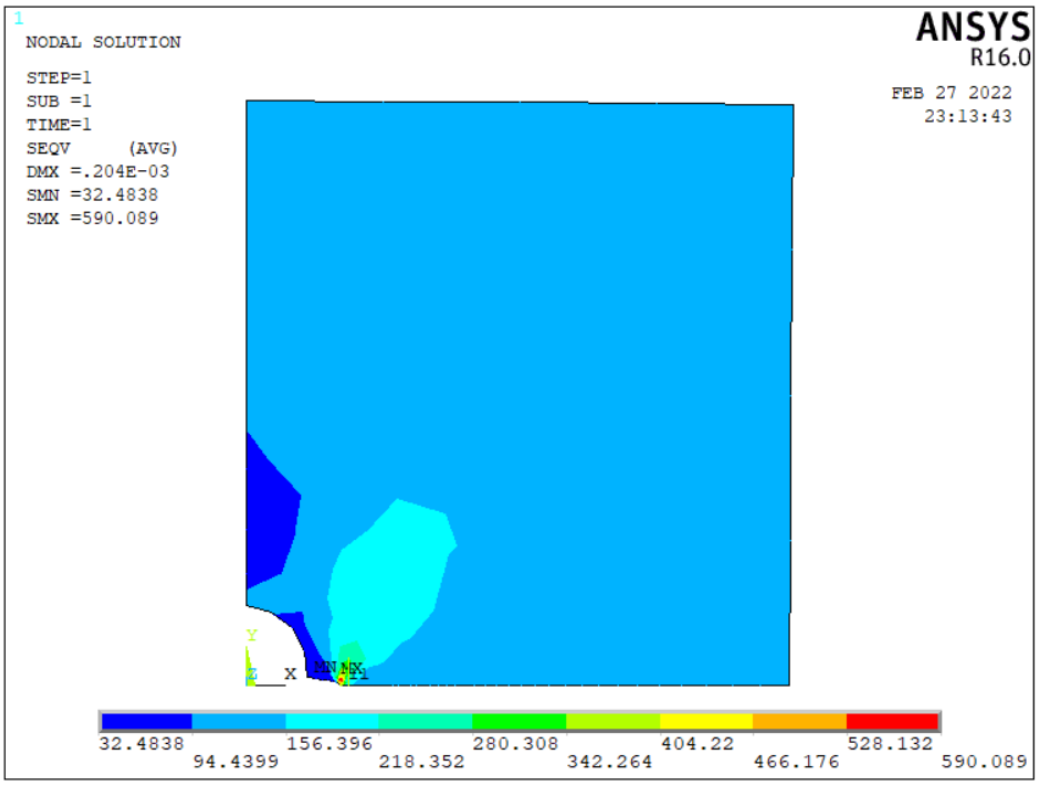

Figure 4.51: Von Mises stress distribution at the tip of the crack due to tension stress in the hoop direction when the longitudinal crack length a = 6.474mm.

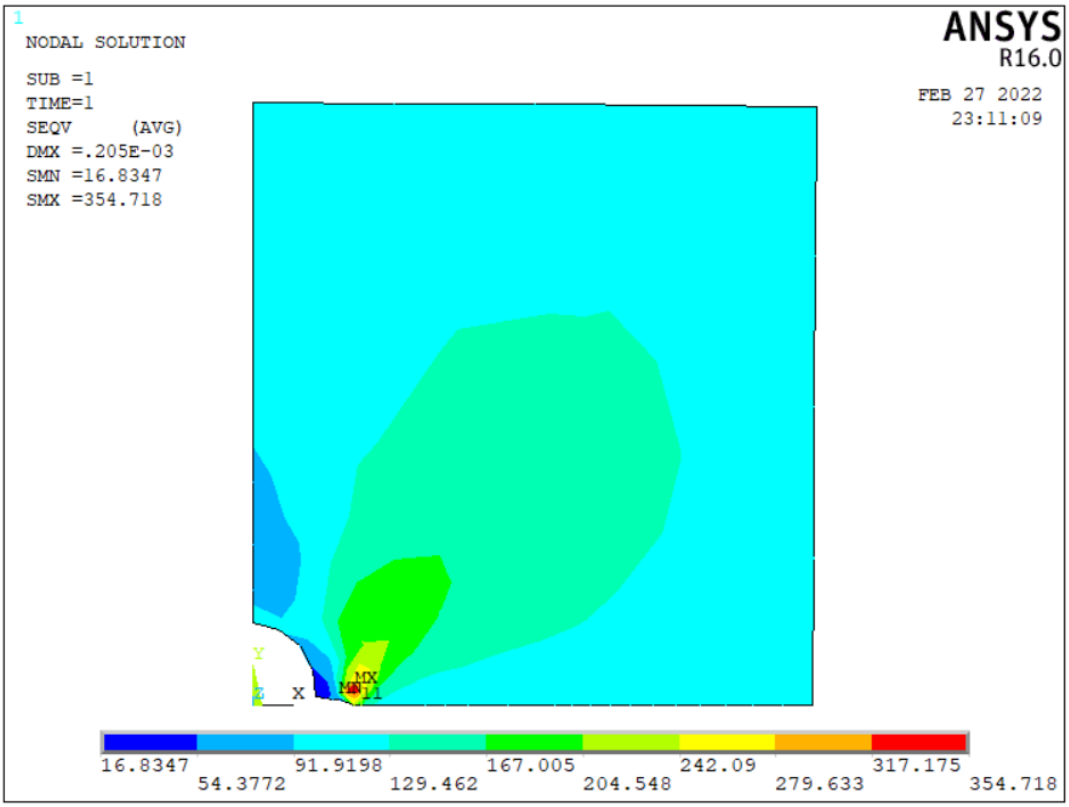

Figure 4.52: Von Mises stress distribution at the tip of the crack due to tension stress in the hoop direction when the longitudinal crack length a = 7 mm.

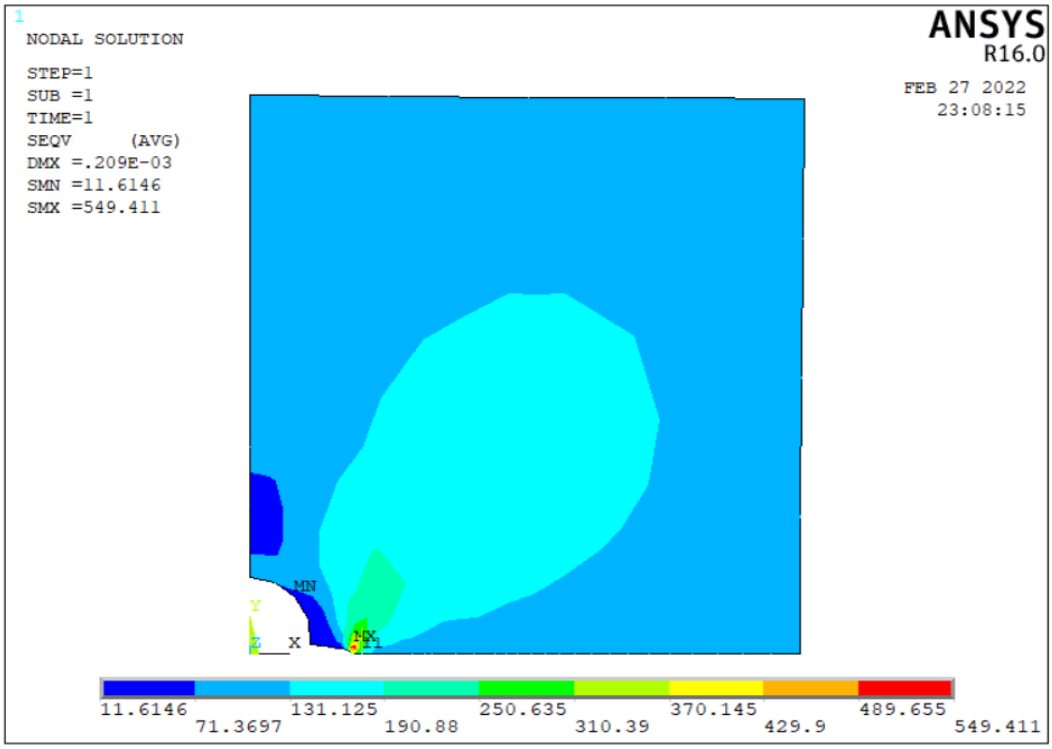

Figure 4.53: Von Mises stress distribution at the tip of the crack due to tension stress in the hoop direction when the longitudinal crack length a = 8 mm.

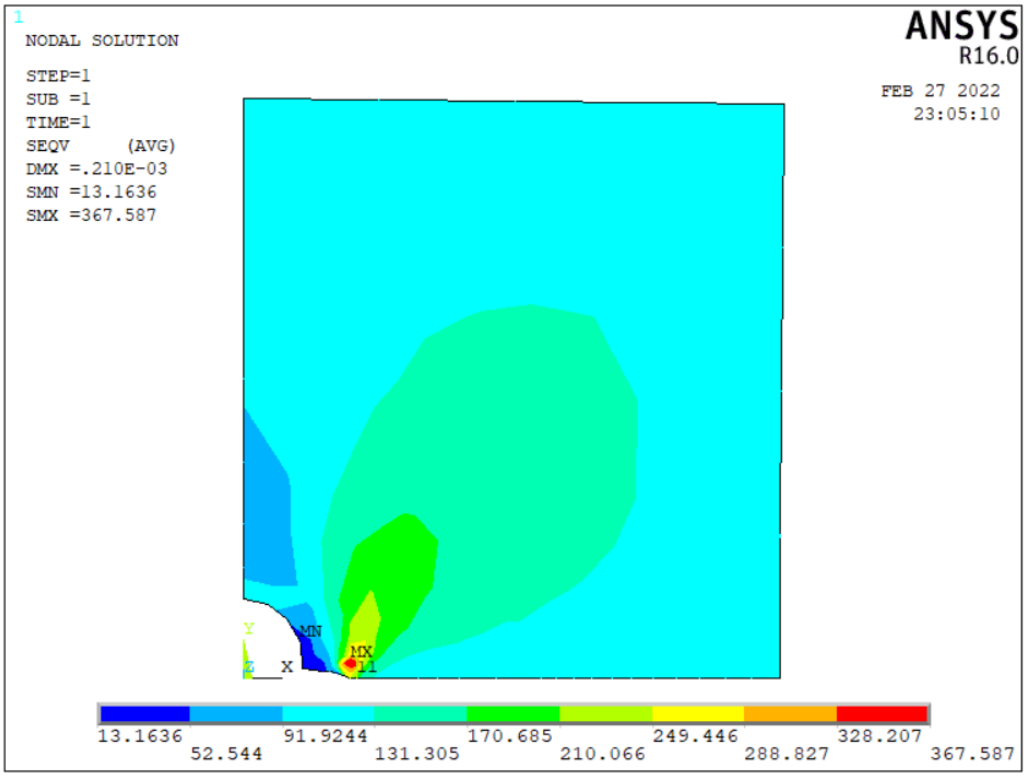

Figure 4.54: Von Mises stress distribution at the tip of the crack due to tension stress in the hoop direction when the longitudinal crack length a = 9 mm.

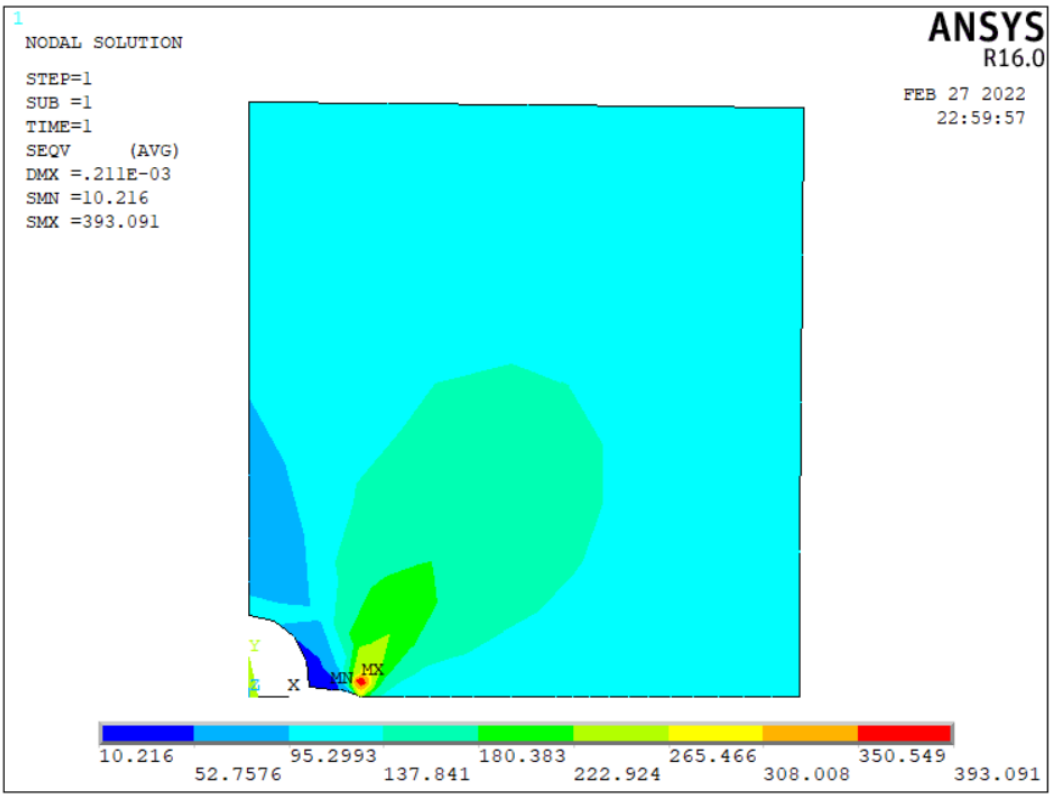

Figure 4.55: Von Mises Stress distribution at the tip of the crack due to tension stress in the hoop direction when the longitudinal crack length a = 9.53 mm.

Table 4.7: The variation of the ANSYS solution for K_I vs. analytical K_I value and the percentage error/discrepancy

Item Number	Crack Length $-a_i$ a (mm)	Stress Intensity Factor, K (MPa.m½)	β	Π*a (m)	Sqrt (Π*a)	$K_I = \beta\ \sigma\sqrt{\pi a}$	The discrepancy
1	1.25	24.375	2.85	0.003929	0.062682	24.83137	0.018379
2	2	28.492	2.56	0.006286	0.079284	28.21252	-0.00991
3	3	32.321	2.5	0.009429	0.097103	33.74331	0.042151
4	4	34.69	2.25	0.012571	0.11212	35.06568	0.010714
5	5	35.494	2	0.015714	0.125355	34.84883	-0.01851
6	6	36.367	1.852	0.018857	0.137321	35.35022	-0.02876
7	**6.47**	**36.879**	**1.8**	**0.020334**	**0.142597**	**35.67785**	**-0.03367**
8	7	37.7	1.75	0.022	0.148324	36.07981	-0.04491
9	8	37.897	1.686	0.025143	0.158565	37.16045	-0.01982

Table 4.8: The relationships between crack length and residual strength and geometric factor

Item Number	Crack Length - a(in)	β	σ_{RS}
1	0.049213	3.5	50.98024516
2	0.059055	3.5	47.10250839
3	0.068898	3.5	43.32796675
4	0.07874	3.5	40.33620207
5	0.088583	3.5	37.8892355
6	0.108268	3.5	34.93217568
7	0.11811	3.5	32.57439432
8	0.129921	3.5	31.12002997
9	0.145669	3.5	29.52305645
10	0.15748	3.5	28.1491328
11	0.169291	3.5	27.11262018
12	0.185827	3.5	26.00800476
13	0.19685	3.5	25.05400794
14	0.206693	3.5	24.39766671
15	0.225197	3.5	23.58343507
16	0.23622	3.5	22.81637822
17	0.254882	3.5	22.11605259
18	0.259843	3.5	21.60260218
19	0.267717	3.5	21.33821577
20	0.275591	3.5	21.02669097
21	0.287402	3.5	20.65581636
22	0.303937	3.5	20.15466195
23	0.314961	3.5	19.70081666
24	0.322835	3.5	19.4067511
25	0.334646	3.5	19.11402908
26	0.346457	3.5	18.77964136
27	0.354331	3.5	18.51400902
28	0.362205	3.5	18.30942724
29	0.36811	3.5	18.1358706
30	0.375197	3.5	17.9766767

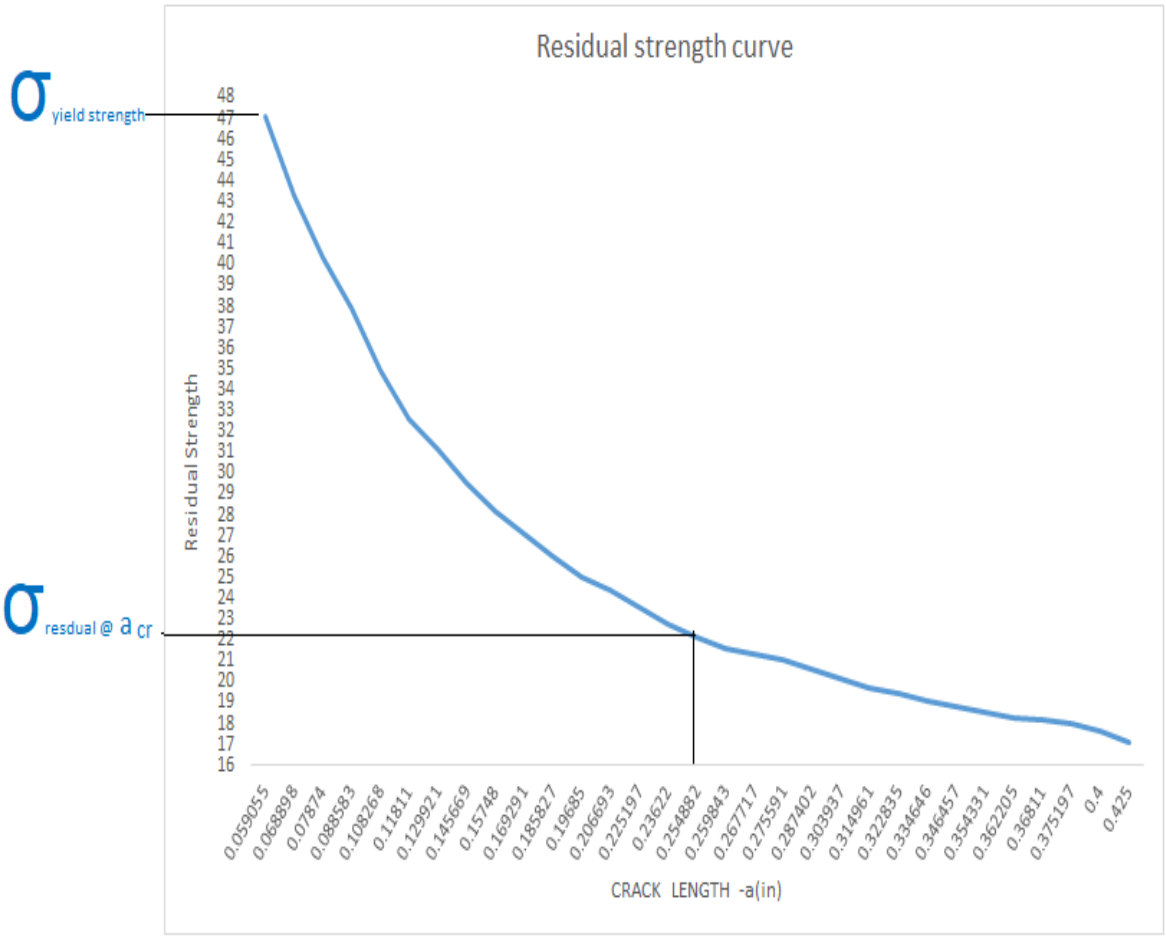

Figure 4.56: Residual Strength Vs Crack Length

Table 4.9: Crack Growth Rate Data: da/dN Vs Stress Intensity Factor: ΔK

Item Nº	a[in]	a=average	β	σ_{max}	K_{max}	a_i-a_{i-1}	da/dN	dN	∑N
1	0.049213		1.5						
2	0.059055	0.054134	1.49	13.52	8.309211	0.009843	0.0000022	4.43E+03	4.43E+03
3	0.068898	0.063976	1.48	13.52	8.972448	0.009843	0.0000029	3.34E+03	7.77E+03
4	0.07874	0.073819	1.47	13.52	9.57282	0.009843	0.0000037	2.63E+03	1.04E+04
5	0.088583	0.083661	1.46	13.52	10.12173	0.009843	0.0000046	2.14E+03	1.25E+04
6	0.108268	0.098425	1.45	13.52	10.90335	0.019685	0.0000061	3.25E+03	1.58E+04
7	0.11811	0.113189	1.41	13.52	11.37	0.009843	0.0000071	1.39E+03	1.72E+04
8	0.129921	0.124016	1.35	13.52	11.39492	0.011811	0.0000071	1.66E+03	1.88E+04
9	0.145669	0.137795	1.33	13.52	11.83335	0.015748	0.0000082	1.92E+03	2.08E+04
10	0.15748	0.151575	1.32	13.52	12.31761	0.011811	0.0000094	1.26E+03	2.20E+04
11	0.169291	0.163386	1.31	13.52	12.69163	0.011811	0.0000106	1.11E+03	2.31E+04
12	0.185827	0.177559	1.3	13.52	13.12967	0.016535	0.0000120	1.38E+03	2.45E+04
13	0.19685	0.191339	1.29	13.52	13.52478	0.011024	0.0000133	8.29E+02	2.53E+04
14	0.206693	0.201772	1.28	13.52	13.78095	0.009843	0.0000144	6.86E+02	2.60E+04
15	0.225197	0.215945	1.27	13.52	14.14537	0.018504	0.0000158	1.17E+03	2.72E+04
16	0.23622	0.230709	1.26	13.52	14.50579	0.011024	0.0000173	6.36E+02	2.78E+04
17	0.254882	0.245551	1.25	13.52	14.84636	0.018661	0.0000189	9.88E+02	2.88E+04
18	0.259843	0.257362	1.23	13.52	14.95604	0.004961	0.0000194	2.55E+02	2.91E+04
19	0.267717	0.26378	1.22	13.52	15.01825	0.007874	0.0000197	3.99E+02	2.95E+04
20	0.275591	0.271654	1.21	13.52	15.11583	0.007874	0.0000202	3.90E+02	2.99E+04
21	0.287402	0.281496	1.2	13.52	15.26007	0.011811	0.0000209	5.65E+02	3.04E+04
22	0.303937	0.295669	1.19	13.52	15.50919	0.016535	0.0000222	7.45E+02	3.12E+04
23	0.314961	0.309449	1.18	13.52	15.73314	0.011024	0.0000234	4.71E+02	3.17E+04
24	0.322835	0.318898	1.17	13.52	15.83619	0.007874	0.0000240	3.28E+02	3.20E+04
25	0.334646	0.32874	1.16	13.52	15.94128	0.011811	0.0000246	4.81E+02	3.25E+04
26	0.346457	0.340551	1.15	13.52	16.08526	0.011811	0.0000254	4.65E+02	3.29E+04
27	0.354331	0.350394	1.14	13.52	16.17417	0.007874	0.0000259	3.04E+02	3.32E+04
28	0.362205	0.358268	1.13	13.52	16.21143	0.007874	0.0000261	3.01E+02	3.35E+04
29	0.36811	0.365157	1.12	13.52	16.22173	0.005906	0.0000262	2.25E+02	3.38E+04
30	0.375197	0.371654	1.19	13.52	17.38822	0.007087	0.0000339	2.09E+02	3.40E+04

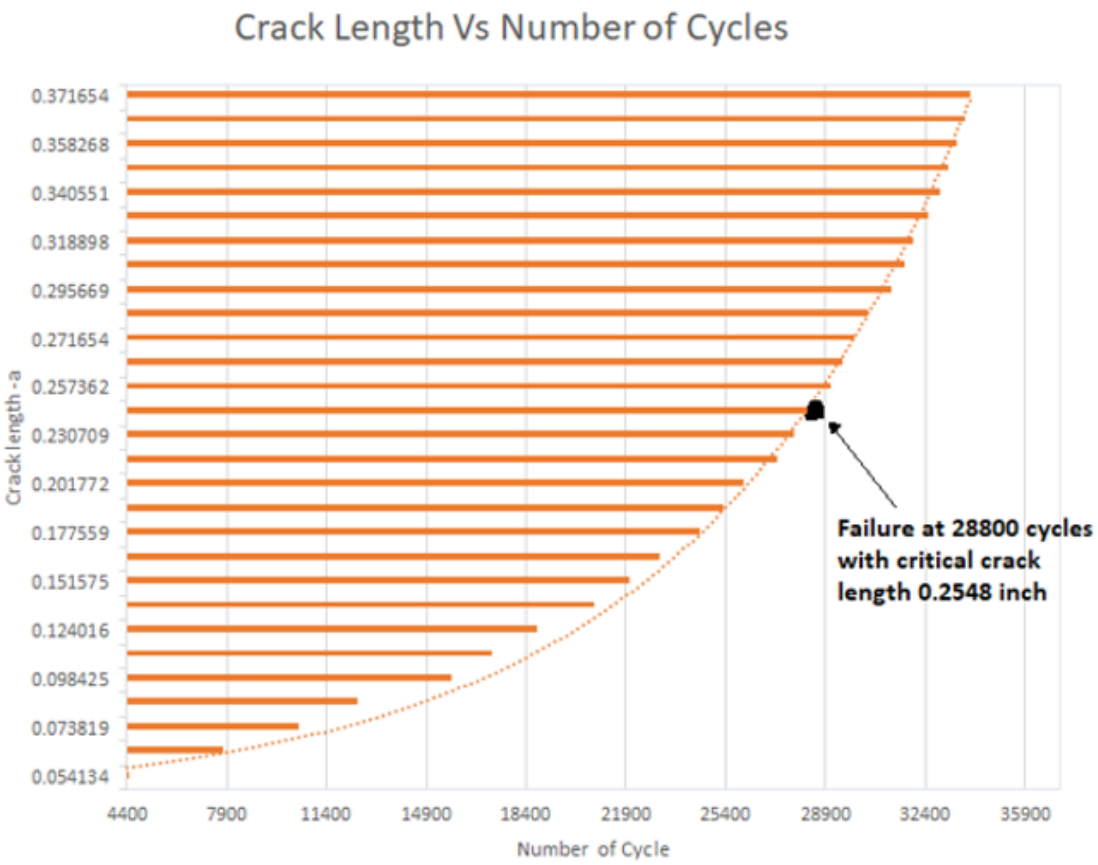

Figure 4.57: Crack Length-a versus number of cycle –N

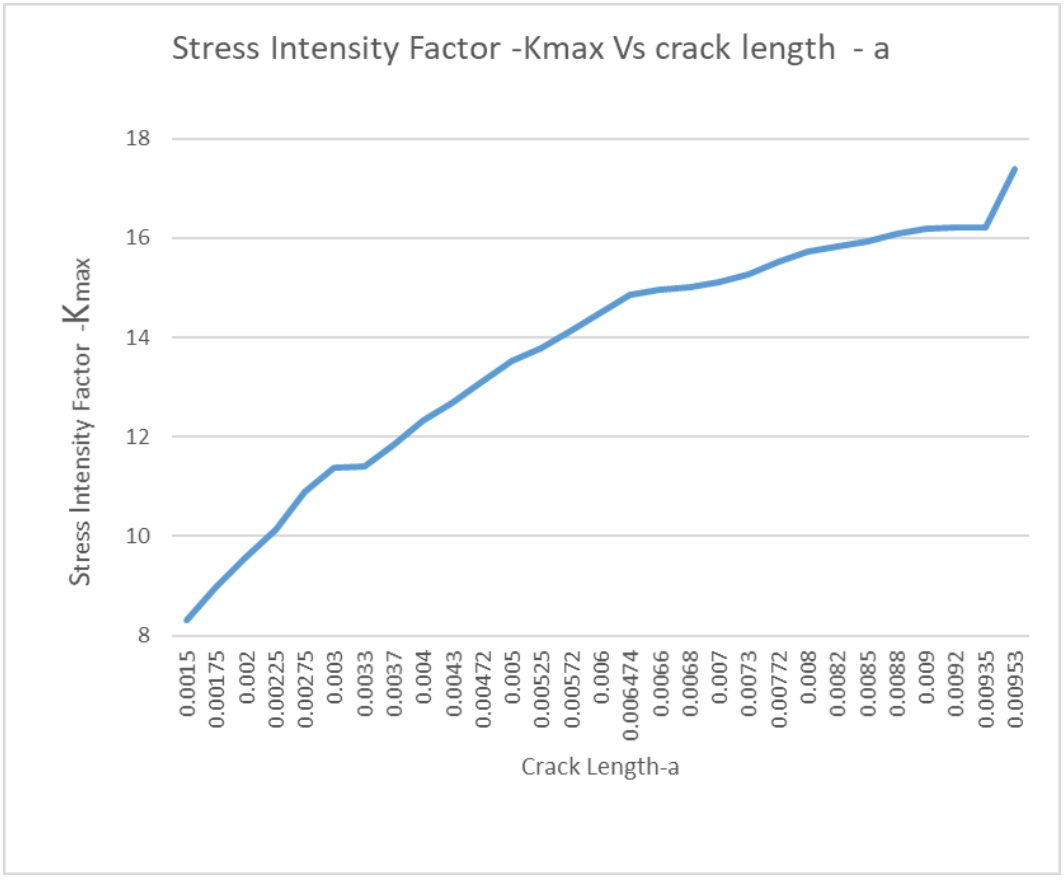

Figure 4.58: Stress Intensity Factor –KI versus crack length-a

4.13.12 Inspection threshold

The inspection threshold or first inspection is the time in cycles or flight hours that inspections should begin. [64] [65]

The inspection threshold, N_1, is the established as the lesser of:

N_d= cycles to detectable crack length, a_d= 4430.00cycles

$1/2N_{cr}$ = ½ of cycles to critical crack length, $a_{crit\ Le}$ = (1/2) *28,800.00=14,400.00 cycles

4.13.13 Inspection interval

The inspection interval is established to assure that there are at least two inspections before a critical crack develops. The interval for repetitive inspections, N_R, is:

$$N_R = (N_{cr} - N_1)/2 = (28800-4430)/2 = 12{,}185.00 \text{ cycles}$$

A graphic description of determining threshold and interval from the damage tolerance characteristics is presented in figure

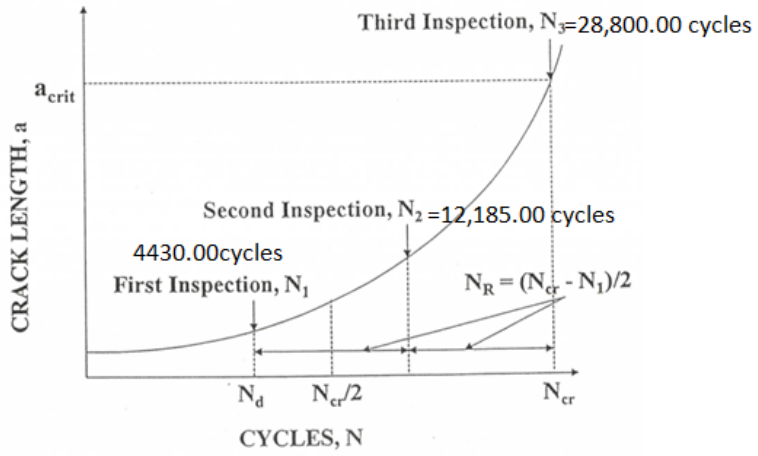

Figure 4.59: Crack Length, cycles, first, second and third inspection

4.13.14 Detectable crack length

Non–Destructive Inspection (NDI) procedures are employed to determine the detectable flaw size. The inspection interval for the repair/modification is based on the crack size detectable by NDI means. All procedures have been qualified and comply with the defined inspection requirements that the defect size to be detected is determined with a probability of detection (POD) of 90 percent at a confidence level of 95 percent. Common NDI methods include visual (3 to 5X magnifying glass) penetrant (dye or

fluorescent) magnetic particles (for ferromagnetic material), X-Ray (radiographic), ultrasonic, and eddy current (high and low frequency). [64] [65]

Ultrasonic method (US) for testing of concealed skin sheet from outside
High Frequency Eddy Current method (HFEC) for testing of external doubler from outside
Low Frequency Eddy Current (LFEC) for Sub-Surface Crack Sizing
Pulsed Eddy Current (PEC) for testing of concealed skin from outside.
Magneto-Optic Imager (MOI) for testing from outside in external double

Chapter Five

5. Conclusion, Recommendation, Validations and Future Work

5.1 Conclusion

In this thesis work, Finite Element Analysis (FEA), i.e., ANSYS application software and analytical methods are used to study "MOUNTING PLATE, STRESS CONCENTRATION AND DAMAGE TOLERANCE ANALYSIS FOR ANTENNA INSTALLATIONS ON PRESSURIZED TRANSPORT AIRCRAFT". First, the best antenna mounting plate is identified. An elliptical antenna mounting plate is compared with those of circular and rectangular mounting plates. Second, based on the first result at the location of antenna installation, from a stress concentration factor point of view, the best antenna cut-out shape was studied by comparing antenna cut-out shapes such as elliptical, circular, and square cut-out at both the mounting plate and aircraft fuselage skin subjected to biaxial tension loads. Finally, damage tolerance analysis (DTA) was performed on the antenna cut out and, based on the damage tolerance analysis (DTA), the inspection type and inspection threshold (damage detection) were established.

5.1.1 Specific objective 1

The static strength of three different mounting plates compared. Using analytical and FEM as indicated in sections ***4.1.1*** and ***4.2.2***, the elliptical antenna mounting plate is compared with those of the circular and rectangular installation mounting plates. Results based on analytical and FEM analysis were compared with each other and explained as follows:

For **Analytically analysis :** For the same area of the mounting plate, all parameters are the same except the mounting plate allowable and margin of safety MS, fastener joint margin of safety MS, and number of rivets used. The circular mounting plate is relatively better than the rectangular mounting plate and elliptical mounting plate.

For FEM/FEA analysis: The effect of various stress and strain types on the mounting plates is considered. The medium value for both stress and strain is considered. The circular mounting plate was found to be better compared with the maximum or the minimum value for rectangular and elliptical mounting plates, respectively.

Using the circular mounting plate for a relatively small surface area or if the area is within the packet/skin bay better. The uniform distribution of rivets around its circumference makes it flawless compared with elliptical and rectangular mounting plates for places where the direction of stress is unknown or where stress is known to change frequently (i.e., fatigue is a more susceptible area).

The determination of the number of rivets/fasteners, rivet pattern, and pitch of the 1st, 2nd, and 3rd row or annulus circles contour for the circular mounting plate is somewhat tiresome compared with the rectangular mounting plate (i.e. preparation of the rectangular mounting plate is the easiest one) and, relatively, it needs less effort compared with the elliptical mounting plate (preparation of the elliptical mounting plate is the most tiresome compared with the circular and rectangular mounting plates).

Finally, after comparing mounting plate types, i.e., elliptical antenna mounting plate compared with those of circular and rectangular mounting plates, the circular mounting plate becomes the better mounting plate.

5.1.2 Specific objective 2

Using analytical and FEM analysis, at the location of antenna installation, biaxial tension load is applied to the skin and mounting plate. Different antenna cut-out shapes compared with each other. As indicated in sections 4.4 and 4.12, the cut-out shapes are elliptical, circular, and square cut-outs.

For Analytically analysis: For a biaxial tension load, an analytical analysis was performed for $K_{tg:}$ Gross Area Stress Concentration factor for antenna cut-outs with different shapes such as circular, square, and elliptical, as indicated in section 4.4. The circular cut out has a relatively low gross area stress concentration factor, with a value of 2.14.

The ANSYS result of K_{tg}: Gross Area Stress Concentration Factor for different geometrical cut-outs performed with different mounting plates and the minimum stress concentration factor result found is as summarized below. also indicated in section 4.12.

- The Elliptical Mounting Plate with a square cut out has a Ktg: Gross Area Stress Concentration factor of 2.68.
- The rectangular mounting plate with a circular cut out has a Ktg: Gross Area Stress Concentration factor of 2.8.
- The Circular Mounting Plate with circular cut out has K_{tg}: Gross Area Stress Concentration factor of 2.83.

Therefore, in Specific Objective 1, a circular mounting plate has been selected among rectangular and elliptical mounting plates. Therefore, in Specific Objective 2, a circular cut out with a circular mounting plate has been selected.

5.1.3 Specific objective 3

Based on results found in specific objective 1 and specific objective 2, damage tolerance analysis at the antenna cut-out was performed for the circular mounting plate with circular antenna cut-out, then estimated inspection type and inspection threshold (damage detection) were performed.

For Analytically analysis: Considering the fracture toughness Kc i.e., K_I value at the critical crack length of the skin material, and taking initial and subsequent cack length predictions of fatigue crack growth using "Linear Elastic Fracture Mechanics" (LEFM) performed. a_c: The Critical Crack Length has been approximately determined with a value of $a_c = 6.47$mm

For FEM/FEA analysis: Starting from Initial Crack Length a_i to ac: Critical Crack Length, the value of facture toughness is calculated and compared with the facture toughness of the skin material, and finally, the Critical Crack Length is fixed.

Based on the above result, an estimated inspection type and inspection threshold (damage detection) were established.

5.2 Recommendation

This study recommends that for small antenna installations, which are typically located on the fuselage skin at the crown area, bounded by frames and longerons away from discontinuities like doors and windows. During the installation of various antennas in aircraft fuselages, the use of a circular mounting plate along with antenna cut out with a diameter of an inch is more preferable and more reliable than elliptical and rectangular mounting plates with different antenna cut outs. The same is verified and discussed in the next section, 5.3.

5.3 Validity and Applicability

Mounting plate effect, antenna cut out effect, and the damage tolerance analysis and study of this thesis is Applicable to small antenna installations that do not span over several pockets on the fuselage. It is valid for demonstrating compliance with CS-23 and possibly FAR-23 regulations.

However, for CS-25 validity, it must be verified using relevant aircraft manufacturer documents or acceptable evidence from different publications. Validity for larger antennas and for large aircraft is further discussed as indicated below.

5.3.1 Specific objective -1: validation points

Table 5.1: **Specific objective 1**- mounting plate validation points comparing the SRM Recommended Value to the actual results obtained with this thesis

	Independent Criteria	Boeing Structural Repair Manual (SRM) Recommended Value	Circular Mounting Plate	Observation
1	The Mounting Plate Allowable and Margin of Safety MS	MS < 0 ⇒ Antenna installation is statically inadequate MS = 0 ⇒ Antenna installation is marginally adequate MS < 0 ⇒ Antenna installation is statically inadequate	6.88	It is acceptable
2	Fastener Joint Margin of Safety MS		3	Fastener Joint Margin of Safety MS
3	The Shear Margin of Safety MS		4	The Shear Margin of Safety MS
4	Stiffness Ratio	The antenna installation is considered adequate if the ratio is between 1.0 and 1.5. The antenna installation is too stiff when the value is greater than 1.5 and not stiff enough when it is less than 1.0.	1.1269	The result is within SRM given value , so it is a value within a valid and safe range.
5	The fastener bending(Q)	For Aluminium fasteners, the bending is important. A Q value above 2 may indicate that the Aluminium rivet will not fill the hole but instead may buckle in the hole	0.536	The result is far less than 2, so it is a value within a valid and safe range.
6	Spacing	4≤(P/D)≤6	P/D=1.1/0.25 = 4.4	greater than 4 and less than 6 it is okay
7	Edge Margin [e or EM]	2D ± 0.05 Inches	0.5	0.45 ≤0.5≤ 0.55 it is okay

5.3.2 Specific objective -2: validation points

Table 5.2: **Specific objective 2-** stress concentration factor (K_{tg}) validation points comparing the SRM Recommended Value to the actual results obtained with this thesis.

Mounting Plate Type	K_{tg}: gross area stress concentration By FEM	K_{tg}: Gross Area Stress Concentration factor Analytical using Pilkey, W.D., and Peterson's Stress Concentration Factors (3rd Ed.).	Observation
Circular Mounting Plate with circular cut out	2.8	2.5	The maximum stress in the circular mounting plate with the circular cut-out is about three times the applied force; hence, the previous observation made by Pilkey et al. (2008) is verified.

5.3.3 Specific objective -3: validation points

Consider the Boeing 767-300 MPD and the SRM. Regarding the repetitive inspection interval for the installed antenna and the 1-inch hole diameter repair, at section 46

i. B767-300 SRM: 53-00-01-2R-6-Fuselage Skin-Small Hole Flush Repair stated that this repair is applicable to skin damage which can be removed with a maximum of 1.0-inch diameter cut-out. Regarding the inspection type**:** This repair is category A (permanent) and no supplemental inspection is necessary.
ii. MPD item number 53-642-91: Mandates, General Visual Inspection of the upper half of the fuselage-external skin between Body Station (BS) 132.5 and BS 1582 and all antenna locations within A threshold interval of 50000 FC and a repetitive interval of 3000 FC
iii. This thesis addressed that: At antenna cut out and at the vicinity of the mounting plate and the parent aircraft skin inspection threshold interval Start at 4430 FC and repetitive interval of 4430 FC

Inference /observation for the validation**:** comparing items i and ii, which are Boeing official documents that are approved by the FAA, With the results found in this thesis, the inspection threshold interval i.e. (damage detection) and the repetitive interval for the damage tolerance analysis, it can be concluded that the result found is acceptable with a 25% variations. On the other hand, this inspection becomes an additional inspection besides the existing 3000 repetitive inspections, and we can conclude that the aircraft could be safe and operational.

5.4 Future Work

- Finish aluminium repair parts and reworked surfaces by applying a chemical conversion coating and one or two coats of primer can be included in the analyses.
- Install mounting plate with faying surface sealant can be included in the analyses
- Liberally apply a corrosion inhibiting compound to completed repair can be included in the analyses [i.e. Bare Metal Surface =>Chemical Conversion Coating => BMS 10-79 TYPE 3 Primer =>BMS 10-60 TYPE 2 Polyurethane Enamel]
- different riveted diameter Vs pitch/spacing Vs rivet patter can be included in the analyses
- In terms of composite aircraft same concepts of antenna installation but force analysis different from metallic aircraft fuselage.
- In a given aircraft fuselage more than 10 to 16 antenna installed on different location of aircraft fuselage which implies the aircraft fuselage possess antenna cut out around 10 to 16 which affect fuselage durability during in-service life of the aircraft. in the future to minimize number of antenna cut-out on the fuselage integrated antenna system design needed in the aviation industry.
- For pressurized aircraft flight at 36,000 feet and above the ground, Temperature swings between [-65F to +180F typical] stress related with temperature fluctuation (thermal stress and strain) fracture related with thermal stress and strain
- For big antenna installation like Sat-com (i.e. Satellite communication) which crossed more than one frames and longerons, the load analysis different from this thesis, frames and longerons effect considered.

Reference

[1] MIL-STD-1530 D Aircraft structural integrity program.

[2] Eastin, R. (presentation) or McGarvey, J. (paper). Chicago ACO paper “Damage tolerance analysis for antenna installations on pressurized transport Airplanes”

[3] Swift, T. 1991. "Repairs to damage tolerant Aircraft," Structural integrity of aging airplanes, edited by Atluri, S. N., Sampath, S.G., and Tong, P. Springer-Verlag. 433–483. http://www.dtic.mil/docs/citations/ADA225742

[4] Boeing. 2016. Aircraft Structural repair for engineers Part III. Version 7.

[5] Fredell, R.S.,1994. Damage tolerant repair techniques for pressurized aircraft fuselages. WRIGHT LAB WRIGHT-PATTERSON AFB OH.

[6] Los Angeles Aircraft certification office policy memo. 1995. «INFORMATION: ANM- 120L Damage tolerance philosophy.

[7] Ethiopian Airlines (ETH) Detail Specification Model 767-360ER Document No. D019T001ETH63E-1

[8] Boeing Model 787-9 DETAIL SPECIFICATION International Lease Finance Corporation (ILF) Ethiopian Airlines (ETH)

[9] Safarian “DTA guidelines for antenna installations”.

[10] Swift, T., 1981. Application of damage tolerance technology to type certification (No. 811062). SAE Technical Paper.

[11] Boeing service bulletin 777-53A0068: [FUSELAGE - Sections 44 and 46 - crown skin panel-corrosion and crack on fuselage skin below SATCOM antenna adapter plate – inspection.

[12] Swift, T., 1987. Damage Tolerance in Pressurized Fuselages-11th Plantema Memorial Lecture. In ICAF Symposium.

[13] Chen, C., Nomura, M., and Yu, J. (1999–2000) "Enhancement to repair assessment procedure and integrated design (RAPID)". Analysis methods enhancements.

[14] Wild, G., Pollock, L., Abdelwahab, A.K. and Murray, J., 2021. The Need for Aerospace Structural Health Monitoring: A review of aircraft fatigue accidents. International Journal of Prognostics and Health Management, 12(3).

[15] WITHEY, P., 2001. Fatigue failure of the de havilland comet i. In Failure Analysis Case Studies II (pp. 185-192). Pergamon.

[16] Boeing. 2016. Aircraft Structural repair for engineers Part III. Version 7.

[17] Ganson, B., 2021. Aircraft Designers and Manufacturers. In Texas Takes Wing (pp. 147-168). University of Texas Press.

[18] Freeman, R., 2021. Failure of joints in service. In Welding and Joining of Aerospace Materials (pp. 427-435). Woodhead Publishing.

[19] Wanhill, R.J., 2018. Fatigue Requirements for Aircraft Structures. In Aircraft Sustainment and Repair (pp. 17-40). Butterworth-Heinemann.

[20] Freeman, R., 2021. Failure of joints in service. In Welding and Joining of Aerospace Materials (pp. 427-435). Woodhead Publishing.

[21] Babish, I.V., Charles, A., Tiffany, C.F. and Gallagher, J.P., 2010. Threats to Aircraft Structural Safety Including a Compendium of Selected Structural Accidents/Incidents. AERONAUTICAL SYSTEMS CENTER WRIGHT-PATTERSON AFB OH DIRECTORATE OF ENGINEERING.

[22] Howard, I.C., 1986. Fracture of an aircraft horizontal stabilizer. ASTM International.

[23] Brot, A., 2006. Development of fatigue life regulations based on lessons learned from several aircraft accidents. In 46 th Israel Annual Conference on Aerospace Sciences.

[24] McEvily, A.J., 2004. Failures in inspection procedures: case studies. Engineering failure analysis, 11(2), pp.167-176.

[25] Saraçyakupoğlu, T., 2020. Fatigue Studies in Aviation in Light of the 1988 Aloha Airlines Incident. Aviation Turkey.

[26] Shimamoto, A., Kosai, M. and Kobayashi, A.S., 1998. National Transportation Safety Board Aircraft Accident Report, Aloha Airlines Flight 243, Boeing 737-200, N73711 National Transportation Safety Board Aircraft Accident Report, Aloha Airlines Flight 243, Boeing 737-200, N73711, NTSB/AAR-89/03, 1989. JSME international journal. Series A, Solid mechanics and material engineering, 41(3), pp.352-358.

[27] Mechanical Property of 2024-T3 Clad Sheet and Plate from The metallic materials properties development and standardization (MMPDS) Handbook.

[28] Structural Repair Manual (SRM) Chapter 51-30-01-0G-0

[29] "Benachour, M., Benguediab, M., Hadjoui, A., Benachour, N., & Hadjoui, F. Fatigue crack growth of different aluminum alloy 2024. In ECF17, Brno 2008. "

[30] Aluminum 2024-T4 - ASM Material Data Sheet, https://asm.matweb.com/search/SpecificMaterial.asp?bassnum=ma2024t4

[31] Aircraft Structural repair for engineers Part I. Version 2.1 7x7 Copy Right © 2013 the Boeing company

[32] White, F.M., 1999. University of Rhode Island. fluid mechanics. McGraw hill series in mechanical engineering, pp.1-960.

[33] "Reynolds Number". www.grc.nasa.gov.

[34] B767-300 Structural Repair Manual (SRM) 51-00-03-0G-0, Rev No. / Date: 109 / 15 Dec 2018

[35] B767-300 Structural Repair Manual (SRM) chapter: 53-00-01

[36] Reference: B767-300 Structural Repair Manual (SRM) chapter 51-00-02-0G-0 Rev No. / Date: 109 / 15 Dec 2018

[37] Munson, B.R., Young, D.F., and Okiishi, T.H. 1998. Fundamentals of fluid mechanics, John Wiley and Sons, Inc.

[38] Falkovich, G. 2011. Fluid mechanics. Cambridge University Press.

[39] White, F.M., 1999. University of Rhode island. fluid mechanics. McGraw hill series in mechanical engineering, pp.1-960.

[40] "Boundary Layer". www.grc.nasa.gov.

[41] Wolfgang Hoffmann Structures Expert, Large Antennas EASA / NAA / DOA Workshop 17th – 18th September 2014

[42] B767-300 Structural Repair Manual (SRM) chapter 53-00-00-0G-0Rev No. / Date: 109 / 15 Dec 2018

[43] Boeing drawing number 146T3151_dwg_0003 and 146T3151_DWG_0004

[44] Component Maintenance Manual (CMM) of respective listed antenna type

[45] Megson, T.H.G., 2021. Aircraft structures for engineering students. Butterworth-Heinemann.

[46] Keçelioğlu, G., 2008. Stress and fracture analysis of riveted joints (Master's thesis, Middle East Technical University).

[47] Aircraft Structural repair for engineers Part I. Version 2.1 7x7 Copy Right © 2013 the Boeing company

[48] Chen, C., Nomura, M., and Yu, J. (1999–2000) "Enhancement to repair assessment procedure and integrated design (RAPID)". Analysis methods enhancements.

[49] Boeing. 2016. Aircraft Structural repair for engineers Part III. Version 7.

[50] Pilkey, W.D., and Peterson's Stress Concentration Factors (3rd Ed.).

[51] Esam M. Alawadhi finite element simulations using ANSYS (2nd Ed.).

[52] Safarian, P. Federal aviation administration, finite element modelling and analysis validation.

[53] Perez, N., 2017. Fatigue crack growth. In Fracture Mechanics (pp. 327-372). Springer, Cham.

[54] Anderson, T.L. 1995. Fracture mechanics: Fundamental and application, CRC Press.

[55] Boeing. 2016. Aircraft Structural repair for engineers Part III. Version 7.

[56] ASTM E-1049-85 Standard Practice for Cycle Counting in Fatigue Analysis".

[57] Brot, A., Peleg-Wolfin, Y., Kressel, I. and Yosef, Z., 2008. The damage-tolerance behavior of integrally stiffened metallic structures. In 48th Israel Annual Conference on Aerospace Sciences IACAS conference.

[58] Swift, T. 1990. FAA-AIR-90-01 "Repairs to damage tolerant Aircraft". Federal Aviation Administration (FAA).

[59] Pacchione, M. and Telgkamp, J., 2006, September. Challenges of the metallic fuselage. In Proceedings of the 25th International Congress of the Aeronautical Sciences-ICAS (Vol. 451, pp. 1-45).

[60] Fagerberg, J., 2020. Development of Damage Tolerance Methodology for Antenna Installations in Pressurized Aircraft.

[61] Pappa, Z., 2018. Damage tolerance design aircraft structures.

[62] Shrestha, B., 2021. Crack propagation in aircraft fuselage stiffened skin panels.

[63] Chen, C., Nomura, M., and Yu, J. (1999–2000) "Enhancement to repair assessment procedure and integrated design (RAPID)". Analysis methods enhancements.

[64] https://www.ndt.net/article/ecndt98/aero/001/001.htm

[65] FAA Chicago aircraft certification office. Damage tolerance analysis for antenna installation on pressurized transport airplanes.

[66] Boeing service bulletin 777-53A0068: [FUSELAGE - Sections 44 and 46 - crown skin panel-corrosion and crack on fuselage skin below SATCOM antenna adapter plate – inspection.

[67] Handbuch Struktur Berechnung. Issue B. IABG mbH. Einsteinstr. 20, 85521 Ottobrunn, 1991.Chap.21031-01.

Appendix

Appendix-I: History of fatigue study /Fatigue Time Line

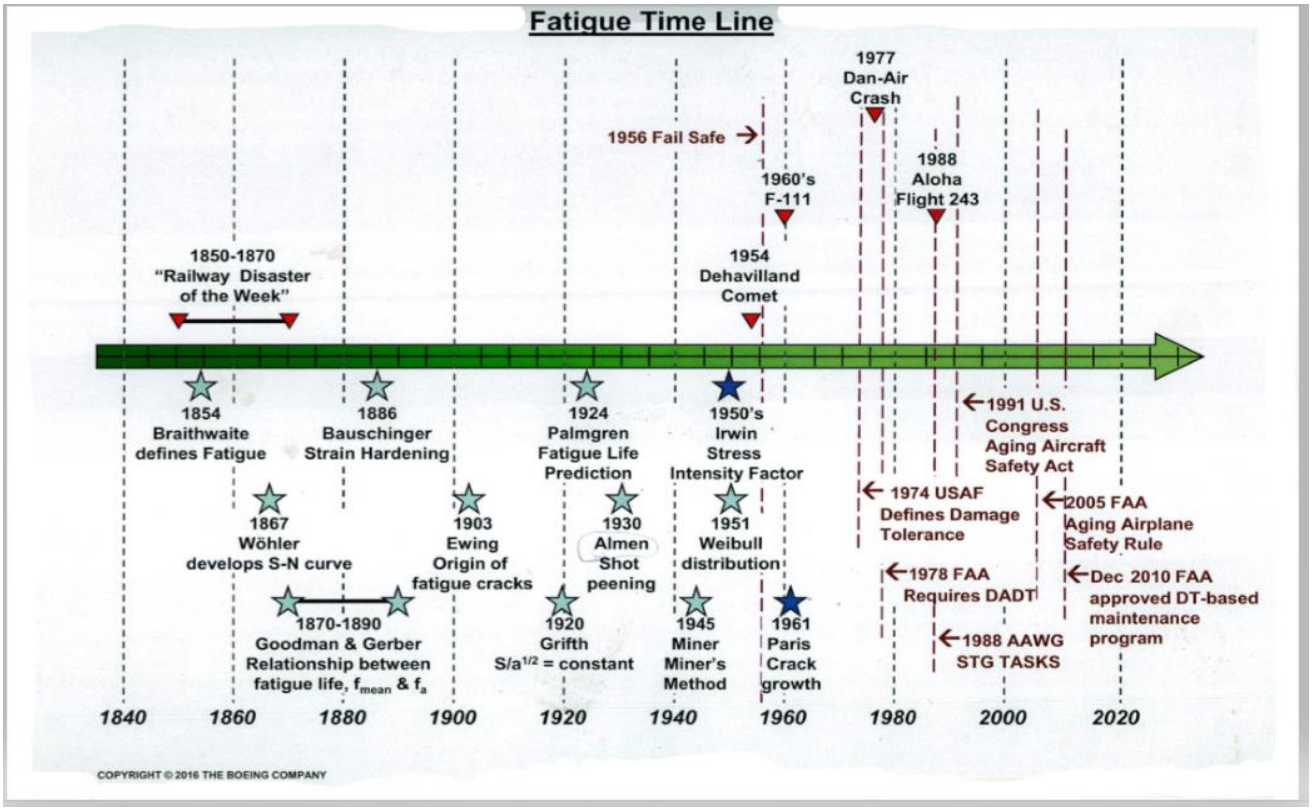

Appendix-II: Esam M.Alawadhi Finite Element Simulations Using ANSYS (2nd Ed.). [46]

7.1 MESH REFINEMENT

The accuracy of the finite element model can be enhanced by either increasing the number of elements in the model or using higher-order elements. Increasing the number of element is called h-refinement, while increasing the order of the element is called p-refinement. Increasing the number of elements or the elements' order will lead to significant increase in the computational time and requires memory to solve the problem. Consider the stress analysis of a plate with holes shown in Figure 7.1a. A linear quadratic element is used to determine the stress concentration factor. The exact solution is available from the theory of elasticity, and Figure 7.1b shows the finite element mesh. The mesh consists of 86 elements. To study the effect of the number of elements on the solution, the number of elements is increased and the stress concentration is obtained for all mesh sizes.

Figure 7.2 shows the error of the stress concentration for different number of elements using linear quadratic elements. The domain is meshed with three different mesh sizes, A, B, and C. The number of elements of mesh C is higher than B, and B is higher than A. The figure indicates that as the number of elements increases, the relative error is decreased to approach a fixed value. Adding more elements to the mesh C will have an insignificant effect in reducing the computational error.

When the number of elements has no effect on the solution, the mesh is called a mesh-independent solution. Increasing the order of the elements reduces error percentage for the same number of elements. Figure 7.3 indicates that replacing the linear quadratic elements with a cubical one reduces the percentage of the error by about 10%.

With a high-order element, the mesh-independent process is faster than a low-order element, as shown in Figure 7.4. In addition, a mesh with the linear quadratic element is becoming mesh independent at a very slow rate.

The higher-order elements lead to more accurate results than lower-order elements. On the other hand, the time required to complete the solution is important, especially for very large meshes. The computational time could take more than 10 days for meshes with more than one million elements. In addition to time, the higher-order elements need large amount of memory that could not be afforded. Figure 7.5 indicates that in spite of a low mesh convergence rate of linear quadratic elements, the time required to solve the problem is nearly independent of the number of elements in the mesh. Also, increasing the order of the elements significantly increases the time required to solve the problem.

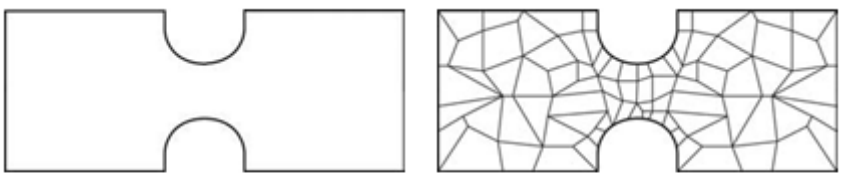

FIGURE 7.1 (a) Geometry of a plate, and (b) finite element mesh.

Appendix-II: Esam M.Alawadhi Finite Element Simulations Using ANSYS (2nd Ed.).[46]

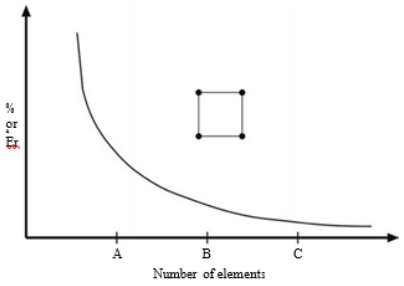

FIGURE 7.2 Error of the stress concentration for different mesh size using linear quadratic elements.

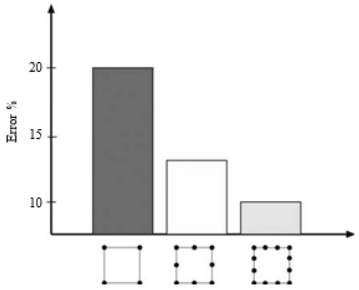

FIGURE 7.3 Percentage of error with different element orders.

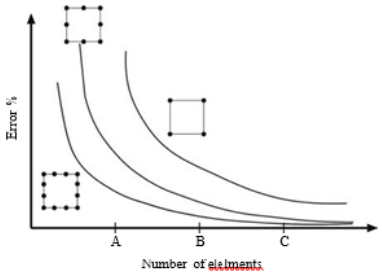

FIGURE 7.4 Error of the stress concentration for different number of elements with different orders.

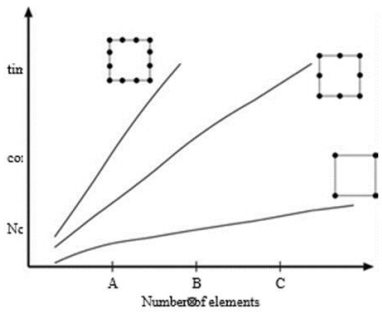

FIGURE 7.5 Computational time for various types and numbers of quadrilateral elements.

Appendix-III: stress gradient along the potential crack growth and normalized stress intensity factor β .[49]

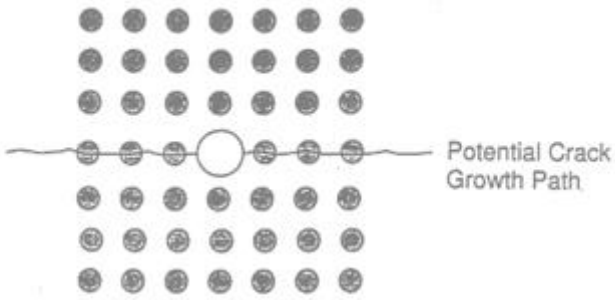

Figure 17. Potential Crack Growth Paths

The stress gradient along the potential crack path subjected to 1,000 psi reference skin stress is shown in Figure 18. The distance d is measured from the center of the hole.

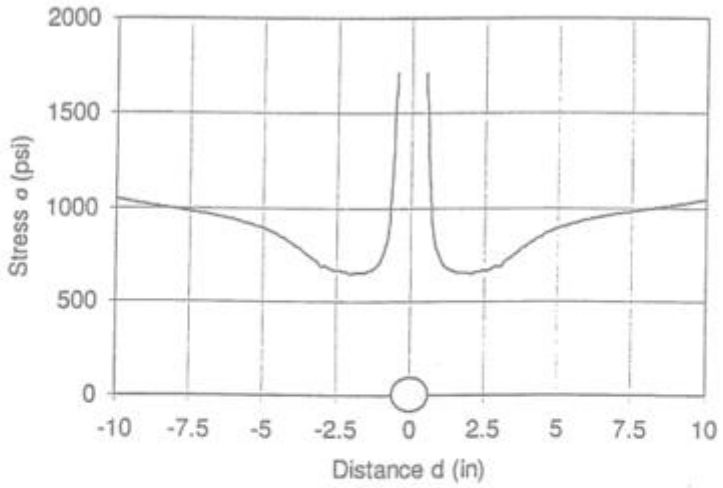

Figure 18. Stress Gradient along Potential Crack Growth Path

Residual Strength and Crack Growth

To demonstrate the residual strength and crack growth analysis of the example problem, analysis is performed for three Scenarios described in Section 3.3.

Appendix-IV: stress gradient along the potential crack growth and normalized stress intensity factor β. [49]

(1) Stress Intensity Factors

Stress intensity factors for a crack initiating from the center or the corner fastener hole due to gross, bearing, and bypass stresses are calculated using the superposition method. The effect of a crack growing toward an adjacent hole is accounted for using the compounding method.

For a crack initiating from the antenna connector hole, the weight function method is used. Using the stress gradients shown in Figure 18, the normalized stress intensity factor or geometry factor is obtained as shown in Figure 19.

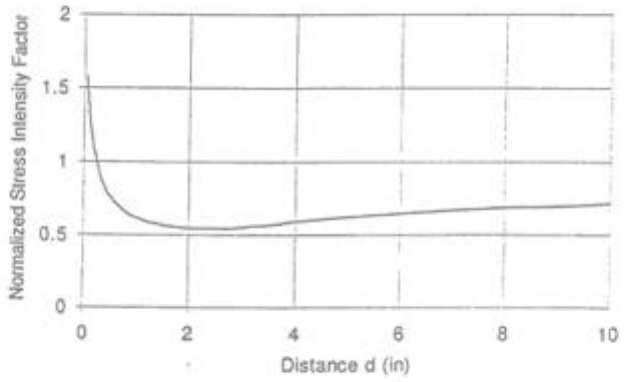

Figure 19. Normalized Stress Intensity Factors

The effect of a crack growing toward an adjacent hole is accounted for using the compounding method.

Appendix-V: Corrosion and Cracking of Fuselage Skin below SATCOM Adapter Plate (777-FTD-53-12001). [66]

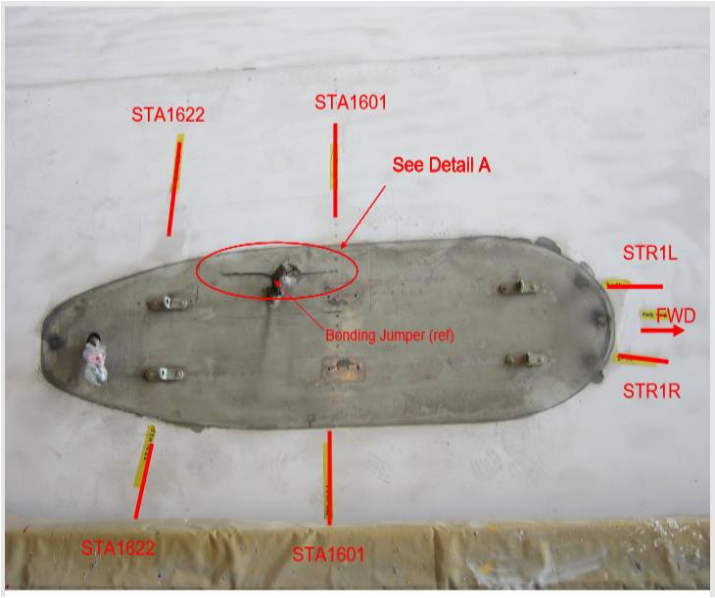

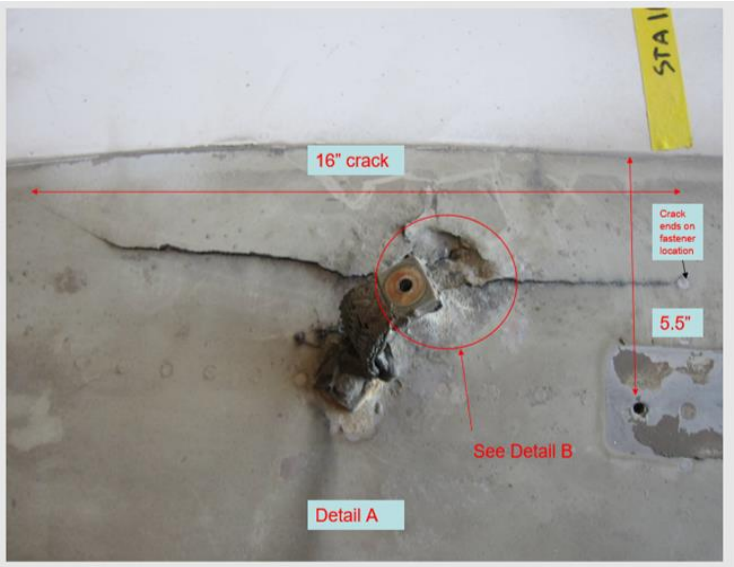

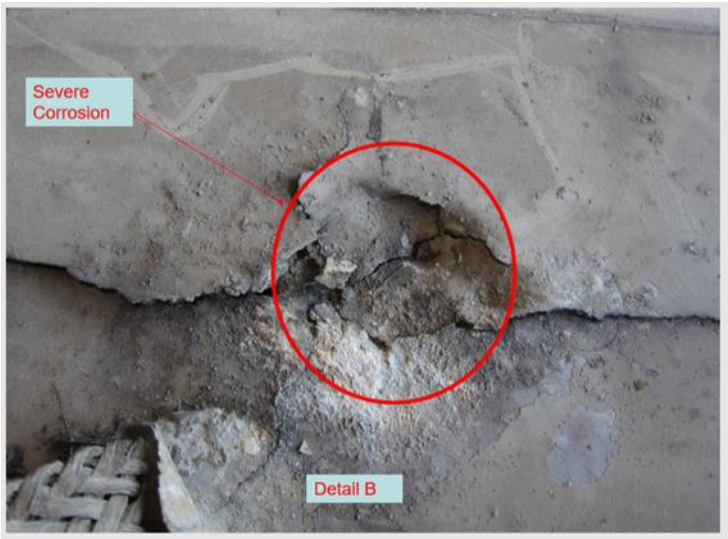

Appendix -V: Compatibility Equations

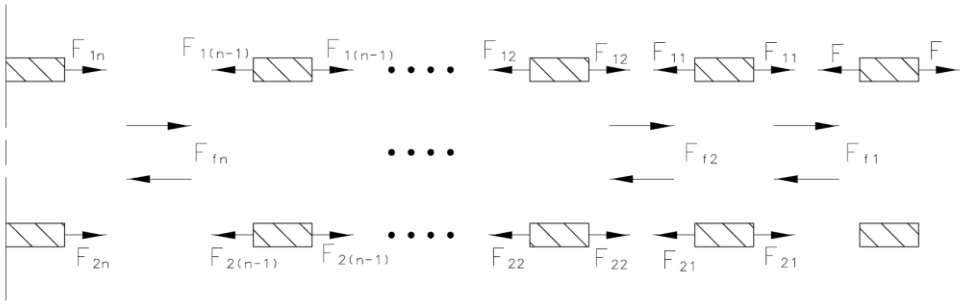

Figure A.1: mounting plate /Skin Free Body Diagram. [67]

- Equilibrium

$$\begin{array}{lllllll} F_{1n} & + & F_{fn} & - & F_{1(n-1)} & = & 0 \\ F_{1(n-1)} & + & F_{f(n-1)} & - & F_{1(n-2)} & = & 0 \\ \ldots & + & \ldots & - & \ldots & = & 0 \\ F_{11} & + & F_{f1} & - & F & = & 0 \end{array}$$

$$\begin{array}{lllllll} F_{2n} & + & F_{fn} & - & F_{2(n-1)} & = & 0 \\ F_{2(n-1)} & + & F_{f(n-1)} & - & F_{2(n-2)} & = & 0 \\ \ldots & + & \ldots & - & \ldots & = & 0 \\ & & F_{21} & - & F_{f1} & = & 0 \end{array}$$

- Compatibility

$$\begin{array}{lllllllllllllll} u_{1n} & & & & & & & - & u_{2n} & & & & & = & u_{fn} \\ u_{1n} & + & u_{1(n-1)} & & & & & - & u_{2n} & - & u_{2(n-1)} & & & = & u_{f(n-1)} \\ u_{1n} & + & u_{1(n-1)} & + & \ldots & + & \ldots & - & u_{2n} & - & u_{2(n-1)} & - \ldots - & \ldots & = & \ldots \\ u_{1n} & + & u_{1(n-1)} & + & \ldots & + & u_{12} & - & u_{2n} & - & u_{2(n-1)} & - \ldots - & u_{22} & = & u_{f2} \\ u_{1n} & + & u_{1(n-1)} & + & \ldots & + & u_{11} & - & u_{2n} & - & u_{2(n-1)} & - \ldots - & u_{21} & = & u_{f1} \end{array}$$

Figure A.2: Compatibility and Equilibrium Equations. [67]